

**DYNAMIC ANALYSIS OF MAGNETORHEOLOGICAL
(MR) FLUID BASED SEMIACTIVE SUSPENSION
SYSTEM FOR VEHICULAR APPLICATION USING
NON-PARAMETRIC APPROACH**

Thesis

Submitted in partial fulfillment of the requirements for the degree of

DOCTOR OF PHILOSOPHY

by

Hemanth K.



DEPARTMENT OF MECHANICAL ENGINEERING
NATIONAL INSTITUTE OF TECHNOLOGY KARNATAKA,
SURATHKAL, MANGALORE – 575025

October, 2016

D E C L A R A T I O N

I hereby *declare* that the Research Thesis entitled “**DYNAMIC ANALYSIS OF MAGNETORHEOLOGICAL (MR) FLUID BASED SEMIACTIVE SUSPENSION SYSTEM FOR VEHICULAR APPLICATION USING NON-PARAMETRIC APPROACH**” which is being submitted to the **National Institute of Technology Karnataka, Surathkal** in partial fulfillment of the requirements for the award of the Degree of **Doctor of Philosophy** in **Department of Mechanical Engineering** is a *bonafide report of the research work carried out by me*. The material contained in this Research Thesis has not been submitted to any University or Institution for the award of any degree.

Register Number : **135021ME13FO4**

Name of the Research Scholar : **Hemanth K.**

Signature of the Research Scholar :

Department of Mechanical Engineering

Place : **NITK-Surathkal**

Date :

C E R T I F I C A T E

This is to *certify* that the Research Thesis entitled “**DYNAMIC ANALYSIS OF MAGNETORHEOLOGICAL (MR) FLUID BASED SEMIACTIVE SUSPENSION SYSTEM FOR VEHICULAR APPLICATION USING NON-PARAMETRIC APPROACH**” submitted by **Mr. Hemanth K. (Register Number: 135021ME13FO4)** as the record of the research work carried out by him, is *accepted as the Research Thesis submission* in partial fulfillment of the requirements for the award of degree of **Doctor of Philosophy**.

Research Guide(s)

Dr. Hemantha Kumar

Assistant Professor

Department of Mechanical Engineering

NITK, Surathkal

Prof. K. V. Gangadharan

Professor

Department of Mechanical Engineering

NITK, Surathkal

Chairman - DRPC

Date:

ACKNOWLEDGEMENTS

With a deep sense of gratitude, I wish to express my sincere thanks to my supervisors **Dr. Hemantha Kumar** and **Prof. K. V. Gangadharan**, Department of Mechanical Engineering, National Institute of Technology Karnataka (N.I.T.K), Surathkal, for their excellent guidance and support throughout the work. I received very useful, encouraging and excellent academic feedback from them, which has stood in good stead while writing this thesis. Their constant encouragement, help and review of the entire work during the course of the investigation were invaluable. I profoundly thank them.

I take this opportunity to thank **Prof. K. V. Gangadharan**, Professor and Head, Department of Mechanical Engineering for his continuous and timely suggestions.

I wish to thank all the members of the Research Program Assessment Committee including **Dr. R.P.Choudhary**, Assistant Professor, Department of Mining Engineering and **Dr. Navin Karanth**, Assistant professor, Department of Mechanical Engineering for their appreciation and criticism all through this research work.

Special thanks to **Prof. Vijay H. Desai**, Professor, Department of Mechanical Engineering for his help and constructive comments and continuous support during my research work.

I acknowledge the funding support from Department of Science and Technology (DST): No.SB/FTP/ETA-0071/2013 and support from SOLVE: The Virtual Lab @ NITK (www.solve.nitk.ac.in) and experimental facility provided by Centre for System Design (CSD): A Centre of excellence at NITK-Surathkal.

I wish to express my sincere gratitude to all the faculty members of the Department of Mechanical Engineering, N.I.T.K Surathkal for their help, encouragement and support all through this research work.

My sincere thanks to all my lab mates Mr. Kiran Vernekar, Mr. Gangadhar N., Mr. Madhusudana C. K., Mr. Gurubasavaraju T. M., Mr. J. Vipin Allien and Mr. A. Ganesha for their help and support to carry out this dissertation work.

I am indebted to my roommates Mr. Nivish George, Mr. V. Shamanth, Mr. Gangadhar N., Mr. H. S. Nithin, Mr. Rakesh K Rajan and Mr. H. S. Ashrith for their constant help and encouragement during the entire research work.

Finally, I would like to thank my parents who have trusted me throughout my life. I would like to share this moment of happiness with my parents, Indramma and C. N. Krishna; My sister Ashwini C.K.; My sister-in-law Asha; My brother Anand C.K. and My brother-in-law Lokesh M.V. for their constant encouragement.

Hemanth K.

ABSTRACT

The magnetorheological (MR) fluid dampers belong to a category of semi-active devices, in which damping force can be varied within a few milliseconds through the application of a magnetic field. The main aim of this project is to investigate the performance of MR damper used as a semi-active suspension system in vehicle models to improve the ride comfort and road holding quality of the vehicle, when subjected to average random road profile and road bump as inputs.

Research work starts with design and development of MR damper, which includes optimization of MR damper to study the variation of magnetic flux density with variation of electromagnetic circuit parameters such as current magnitude, number of turns in the coil, coil core length, fluid flow gap and flange length. The optimization study shows that, the magnetic flux density induced in the fluid flow gap increases with increase of applied current, number of turns in the coil and coil core length. The magnetic flux density is seen to decrease with increase of fluid flow gap and flange length. The optimum fluid flow gap, which is obtained from the optimization technique has been considered for fabrication of MR damper.

Experimental studies on a developed MR damper with different proportion of MR fluid have been conducted by using dynamic testing facilities at 1.5Hz and 2Hz operating frequencies. Based on the experimental results, the optimum level of parameters such as proportion of MR fluid and operating frequency are evaluated by using Taguchi design of experiments. Then, dynamic behaviour of MR damper with optimum level of parameters has been investigated. Developed damper shows the capability of improving both stiffness and damping properties with variation of electric current.

Magnetostatic analysis of MR damper has been carried out, in order to find total magnetic flux density induced in the fluid flow gap. Total magnetic flux density induced in the fluid flow gap is divided into five categories by using statistical categorization technique. The average total magnetic flux density obtained from the

statistical categorization technique has been used to evaluate the damper force. Based on this, non-parametric model has been developed and polynomial function is used to relate the damper force as a function of current. Bouc-Wen model has been used to benchmark the developed non parametric model. The parameters of the Bouc-Wen model are evaluated by minimizing the error between the experimental and predicted force using non-dominated sorting genetic algorithm II (NSGA-II) optimization technique. The hysteresis behaviour of the MR damper is predicted by both models (non-parametric model and Bouc-Wen model) and validated with the experimental investigations. Both parametric and non-parametric models predict the behaviour, which is having good agreement with experimental results.

Different mathematical models such as quarter car model (2 DOF), half car model (4 DOF) and full car model (7 DOF) of the vehicle with passive and semi-active suspension systems are formulated. Newly developed non-parametric model of MR damper is used in vehicle model as semi-active suspension system with suitable control strategy. Ride comfort and road holding performances of passive and semi-active suspension systems are found under average random road profile as input. In comparison, the vehicle with MR based suspension system provides better vibration isolation for a vehicle than passive suspension system.

Key words: - MR damper, Non-parametric model, Random road profile, Road bump, Semi-active suspension, Quarter car model, Half car model, Full car model.

CONTENTS

	Page No.
Declaration	
Certificate	
Acknowledgements	
Abstract	
List of contents	i
List of figures	v
List of tables	ix
Abbreviations	x
1. INTRODUCTION	1
1.1. INTRODUCTION	1
1.1.1. Ride comfort	1
1.1.2. Road holding	2
1.1.3. Handling	2
1.2. TYPES OF SUSPENSION SYSTEM	2
1.2.1. Passive suspension system	2
1.2.2. Active suspension system	3
1.2.3. Semi-active suspension system	4
1.3. MAGNETO RHEOLOGICAL (MR) FLUID	6
1.4. MAGNETO RHEOLOGICAL FLUID DAMPER	9
1.4.1. Types of MR damper	10
1.4.1.1. Monotube MR damper	10
1.4.1.2. Twin tube MR damper	10
1.4.1.3. Double ended type MR damper	11
1.5. MAGNETO RHEOLOGICAL DAMPER MODELS	12
1.5.1. Parametric modeling	12
1.5.2. Non-parametric model	12
1.5.2.1. Magnetostatic analysis	13
1.5.3. Vehicle model	13

1.6. ORGANIZATION OF REPORT	14
2. LITERATURE REVIEW	16
2.1. INTRODUCTION	16
2.2. MAGNETORHEOLOGICAL (MR) FLUID	16
2.2.1. MR fluid brake and MR clutch	18
2.2.2. MR fluid polishing	20
2.2.3. MR fluid damper	20
2.3. DYNAMIC CHARACTERIZATION OF MR DAMPER	22
2.4. OPTIMIZATION OF MR DAMPER	24
2.5. MR DAMPER MODELS	27
2.5.1. Parametric modeling	27
2.5.2. Non-parametric model	34
2.6. ACTIVE VIBRATION CONTROL OF VEHICLES	36
2.7. SEMI-ACTIVE VIBRATION CONTROL OF VEHICLES	38
2.7.1. Quarter car model	38
2.7.2. Half car model	41
2.7.3. Full car model	42
2.8. SCOPE AND OBJECTIVE	43
2.8.1. Objectives	44
2.9. SUMMARY	44
3. METHODOLOGY AND EXPERIMENTAL SETUP	45
3.1. INTRODUCTION	45
3.2. METHODOLOGY	45
3.2.1. Design of MR damper	47
3.2.2. Optimization of MR damper	47
3.2.3. Preparation of MR fluid	47
3.2.4. Evaluation of optimum proportion of MR fluid	48
3.2.5. Dynamic characterization of MR damper	48
3.2.6. Development of nonparametric model of MR damper	48
3.2.7. Ride comfort and road holding analysis of vehicle	48
3.3. EXPERIMENTAL SETUP	49

3.3.1.	APS 420 electro-dynamic shaker	50
3.3.2.	APS-145 power amplifier	50
3.3.3.	Signal Generator	51
3.3.4.	Data acquisition using LabVIEW	52
3.3.4.1.	<i>Displacement transducer (Honeywell-LVDT)</i>	52
3.3.4.2.	<i>Force transducer</i>	53
3.3.4.3.	<i>NI-DAQ system</i>	54
3.3.5.	Software interface	55
3.4.	SUMMARY	55
4.	DESIGN, FABRICATION AND OPTIMIZATION OF ELECTROMAGNETIC CIRCUIT OF MR DAMPER	56
4.1.	INTRODUCTION	56
4.2.	DESIGN OF MR DAMPER	56
4.3.	MAGNETIC FIELD ANALYSIS	61
4.4.	OPTIMIZATION OF MR DAMPER	63
4.4.1.	Finite element modeling of MR damper	66
4.4.1.1.	<i>FEA Assumptions and model details</i>	68
4.4.1.2.	<i>Boundary conditions</i>	68
4.5.	RESULTS AND DISCUSSION	70
4.6.	SUMMARY	74
5.	EVALUATION OF OPTIMAL LEVEL OF PARAMETERS ON THE PERFORMANCE OF MR DAMPER	75
5.1.	INTRODUCTION	75
5.2.	CONSTITUENTS OF MR FLUID	75
5.2.1.	Carrier fluid	77
5.2.2.	Magnetizable and additives material	77
5.3.	MR FLUID PREPARATION	78
5.4.	EXPERIMENTAL ANALYSIS OF MR DAMPER	79
5.5.	TAGUCHI METHOD DESIGN OF EXPERIMENTS	81
5.5.1.	Selection of process parameters and their levels	83
5.5.2.	Orthogonal array	83

5.5.3. Signal-noise ratio analysis	85
5.5.4. Confirmation test	86
5.6. RESULT AND DISCUSSION	86
5.6.1. Experimental results	89
5.7. SUMMARY	91
6. DEVELOPMENT OF NOVEL NON-PARAMETRIC MR DAMPER MODEL	92
6.1. INTRODUCTION	92
6.2. DEVELOPMENT OF NONPARAMETRIC MODELING	92
6.2.1. Magneto-static analysis	94
6.3. DEVELOPMENT OF PARAMETRIC MR MODEL	97
6.3.1. Bouc-Wen MR model	98
6.3.2. Results and discussion	99
6.4. SUMMARY	102
7. VERTICAL DYNAMIC ANALYSIS OF A VEHICLE WITH MRDAMPER	103
7.1. INTRODUCTION	103
7.2. ROAD PROFILE	103
7.2.1. Random road profile model	103
7.2.2. Road bump profile	105
7.2.3. Performance indices	106
7.3. MATHEMATICAL MODELING OF VEHICLE	106
7.3.1. Semi-active control strategy	107
7.3.1.1. <i>Sky-hook control strategy</i>	107
7.3.1.2. <i>Proportional integral derivative control strategy</i>	108
7.3.1.3. <i>Fuzzy logic control strategy</i>	110
7.3.2. Dynamic analysis of quarter car model	112
7.3.2.1. <i>Dynamic response analysis of quarter car model subjected to random road</i>	115
7.3.2.2. <i>Dynamic response analysis of quarter car model subjected to road bump</i>	117

7.3.3. Dynamic analysis of half car model	118
7.3.3.1. <i>Dynamic response analysis of half car model subjected to random road</i>	120
7.3.3.2. <i>Dynamic response analysis of half car model subjected to road bump</i>	123
7.3.4. Dynamic analysis of full car model	124
7.3.4.1. <i>Dynamic response analysis of full car model subjected to random road</i>	129
7.3.4.2. <i>Dynamic response analysis of full car model subjected to road bump</i>	133
7.4. SUMMARY	135
8. CONCLUSIONS	136
8.1. SUMMARY	136
8.2. CONTRIBUTIONS	137
8.3. CONCLUSIONS	137
8.4. SCOPE OF FUTURE WORK	139
Reference	140
Appendix-I	163
Appendix-II	167
Publication list	171

LIST OF FIGURES

Figure No.	Description	Page No.
Figure 1.1	Passive suspension system	3
Figure 1.2	Active suspension system	4
Figure 1.3	Semi-active suspension system	4
Figure 1.4	Variable orifice damper	5
Figure 1.5	MR fluid damper	6
Figure 1.6	Dipole alignments of ferrous particles	7
Figure 1.7	Squeeze mode	8
Figure 1.8	Share mode	9
Figure 1.9	Valve mode	9
Figure 1.10	Mono tube MR damper	11
Figure 1.11	Twin tube MR damper	11
Figure 1.12	Double ended MR damper	11
Figure 1.13	Generalized vehicle model	14
Figure 2.1	MR fluid brake	19
Figure 2.2	MR clutches	19
Figure 2.3	MR polishing device	20
Figure 2.4	MR fluid damper	20
Figure 2.5	MR damper in structural application	21
Figure 2.6	MR damper for vibration reduction in washing machine	21
Figure 2.7	MR damper in prosthetic leg application	21
Figure 2.8	MR damper in tool vibration isolation application	22
Figure 2.9	MR damper suspension for vehicular application	22
Figure 2.10	Bingham model	27
Figure 2.11	Gamota – Filisko model	28
Figure 2.12	Bouc-Wen model	29
Figure 2.13	Modified Bouc-Wen model	30
Figure 2.14	Viscous Dhal model	30
Figure 2.15	Viscoelastic–plastic model	31

Figure 2.16	Stiffness-viscosity-elasto slide model	32
Figure 2.17	Neural network model of MR	35
Figure 2.18	Quarter car model	39
Figure 2.19	Half car model	41
Figure 2.20	Full car model	42
Figure 3.1	Research methodology	46
Figure 3.2	Schematic representation of damper testing machine	49
Figure 3.3	APS 420 electro-dynamic shaker	50
Figure 3.4	APS 145 power amplifier	51
Figure 3.5	Signal generator	52
Figure 3.6	Displacement transducer	53
Figure 3.7	Force transducer	53
Figure 3.8	NI-9234 module	54
Figure 3.9	NI-9215 module	54
Figure 3.10	VI Block diagram for the data acquisition	55
Figure 4.1	Free body diagram of piston	57
Figure 4.2	Schematic representation of twin tube damper	58
Figure 4.3	Electromagnetic circuit structure	60
Figure 4.4	Components of MR damper	61
Figure 4.5	Methodology for optimization of MR damper using FEA	65
Figure 4.6	MR valve of twin tube MR damper	66
Figure 4.7	Finite element model of MR damper	67
Figure 4.8	Mesh FE model of MR damper	67
Figure 4.9	B-H curve of steel	69
Figure 4.10	B-H curve of MR fluid	69
Figure 4.11	Magnetic flux density v/s Current magnitudes	71
Figure 4.12	Magnetic flux density v/s numbers of turns in the coil	71
Figure 4.13	Magnetic flux density v/s Core length of coil	72
Figure 4.14	Magnetic flux density v/s Flange length	72
Figure 4.15	Magnetic flux density v/s Fluid flow gap	73

Figure 4.16	Surface plot of Magnetic flux density v/s fluid flow gap and flange length	73
Figure 5.1	Constituents of MR Fluid	76
Figure 5.2	Preparation of MR fluids	79
Figure 5.3	MR damper test set up	80
Figure 5.4	Detail procedure of Taguchi design of experiment	82
Figure 5.5	S/N ratio v/s variations in parameters	88
Figure 5.6	Force v/s displacement curve	89
Figure 5.7	Variation of stiffness and energy dissipation v/s current	90
Figure 6.1	Detail procedure for development of nonparametric model	93
Figure 6.2	Finite element model of MR damper piston	94
Figure 6.3	Total magnetic flux density in the fluid flow gap	95
Figure 6.4	Bouc-Wen model	98
Figure 6.5	Comparison of experimental and MR models result	101
Figure 7.1	Random road roughness in time domain and its PSD	105
Figure 7.2	Road bump profile	105
Figure 7.3	Sky-hook control strategy	108
Figure 7.4	Control structure for half car model with PID controller	109
Figure 7.5	Control structure for full car model with fuzzy logic controller	110
Figure 7.6	Fuzzy membership functions	112
Figure 7.7	Quarter car model with semi-active suspension	113
Figure 7.8	Responses of quarter car model with different control strategies	114
Figure 7.9	Sprung mass acceleration response in time domain and its spectrum	115
Figure 7.10	RMS acceleration of sprung mass v/s velocity	116
Figure 7.11	RMS road holding v/s velocities	116
Figure 7.12	Acceleration of vehicle body under road bump	117
Figure 7.13	Half car model of vehicle	118

Figure 7.14	Half car sprung mass acceleration in time domain	121
Figure 7.15	Half car pitch rate in time domain	121
Figure 7.16	Vertical acceleration of Sprung mass	122
Figure 7.17	Pitch acceleration of Sprung mass	122
Figure 7.18	Road holding of front wheel	123
Figure 7.19	Road holding of rear wheel	123
Figure 7.20	Acceleration of vehicle body under road bump	124
Figure 7.21	Pitch angle of vehicle body under road bump	124
Figure 7.22	Full car semi-active suspension system	125
Figure 7.23	Acceleration of sprung mass in time domain	129
Figure 7.24	Full car roll rate in time domain	129
Figure 7.25	Full car pitch rate in time domain	130
Figure 7.26	RMS acceleration of sprung mass v/s velocity	130
Figure 7.27	RMS acceleration of roll rate v/s velocity	131
Figure 7.28	RMS acceleration of pitch rate v/s velocity	131
Figure 7.29	Road holding of front left wheel	132
Figure 7.30	Road holding of front right wheel	132
Figure 7.31	Road holding of rear right wheel	133
Figure 7.32	Road holding of rear left wheel	133
Figure 7.33	Acceleration of vehicle body under road bump	134
Figure 7.34	Roll angle of vehicle body under road bump	134

LIST OF TABLES

Table No.	Descriptions	Page No.
Table 3.1	Specification of APS 420 shaker	50
Table 3.2	Specification of APS 145 amplifier	51
Table 3.3	Specification of displacement transducer	53
Table 3.4	Specification of force transducer	53
Table 3.5	Specification of NI-9234 and NI-9215	54
Table 4.1	Dimension of twin tube MR damper	60
Table 4.2	Magnetic properties of MR damper	68
Table 4.3	Lower and upper bounds of the parameters	70
Table 4.4	Optimal parameters obtained from FEA	74
Table 5.1	The different properties of carrier fluids	77
Table 5.2	Parameters and their levels	83
Table 5.3	Experimental design layout of L_{25} orthogonal array	84
Table 5.4	Factors assigned to L_{25} orthogonal array and experimental result	87
Table 5.5	Response table of mean S/N ratios for damper force	88
Table 5.6	Equivalent damping at different current value	90
Table 6.1	Categorized data	96
Table 6.2	The optimal parameters of Bouc-Wen MR model	99
Table 7.1	Road roughness detail	104
Table 7.2	Nomenclature and vehicle parameters	107
Table 7.4	Optimal parameter of PID controller	109

ABBREVIATIONS

$\alpha, \delta, \gamma, \beta$ and n	Parameters of parametric models
ω / ω_0	Angular Frequency
ϕ	Magnetic flux
μ_0	Magnetic permeability of free space
μ_r	Relative permeability of material
θ	Pitch movement
S/N	Signal-noise (S/N) ratio
η_m	Mean of the S/N ratio
$\bar{\eta}_m$	Mean of the S/N ratio at the optimal level
$\hat{\eta}$	Predicted S/N ratio
n_0	Reference spatial frequency
τ_y	Field-induced stress
A	Cross sectional area magnetic circuit
A_p	Area of piston
A_r	Area of piston rod
a	Amplitude of the bump
a_1	Location of center of gravity from front axle
a_2	Location of center of gravity from rear axle
B	Magnetic flux density
B_g	Magnetic flux density in the fluid flow gap
$B_{g,r}$	Reference magnetic flux density
b_1	Distance between left wheels and Center of Gravity
b_2	Distance between right wheels and Center of Gravity
BNC	Bayonet Neill–Concelman
C_0 and C_1	Damping coefficient in Bouc-Wen model
C_{eq}	Equivalent magnetic field dependent damping coefficient
$C_s, C_{sf}, C_{sr}, C_{s1}, C_{s2}, C_{s3}$ and C_{s4}	Suspension damping coefficient

$C_t, C_{tf}, C_{tr}, C_{t1}, C_{t2}, C_{t3}$ and C_{t4}	Tyre damping coefficient
C_v	Viscous damping coefficient
D	Dynamic range
DAQ	Data acquisition
EHM	Elementary hysteresis model
ER	Electro-rheological
f_0	Accumulator force
F_d	Damper force
F_f	Friction force
F_η	Fluid viscosity force
F_e	Experimental force
F_p	Bouc-Wen model Predicted force
f_c	Friction force
F_{ve}	Viscoplastic force
$F(x)$	Fitness function
F_{Max} and F_{min}	Maximum and minimum damper force
F_τ	Controllable force due to the field-induced stress
FEA	Finite element analysis
FEM	Finite element method
FEMM	Finite element method magnetics
FNN	Feed forward neural network
$G_q(\Omega_0)$	Random road roughness coefficient
g	Clearance between piston and inner cylinder
GA	Genetic algorithm
H	Magnetic field intensity
h	Radial distance from piston rod to coil width
I	Applied current
I_x	Roll Axis Moment of Inertia
I_y	Pitch Axis Moment of Inertia
J	Current density

K_0 and K_l	Stiffness in Bouc-Wen model
K_{eff}	Effective field dependent stiffness
K_s , K_{sf} and K_{sr}	Suspension Stiffness
K_t , K_{tf} and K_{tr}	Tire stiffness
L	Flange length
l	Distance between poles
LVDT	Linear variable differential transducer
LQG	linear quadratic Gaussian
LQR	Linear quadratic regulator
MR	Magneto rheological
M_s	Sprung mass
M_u , M_{uf} , M_{ur} , M_{u1} , M_{u2} , M_{u3} and M_{u4}	Unsprung mass
n	Number of observation
N	Number of turns
NI	National Instruments
P_0	Initial pressure of gas chamber
P_{x_i}	Exterior penalty function for the design variable
P	population
P_c	Compression chamber pressure
P_E	Extension chamber pressure
P_R	Reservoir pressure
PID	Proportional integral derivative
q	Number of process parameters
R	Equivalent inertial mass
R_c	Cylinder reluctance
R_{core}	Magnetic core reluctance
R_g	Annular flow path reluctance
R_m	Total reluctance of the magnetic circuit
R_y	Yoke reluctance
S_j	Search parameter

s_y^2	Variance of the observed data
SVES	Stiffness-viscosity-elasto slide
t_1	Thickness of inner cylinder
t_2	Thickness of outer cylinder
u	Vehicle forward velocity
V_0	Initial volume of gas chamber
w	Coil width
$w(t)$	White noise signal
w_d	Energy dissipation
x_i	Design variable
y	Observed data
\bar{y}	Average of the observed data
z	Hysteresis variables
$Z_r(t)$ and $Z(t)$	Road profile

CHAPTER-1

INTRODUCTION

1.1. INTRODUCTION

Nowadays, improvements in driving safety and comfort are over lasting subjects in vehicle design. It is not only a need, but also a challenge for automobile engineers to construct “best quality” vehicle. Ride comfort problems arise from vibrations of the vehicle, which may be due to various sources, including road surface irregularities, aerodynamic forces and vibrations of the engine and transmission. These problems could be tackled by designing a proper suspension system.

Vehicle suspension system is responsible for isolating forces from road to the body, for directional control during handling, ride comfort and safety. Good ride comfort requires a soft suspension, whereas a hard suspension is requisite for carrying heavy loads transmitted by the vehicle body. Good handling requires the suspension system to be a via-media between these two criteria (Liu *et al.* (2005)). In order to fulfil these conflicting requirements, a strong demand for good suspension system exists to improve these criteria.

All vehicle suspension systems should be capable of performing the following basic functions

1.1.1. Ride comfort

One of the primary functions of a suspension system is to isolate the forces being transmitted from the road disturbance to the vehicle body in order to provide better ride comfort. The ride quality is associated with vehicle responses to various road disturbances and can be measured by displacement and root mean square (RMS) acceleration of the sprung mass (Eslaminasab *et al.* (2007)).

1.1.2. Road holding

Suspension system is also responsible to keep the tire always in contact with road surfaces to accomplish good road holding of vehicle. The road holding performance can be described by the relative displacement between unsprung (tire) masses and road surface (Prabakar et al., 2013). Contact force between the tires and road surface create friction forces, which prevent the tire from sliding on the road surface.

1.1.3. Handling

The roll and pitch acceleration of a vehicle during cornering, braking and traction are the parameters which describe the good handling performance of vehicle (Rajamani, 2012). Half car and full car models can be used to study the pitch and roll performance of a vehicle.

1.2. Types of suspension systems

The suspension system can be mainly classified into three types, such as

1. Passive suspension system
2. Active suspension system and
3. Semi-active suspension system

1.2.1. Passive suspension system

Passive suspension systems are the most common system, currently used in most vehicles. These systems are composed of simple mechanical elements such as spring and damper with fixed parameters and they do not require any external energy for suppression of vibration. The designer has to decide the spring and damper property according to the design goal and intended applications. A schematic representation of passive suspension system is as shown in Figure 1.1.

An early design for automobile suspension systems focused on optimization of a passive suspension system, which is suitable for only adoptable road condition and its

parameters are generally fixed. It reacts automatically to the loads applied to them at the road surface.

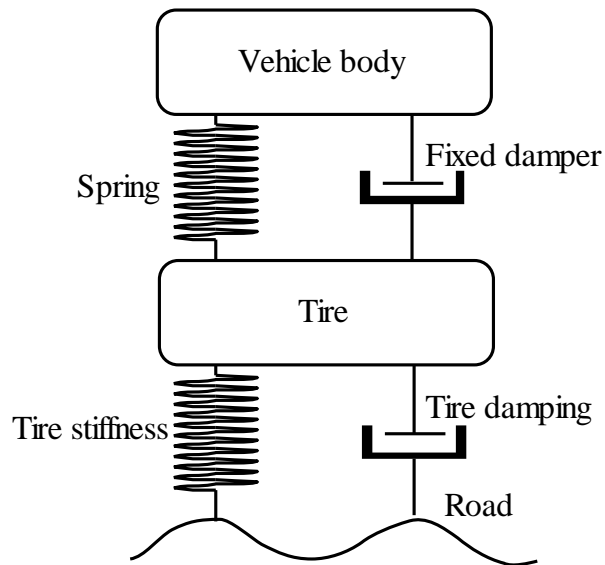


Figure 1.1 Passive suspension system

1.2.2. Active suspension system

Figure 1.2 illustrates schematic representation of active suspension system, in which the reactions to the applied loads are positively supplied by automatically controlled powered actuator. Typically, it consists of a spring, a shock absorber and a hydraulic actuator at each corner of the vehicle. The role of active suspension system is to improve both ride comfort and road holding by appropriately transmitting and filtering all forces between the body of the vehicle and the road. But active suspension system possesses inherent drawbacks, as it requires large power to activate the actuator. The cost of suspension system will be high, complex in design and difficulties arise while implementation of control hardware.

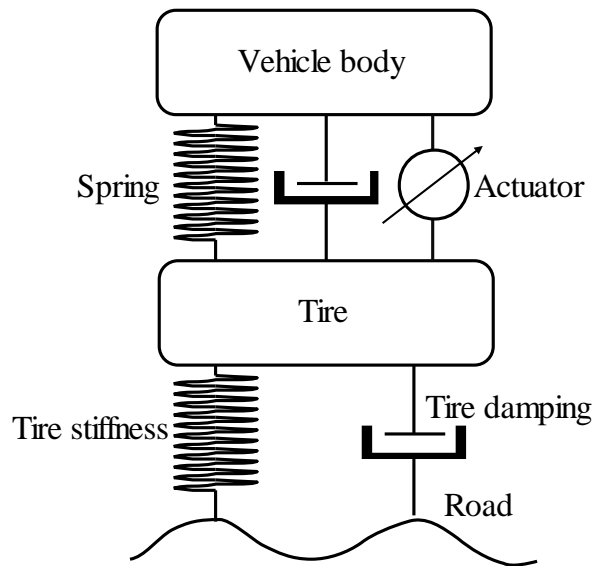


Figure 1.2 Active suspension system

1.2.3. Semi-active suspension system

In a semi-active suspension, the passive damper is replaced with an adjustable damper as shown in Figure 1.3. Semi-active suspension system combines the advantage of the active suspension in terms of improved vehicle performance and the robustness of the passive suspension, without requiring large power source (Harris, (1987)) and the amount of damping can be tuned in real time.

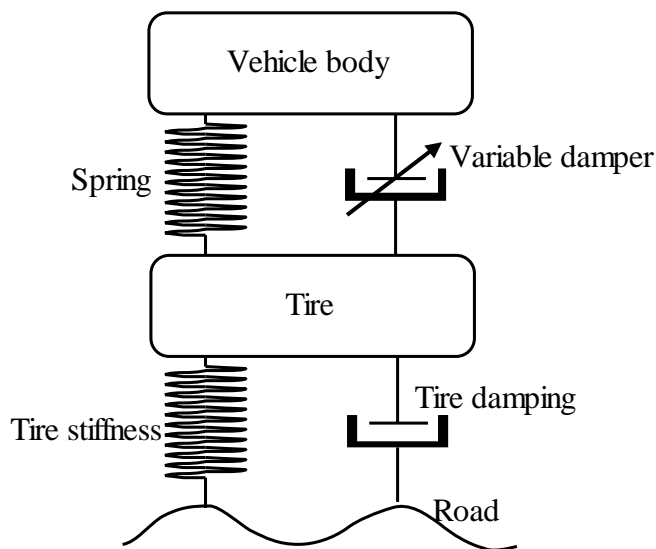


Figure 1.3 Semi-active suspension system

The basic theory of a semi-active suspension is to control the damping level of the suspension. The damping level is controlled by using the controllable damper. In semi-active suspension system, the variable damping can be achieved by two methods such as

1. Variable orifice damper
2. Electro-rheological (ER)/Magneto-rheological (MR) fluid dampers

Figure 1.4 shows the schematic of a variable orifice damper in which orifice diameter can be varied with electronic control. As the piston moves inside the cylinder, it causes fluid flow through the orifice. A larger orifice provides less dissipative resistance, while a smaller orifice provides increased dissipative resistance. The opening of the orifice is determined in real time by feedback control laws. Thus, the damping provided by the device is varied in real time by feedback control.

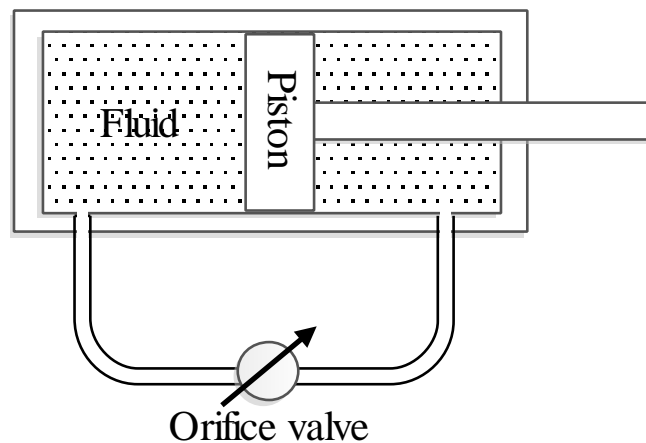


Figure 1.4 Variable orifice damper

In the second method, the viscosity of the oil in the damper (Figure 1.5) is varied in order to achieve the variable damping rate. Electro rheological fluid and magnetorheological fluid are the two fluids, which are most suitable for this application. In electro rheological fluid, the viscosity is varied by changing the electric field, while in magnetorheological fluid, viscosity is varied by changing the magnetic field.

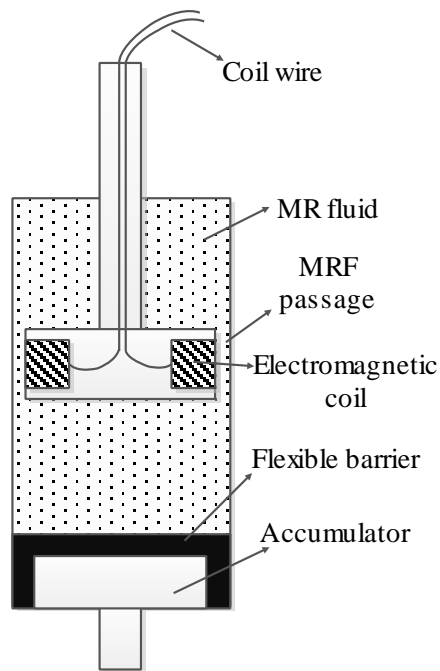


Figure 1.5 MR Fluid damper

1.3. MAGNETO-RHEOLOGICAL (MR) FLUID

Electrorheological (ER) and magnetorheological (MR) dampers are semi-active control devices that use ER or MR fluids to produce controllable damping force. Electrorheological (ER) fluid is composed of polarizable particles such as silica, alumina, zeolites, semiconductors and conducting polymers (Parthasarathy and Klingenberg (1996)) in non-conducting oil. Rheological properties of ER fluid changes rapidly with the application of electric field (Zhao et al. (2000)) and it exhibit yield strength of 2-5 kPa for applied electric field of 3-5 kV/mm. MR fluids are also similar to ER fluid, but MR fluids are 20 to 50 times stronger than ER fluid (Kciuk and Turczyn 2006) and it can be activated from low voltage power supply (less than 10V and 1to 2A). MR fluids are far less sensitive to contamination and extreme in temperature.

A typical magnetorheological (MR) fluid consists of 20-40 percent by volume of relatively pure (3-10 micron diameter size) magnetizable particles, suspended in a carrier liquid such as mineral oil, synthetic oil, water or glycol. Varieties of proprietary additives, similar to those found in commercial lubricants to discourage

gravitational setting and promote particle suspension, are commonly added to MR fluids to enhance lubricity, modify viscosity and inhibit wear.

MR fluids made from iron particles exhibit maximum yield strengths of 50-100 kPa for applied magnetic fields of 150-250 kA/m (Kciuk and Turczyn 2006). MR fluids are not highly sensitive to moisture or other contaminants that might be encountered during manufacture and usage (Milecki, 2001). Further, since magnetic polarization mechanism is unaffected by temperature, the performance of MR-based devices is relatively insensitive to temperature over a broad temperature range (including the range for automotive use).

Figure 1.6 shows the alignment of ferrous particle before and after application of magnetic field. When exposed to a magnetic field, particles in the fluid form chains like structure in the direction of applied magnetic field and the fluid becomes like a semisolid material in a few milliseconds which creates a resistance against the fluid flow. Because of this, the pressure reaction on the MR fluid is called "MR Effect". This effect is completely reversible when the magnetic field is removed (Premalatha et al. 2012).

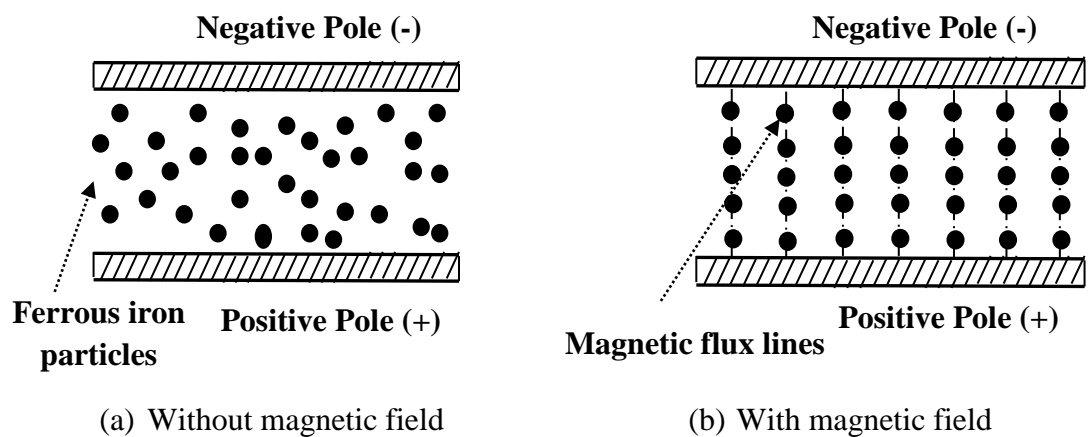


Figure 1.6 Dipole alignments of ferrous particles

MR fluids are used in various applications such as dampers, brakes, clutches, hydraulic valves, seals, flexible fixtures, pneumatic actuators and polishing devices (Wang and Meng, 2001). Based on the different engineering applications the MR fluids can be used in three different operating modes. They are

1. Squeeze mode
2. Shear mode and
3. Valve mode.

In squeeze mode, the fluid is located between a pair of moving poles. Relative displacement is perpendicular to the direction of the fluid flow (Figure 1.7). The compression force applied to the fluid periodically varies. Displacements are small compared to the other modes, but resistive forces are high. This mode is used mainly in bearing applications.

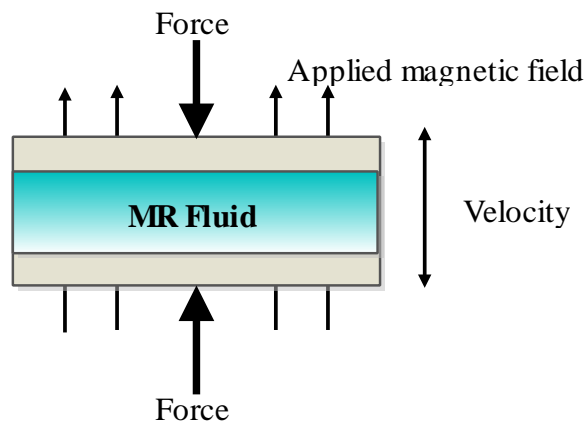


Figure 1.7 Squeeze mode

In shear mode, the fluid is located between a pair of moving poles. Relative displacement is parallel to the poles. The apparent viscosity, and thus the “drag force” applied by the fluid to the moving surfaces can be controlled by modifying the magnetic field between the poles (Figure 1.8). This mode of operation is suitable for clutches, brakes, and locking devices applications.

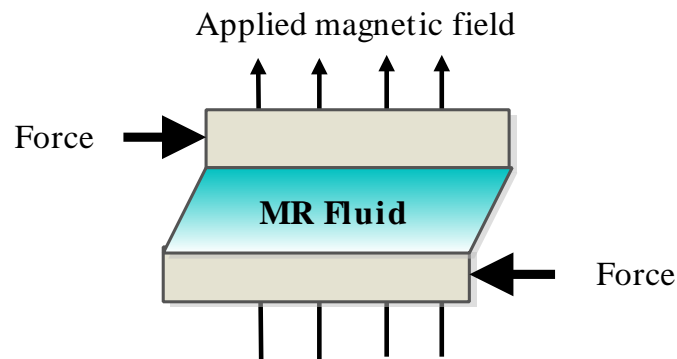


Figure 1.8 Shear mode

In valve mode, the fluid is located between a pair of stationary poles. Resistance to the fluid flow is controlled by modifying the magnetic field between the poles in a direction perpendicular to the flow (Figure 1.9). Devices using this mode of operation include servo-valves, dampers, shock absorbers and actuators applications.

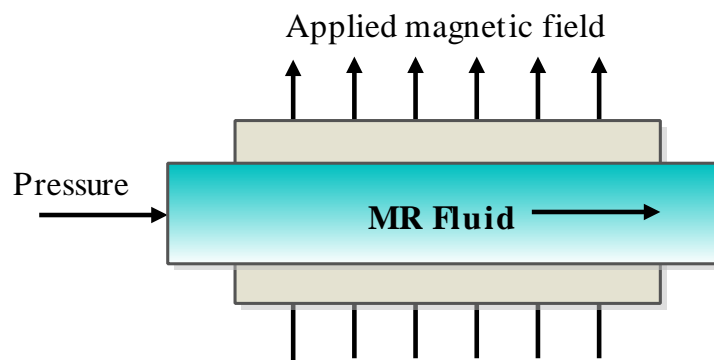


Figure 1.9 Valve mode

1.4. MAGNETO-RHEOLOGICAL (MR) FLUID DAMPER

Magnetorheological damper is a semi-active device filled with magnetorheological fluid. In MR dampers, the damping forces are controlled by the action of magnetic field on the MR fluid. This allows the damping characteristics of the shock absorber to be continuously controlled by varying the magnetic field. Construction of MR damper is quite similar to the conventional hydraulic damper. Along with the regular configuration of the viscous dampers, MR dampers have an iron core with copper

windings fitted to the piston. Leads of the windings are connected to a direct current (dc) source. Because of road undulations, hollow piston head moves inside the cylinder, application of electric current will magnetize the iron core and ferrous particles dispersed in fluid will align themselves along the lines of magnetic flux, which in turn increases the apparent viscosity of the fluid.

1.4.1. Types of MR fluid dampers

MR damper configuration is similar to conventional hydraulic damper and it has additionally an electromagnetic coil in the piston head. MR damper can be classified as

- Mono tube MR damper
- Twin tube MR damper and
- Double ended MR damper

1.4.1.1. Monotube MR Damper

Mono tube MR damper consists of single reservoir for MR fluid and accumulation mechanism to accommodate the volume displaced by piston rod movement. The accumulator piston provides a barrier between MR fluid and compressed gas/compressed spring as shown in Figure 1.10.

1.4.1.2. Twin tube MR damper

Twin tube MR damper (Figure 1.11) consists of two reservoirs namely inner reservoir and outer reservoir. The inner housing guides the piston rod similar to mono tube damper. MR fluid fills the inner reservoir when the piston moves the fluid displaces from inner reservoir to outer reservoir through the base valve provided at the bottom of the inner reservoir. The amount of fluid displaced from the inner reservoir to the outer reservoir is equal to the volume of fluid displaced by the piston rod as it enters the inner housing.

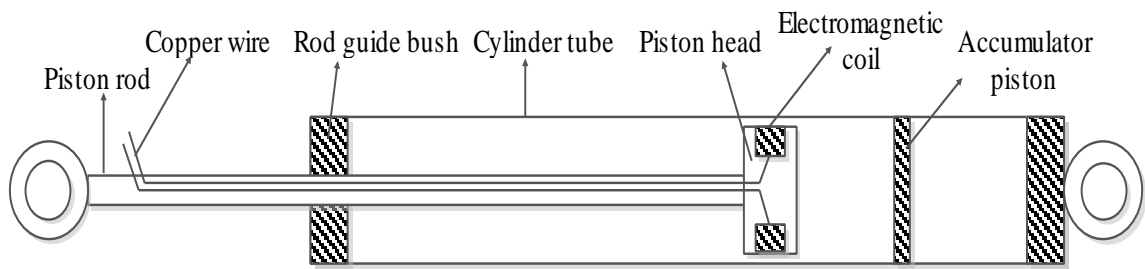


Figure 1.10 Mono tube MR damper

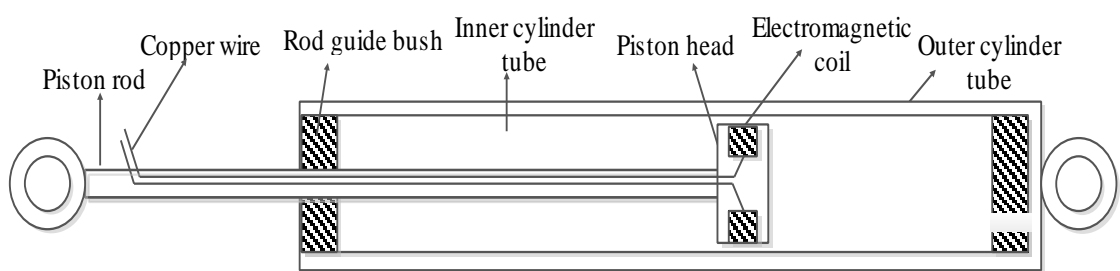


Figure 1.11 Twin tube MR damper

1.4.1.3. Double end type MR damper

Double ended type MR damper consists of a piston rod of equal diameter that extends from both the ends of the damper housing and in this damper, there is no change in volume as the piston moves and it does not require accumulator mechanism as shown in Figure 1.12.

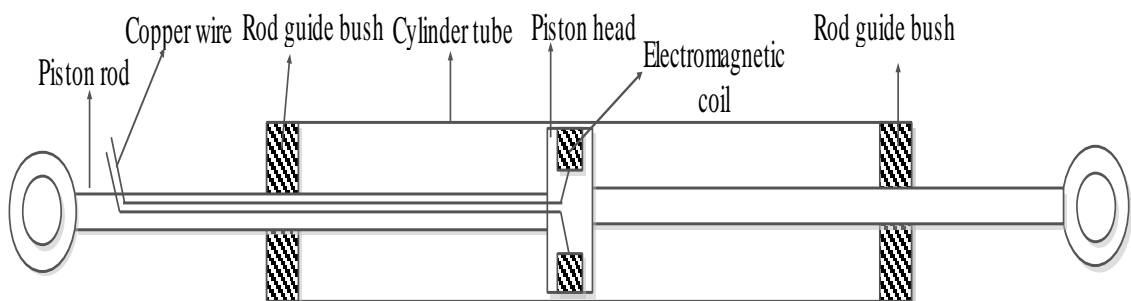


Figure 1.12 Double ended MR damper

1.5. MAGNETO-RHEOLOGICAL DAMPER MODELS

There are two methods of modeling to predict the behavior of the MR damper such as

- Parametric modeling
- Non-parametric modeling

1.5.1. Parametric modeling

In parametric approach, the behaviour of the damper can be predicted by using different phenomenological models. Basically, these models consist of arrangements of mechanical elements such as springs and dashpots to simulate the device behaviour. The parameters of these elements are determined by fitting experimental results by using optimization technique. The different parametric models used to predict the damper behaviour are as follows

- Bingham model
- Gamota and Filisko
- Bouc-Wen model
- Modified Bouc-Wen model
- Viscous Dhal model
- Viscoelastic–plastic model
- Stiffness-viscosity-elasto slide model

1.5.2. Non-parametric modeling

In non-parametric approach, the behavior of the damper can be described by combining the analytical expression (Wereley et al. (1998)) that try to give close results to the actual scenario. The advantage of the non-parametric modelling methods is that, they can avoid the pitfalls of parametric approaches while being robust and applicable to linear, non-linear and hysteresis system (Ehrgott and Masri, 1992; Gangrou Peng, 2011). Non-parametric models can be classified as, (Sims and Stanway (2007))

- Interpolation techniques
 - Simple polynomial model (Choi et al (2001))
 - Non-parametric linearized data modeling
 - Restoring force surface techniques (e.g. Chebyshev polynomial interpolation)
- Neural-based methods:
 - Neural networks (Wang and Liao (2005))
 - Adaptive neuro-fuzzy inference system

Non parametric modelling involves the following steps.

- Evaluation of the experimental force characteristic of MR damper
- Combining of differential and continuous data that captures the various trends in the experimental data
- Using various mathematical techniques, finding the coefficient of the equations (polynomial curve fitting method)

1.5.2.1. Magnetostatic analysis

Magnetostatic analysis is used to evaluate the magnetic field and its related quantities such as magnetic flux density, field intensity, inductance and flux linkage due to the application of electric current. It is also used to verify the risks of magnetic saturation in the devices, which could limit the performance of the devices. In the present study, magnetostatic analysis of MR damper has been conducted in order to evaluate the magnetic field induced in the fluid flow gap by using finite element analysis (FEA). Based on this result, non-parametric MR model has been developed by adopting fifth order polynomial function.

1.5.3. Vehicle model

Figure 1.13 illustrates generalized vehicle model, which consists of vehicle body and tire assembly. Vehicle body mass can be represented by sprung mass and masses of tire-axles represented as unsprung mass respectively. The sprung and unsprung mass is connected by mechanical element such as spring and damper element called

suspension system. The suspension system is used to isolate the vibration being transmitted from the road disturbances to vehicle body in order to provide better ride comfort and road holding to the vehicle when travelling over rough road.

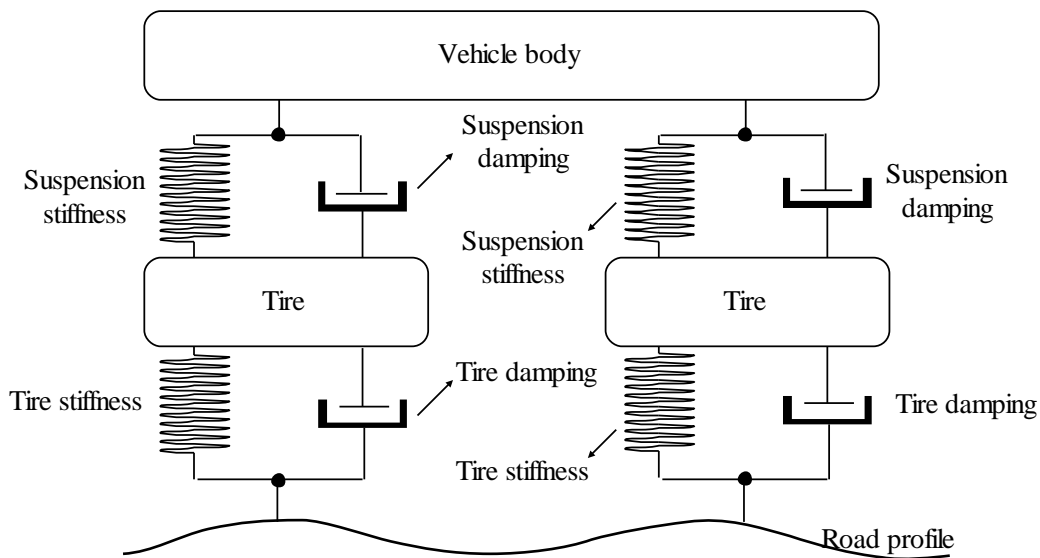


Figure 1.13 Generalized vehicle model

1.6. ORGANIZATION OF THE REPORT

This thesis consists of eight chapters namely Introduction, literature review, methodology and experimental setup, design fabrication and optimization of MR damper, evaluation of optimum level of parameters on the performance of MR damper, development of non-parametric MR damper model, vertical dynamic analysis of vehicle with MR damper, conclusion and future work.

In the first chapter, a brief description of suspension system, MR fluid, working principle of MR fluid, MR damper and mathematical models of MR damper used to predict the behaviour are discussed.

In the second chapter, review of various literature featuring the characterization of MR damper, optimization of MR damper, parametric, non-parametric MR model and semi active control for MR damper are discussed.

Detailed research methodology involved in the present research work, design of damper, experimental setup, sensors used in experimentation and data acquisition system are discussed in the third chapter.

Fourth chapter discusses about the variation of magnetic flux density in the fluid flow gap with respect to the various parameters of electromagnetic circuit of an MR damper by using FEA.

In the fifth chapter, the evaluation of optimum parameters such as proportion of MR fluid, operating frequency and applied current on the damper performance using Taguchi design of experiments is discussed. This chapter also presents dynamic behaviour of the MR damper with optimum parameters obtained from the Taguchi experiments.

In the sixth chapter, development of novel non-parametric MR model based on the magnetic flux density induced in fluid flow gap and Bouc-Wen MR model has been presented and validated with experimental results.

The vertical dynamic behaviour of a passive and semi-active quarter car, half car and full car model have been discussed in seventh chapter. In semi-active suspension system, developed non-parametric MR model has been considered as suspension element.

The important conclusions of the investigation, main contribution, scope for future work have been discussed in eighth chapter. This chapter is followed by references, where details regarding research papers and journals used for investigation are mentioned.

CHAPTER-2

LITERATURE REVIEW

2.1. INTRODUCTION

Previous chapter presented an overview of the vehicle suspension system, MR fluid and its working principle, MR damper and different mathematical formulations of MR dampers to predict behaviour of the MR damper. This chapter discusses the state of art related to experimental study of the MR fluid and damper, optimization of the MR damper, development of parametric and non-parametric modelling of the MR damper used to predict the damper behaviour, active and semi-active vibration control of vehicle suspension system.

2.2. MAGNETORHEOLOGICAL (MR) FLUID

Magnetorheological fluid consists of micron sized magnetically permeable particles dispersed throughout the non-magnetic carrier fluid (Sarkar and Hirani, 2013). When MR fluid is exposed to the external magnetic field, the fluid transforms from a free flowing liquid state to a solid state, because the dispersed magnetic particles attract each other to form fibril structures aligning along the applied magnetic field direction, consequently inhibiting the fluid flow. This makes a change of rheological properties of the MR fluids such as an improvement of yield stress, shear viscosity and storage modulus with external magnetic field strength (Hong et al., 2009). Grunwald and Olabi (2008) presented a state of the art actuator with a control arrangement based on magnetorheological fluid technology and they also reported that magneto rheological fluid technology has excellent features such as fast response, simple interface between input and output and a good controllability. Bossis et al. (2002) analyzed the basic phenomena between the interparticle magnetic forces and hydrodynamic forces. They also reported, analytical prediction for yield stress, rheology with hysteresis and shear

induced phase separation. Kuzhir et al. (2003) conducted experimental and theoretical analysis on flow of MR fluid in the different types of porous media. Kim and Park (2005) analyzed the effect of magnetic field on MR fluid at high frequency range (50-100 Hz) for smart structure applications. They also carried out investigations on effect of magnetic field, when applied in parallel and orthogonal to wave propagation direction.

Jolly et al. (1998) conducted comparative study of rheological and magnetic properties of different commercially available MR fluid and few of its applications were also reported. Li et al. (2003) studied the rheological properties of MR fluid under large step strain share by using parallel plate rheometer. They also developed a mathematical model based on the principle of time-strain separability to predict the behaviour of MR fluid. Jha and Jain (2009) studied the rheological properties of magnetorheological fluid in homogenous magnetic field applied perpendicular to the fluid flow direction. They used Bingham plastic, Herschel–Bulkley and Casson MR fluid models to predict the rheological behaviour of magnetorheological fluid and validated it with experimental results. Lee et al. (2002) evaluated the performance of MR fluid based on impact damper system using Herschel-Bulkley shear model. The effect of shear thinning and shear thickening has been considered during modeling. Kargulewicz et al. (2012) developed an MR fluid model using the discrete element method. The behavior of the MR fluid can be analyzed by examining the time evolution of the ensemble of particles, inter-particle forces found out by a force-displacement law and trajectories were calculated using Newton's second law. Particle magnetization and magnetic interactions between particles were also studied. Simon et al. (2001) studied the effective magnetic behavior of MR composite and formulated a mathematical model based on homogenization theory.

Hato et al. (2011) prepared a carbonyl iron (CI) based magnetorheological fluids containing three different submicron sized organoclay additives. They have investigated viscoelastic properties and sedimentation. They have studied dispersion stability of prepared MR fluid due to presence of submicron sized organoclay particles. Kciuk et al. (2009) carried out an investigation on MR fluids composed of

carbonyl iron particles and demonstrated the flow behavior under the magnetic field. They also investigated the sedimentation of carbonyl iron particles hindered due to addition of the fumed silica particle (1% with CI amount). Jun et al. (2005) prepared MR fluid with 30% weight of mono-disperse magnetic composite (MMC) particles in silicon oil and evaluated magnetic field response on fluid. Chaudhuri et al. (2006) considered 27.5% weight fraction of ferrous nano-particle for preparing MR fluid and evaluated the rheological parameters of fluid by using gradient based least mean square minimization procedure and genetic algorithm. Wong et al. (2001) examined the size, shape and distribution of iron particle in the MR fluid using scanning electron microscopy (SEM) and measured the surface roughness.

Gong et al. (2005) studied the dynamic visco-elastic property and micro structure of MR elastomer with two different classes of MR constituents. Firstly, they have considered 60% iron particle weight and varied silicon oil percentage from 0%, 10%, 20% and 30%. While in the latter case, they have considered 20% of silicon oil and percentage of iron particle varied from 20 to 70%. Bajkowski and Skalski (2012) demonstrated the mathematical model and visco-elastic analysis of MR fluid under damper operational condition. They considered harmonic function as a displacement function and amplitude kept constant with variable rotational speed. Chooi et al. (2008) described the general expression of yield stress and studied the effect of yield stress of fluid flow through the annuli by utilizing derived general expression. In addition to that, computational fluid dynamic analysis has been carried out to validate the obtained general expression.

MR fluids are used in various applications such as dampers, brakes, clutches, hydraulic valves, seals, flexible fixtures, pneumatic actuators and polishing devices (Wang and Meng, 2001).

2.2.1. MR fluid brake and MR clutch

Both MR brake and MR clutch are operating in share mode. In MR fluid brake (Figure 2.1), MR fluid is located in between stator and rotor, the particles in the MR

fluid get aligned in the form of chain like structure due to the application of magnetic field, which opposes the friction between the rotor and stator (Kumbhar et al., 2015).

In MR clutch (Figure 2.2), torque is transmitted from input shaft to the output shaft by shear stress of the MR fluid. MR fluid is located in the sharing gap provided (Bose et al., 2013) between input and output shaft, MR fluid viscosity changes by magnetic field, which causes transfer of torque from input shaft to the output shaft (Kciuk and Turczyn, 2006).

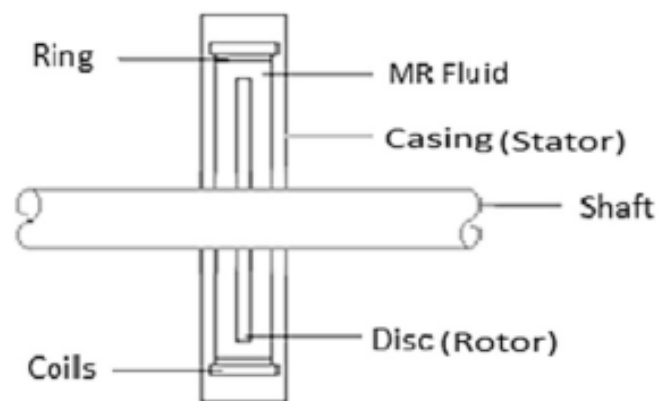


Figure 2.1 MR fluid brake (Courtesy: - Kumbhar et al, 2015)

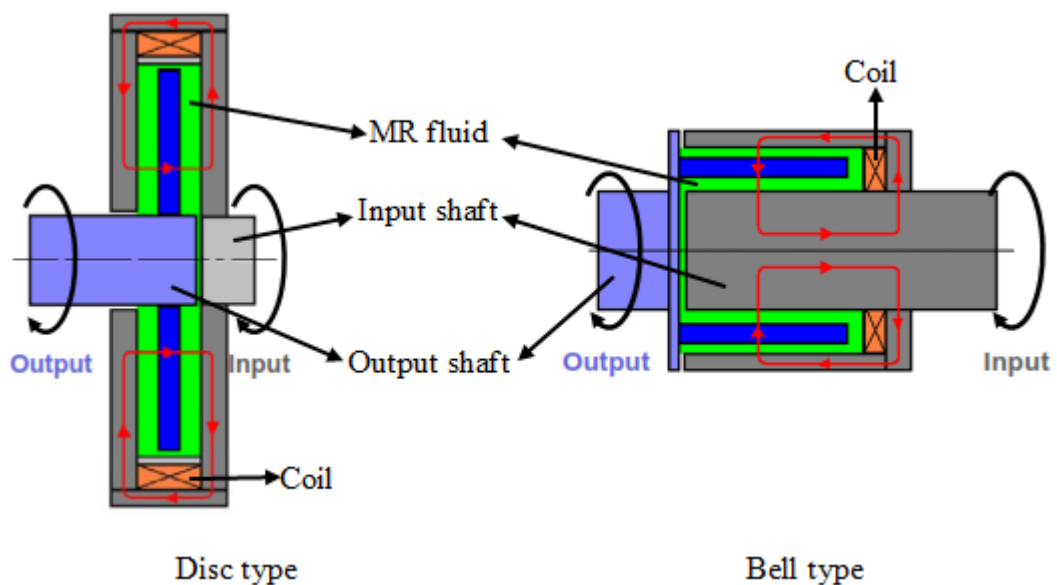


Figure 2.2 MR fluid clutches (Courtesy: - Bose et al., 2013)

2.2.2. MR fluid polishing

In MR fluid polishing, MR fluid acting as abrasive fluid, flows through the predefined converging fluid flow gap provided between working surface and moving wall to polish the materials (Kordonski and Golini, 1999) used mainly for polishing optical glasses, ceramics, plastic and non-magnetic materials (Wang and Meng, 2001).

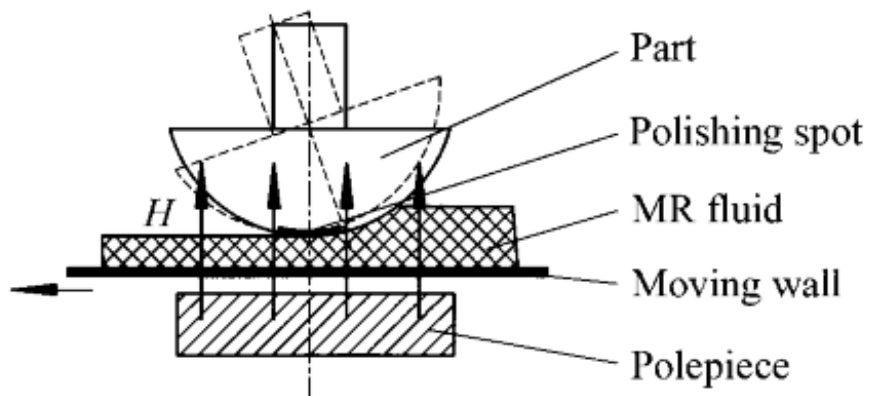


Figure 2.3 MR polishing device (Courtesy: - Kordonski and Golini, 1999)

2.2.3. MR fluid damper

Magnetorheological fluid damper (Figure 2.4) is one of the semi-active device filled with magnetorheological fluid. In MR dampers, the damping forces are controlled by the action of magnetic field on the MR fluid. This allows the damping characteristics of the damper to be continuously controlled by varying the magnetic field (Paul et al., 2015).

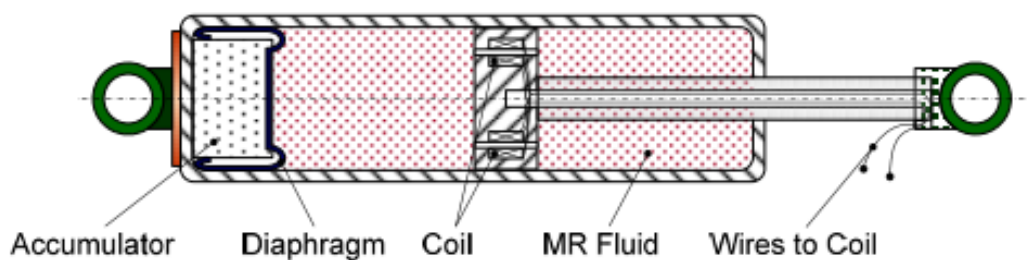


Figure 2.4 MR fluid damper (Courtesy: - Truong and Ahn, 2012)

The applications of MR dampers are found in various fields such as civil structures in earthquake resistant buildings and bridges, vehicles, household applications such as washing machine, prosthetic leg and hard turning machine tool vibration isolation applications. Figures 2.5-2.9 illustrate different application of MR fluid damper.

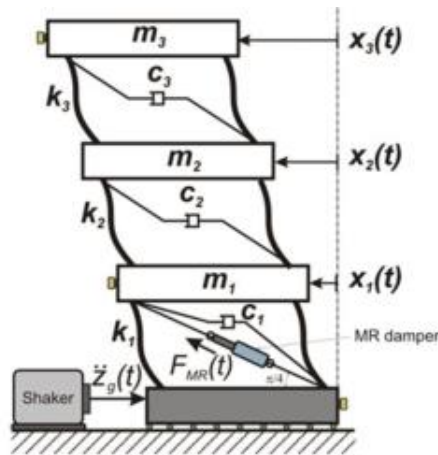


Figure 2.5 MR damper in structural application
(Courtesy: - Enríquez et al., 2015)

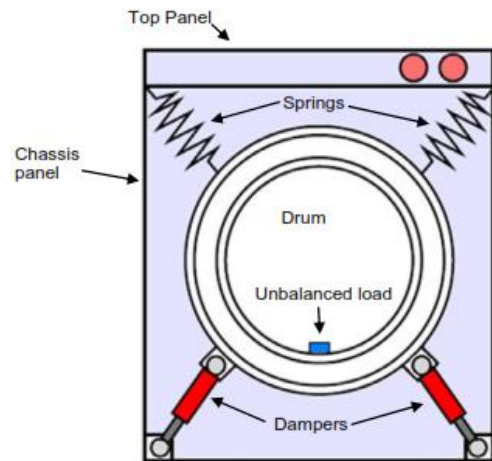


Figure 2.6 MR damper for vibration reduction in washing machine
(Courtesy: - Spelta et al., 2009)

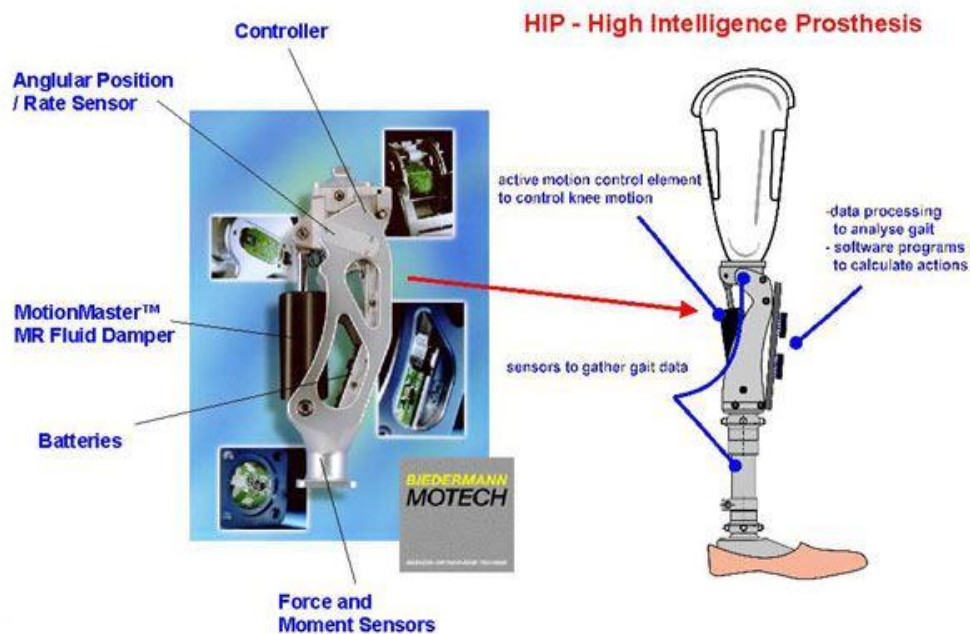


Figure 2.7 MR damper in prosthetic leg application (Courtesy: - Klingenberg, 2001)

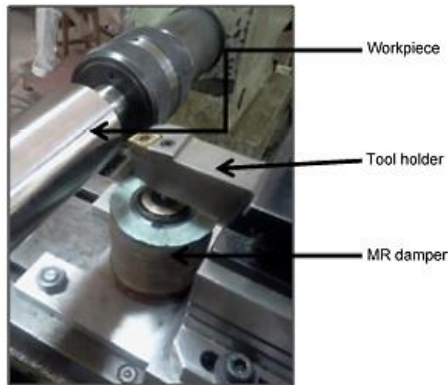


Figure 2.8 MR damper in tool vibration isolation application
(Courtesy: - Paul et al., 2015)

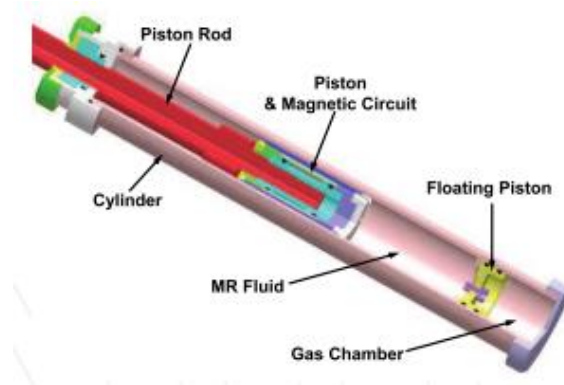


Figure 2.9 MR damper suspension for vehicle application
(Courtesy: - Seong et al., 2011)

2.3. DYNAMIC CHARACTERIZATION OF MR DAMPER

Magnetorheological damper is one of the semi-active devices used to control the vibration of a system with suitable control strategy. In MR damper, the controllable damping force is produced by applying appropriate magnetic field on the MR fluid and variable damping can be achieved in real time.

Gravat (2003) designed and fabricated an MR damper for super-sport motorcycle applications and characterized its performance both experimentally as well as analytically. Ashfak et al. (2011) designed, fabricated and evaluated the performance of MR damper. Ahmadian and Norris (2008) characterize the MR damper under impact and shock loading. They developed drop tower to apply impact load on the MR damper and studied the damper performance by dropping the mass from different heights. Liao and Lai (2002) studied the single degree of freedom (SDOF) system with an MR fluid damper under harmonic excitations. They proposed mathematical model of SDOF with MR damper and validated it with experimental investigations. They also compared results obtained from mathematical model of MR damper with conventional viscous damper. Yang et al. (2002) designed and developed large scale MR damper and proposed two quasi-static models such as axi-symmetric and parallel plate models to predict the hysteresis behaviour of MR damper.

Dutta and Chakraborty (2014) studied the effectiveness of vibration isolation by using nonlinearity in the magnetorheological damper under harmonic excitation. McLaughlin et al. (2014) evaluated the performance of a magnetorheological damper with spiral channel bypass valve under sinusoidal excitation. Esteki et al. (2014) studied dynamic analysis of electrorheological and magnetorheological fluid damper in flow and mix mode configuration under harmonic and random excitation. Avinash et al. (2014) developed the twin tube MR damper and conducted experiments to analyze the damping characteristics of the MR damper under different conditions such as air damping, viscous damping and MR damping. Hu et al. (2015) developed linear variable differential sensor based magnetorheological damper and evaluated its performance under static and dynamic condition. Costa and Branco (2009) conducted experimental and analytical studies of MR damper to evaluate the dynamic performance and also studied the friction force effect between MR fluid and the device wall. Zhang et al. (2008) conducted experimental study of MR damper with two different type of prepared MR fluid by using different carrier fluids with different volume fraction (50%, 60%, 70% and 80%) of fluid. Berasategui et al. (2014) evaluated the power dissipation capacity of MR damper in pre-yield and post-yield damping region under imposed and unrestrained harmonic excitation. Imaduddin et al. (2013) described an overview of recent developments in rotary MR damper in terms of different proposed concepts of structural design, magnetic circuit configuration and modelling techniques. Ali and Ramaswamy (2009) developed two nonlinear model based control algorithms to monitor the magneto-rheological damper voltage required to control the structural vibration.

Kciuk et al. (2010) experimentally investigated the response of a prototype magneto rheological damper at various magnitudes of control current and also analyzed MR damper model employing Finite Element Method (FEM). Kulkarni et al. (2003) studied the performance of designed MR damper with different current, operating frequency and amplitude under squeeze mode, torsional mode and combined mode. Li et al. (2009) developed MR fluid based variable damping and stiffness damper and reviewed its application in vibration isolation. Sahasrabudhe et al. (2005) developed a smart sliding isolation system using controllable MR damper

and its performance has been evaluated analytically as well as experimentally. Kim et al. (2011) estimated the performance of MR damper by using a vehicle. They have measured the dynamic responses of the vehicle both experimentally and numerically by using single-lane change and rapid braking test. Liu et al. (2006) proposed a new configuration of suspension system using two controllable dampers and two constant springs for controlling the variable stiffness. Cronje et al. (2005) developed a variable stiffness and damping vibration MR isolator with a closed-loop displacement and velocity feedback control system. Potter et al. (2011) studied the quasi-active damping method of coupled mechanical and control system design using multiple semi-active dampers. Anakwa et al. (1998) developed a prototype pneumatic active suspension system using a pneumatic actuator for active control of vibration.

2.4. OPTIMIZATION OF MR DAMPER

Force developed in the MR damper is highly influenced by the magnetic flux density induced in the fluid flow gap. In the recent past, optimization of MR damper by considering various geometric parameters, electric parameters and damping force has been conducted by researchers. Gavin et al. (2001) compared electrorheological and magnetorheological fluid devices based on the electrical power requirement and optimized MR damper in order to minimize the electrical power consumption. Parlak et al. (2010) studied the geometrical optimization of MR damper to achieve optimal vibration control by using Taguchi experimental design. The optimal solutions of the MR damper were evaluated using analytical equations. Parlak et al. (2013) carried out geometric optimisation of MR damper using the Taguchi design of experiments. Present work is concentrated on maximising the magnetic flux density at the annular gap of the MR damper and classifying the design variables, which has high influence on the objective function. The optimal damper configurations obtained from this study are fabricated and tested for verification.

Mangal and Ashwin (2015) studied the optimization of geometrical parameters of MR damper to maximize the damper force by using statistical tool (Taguchi design of experiment approach) coupled with the finite element method (FEM). Nguyen et al. (2007) evaluated the optimal geometrical dimensions of MR

valve to improve the valve performance and pressure drop by using golden section algorithm and local quadratic fitting technique through FEM. Nguyen and Choi (2009) determined the optimal level of geometrical parameters such as coil width, flange thickness, piston radius and flow gap of MR shock absorber to minimize the damping force, dynamic range and inductive time constant of the damper by using FEA. Nguyen et al. (2014) optimized the MR damper of front loaded washing machine using finite element analysis in conjunction with golden section algorithm.

Parlak et al. (2012) geometrically optimized the MR damper based on damper force and maximum magnetic flux density as objective function by using goal driven optimization. Tu et al. (2012) designed the damper for an automobile front suspension, wherein magnetic circuit in the piston has been examined by using FEM and properties of the designed damper were determined by conducting experiments. Zhu (2005) conducted experiments on disk type MR damper and performed magnetic field analysis by using FEM. The effect of excitation current in a coil on magnetic flux density induced in the fluid flow gap has been analyzed by both theoretical and experimental studies. Shivaram and Gangadharan (2007) designed a statistical model of MR damper using the design of experiment approach by which various factors such as magnetic field strength, volume fraction of the magnetic particle, shearing gap between piston and cylinder, amplitude and frequency of vibration were considered in their experimentation.

Yazid et al. (2014) conducted studies on MR damper with combination of shear and squeeze mode by using finite element method magnetics (FEMM). Zhou and Zhang (2013) conducted multi-objective optimization of electromagnetic circuit of an MR damper in order to minimize the area of magnetic circuit and enhance the damper force by using finite element method. Javareshkian et al. (2015) analytically investigated the effect of parameters such as number of turns, pole length, gap thickness and spool length in MR damper. They also conducted optimization study of these parameters on minimization of electrical power consumption and improvement of damper force by using response surface method. Goldasz and Sapinski (2011) conducted the magneto-static analysis of MR damper by using FEM and numerical

simulation with two different operation modes (flow and squeeze mode). Sallom and Samad (2011) designed MR valve based on the optimization result, which maximize the magnetic flux density at the valve gap. Yu et al. (2012) studied the optimization of the magnetic circuit in MR dampers by adjusting the fluid flow gap in order to achieve a greater magnetic field strength.

Ferdaus et al. (2014) conducted studies on optimization of MR damper for different configuration of damper piston, MR flow gap and damper housing by using finite element analysis (FEA). Fengchen et al. (2012) conducted finite element analysis of electromagnetic circuit of MR damper to verify the risk of the magnetic saturation of the device. They also carried out experimentation of MR damper and with the help of experimental results, damping force is modeled as a function of current by using cubic polynomial model. Thakkar et al. (2013) conducted electromagnetic analysis of MR damper to identify the saturation limit of supplied current by using FEM. Rosenfield and Wereley (2004) proposed an analytical optimization design method for MR valves and dampers based on the assumption of constant magnetic flux density throughout the magnetic circuit. Parlak and Engin (2012) analyzed the fluid flow through the annular gap by quasi-static analysis and conducted CFD analysis of the MR damper. Paul et al. (2014) used COMSOL software for CFD analysis of the MR damper and compared the results with experimental results. Hu et al. (2015) proposed a double coil MR damper which obtained force and dynamic range though quasi-static model. They also considered seven different configurations of piston head for investigating the performance of double coil damper and obtained optimal parameters.

Nguyen et al. (2009) developed a quasi-static model using Bingham fluid model for the MR valve and demonstrated geometric optimisation of the design parameters to maximise the yield stress damping force. Gudmundsson et al. (2010) evaluated the rheological properties of perfluorinated polyether based MR fluid. They also conducted geometrical optimization study of MR brake to maximize the brake torque. Park et al. (2008) developed an electromechanical brake system using magnetorheological fluid and performed multidisciplinary finite element analysis

which involved magnetostatic, computational fluid dynamics and heat transfer analysis to study the behavior of the system.

2.5. MR DAMPER MODELS

Majority of literature on MR damper mathematical model can be classified into two categories; they are (1) parametric models and (2) Non-parametric models. Both the models are used to predict the hysteresis behavior of MR damper.

2.5.1. Parametric model

In parametric approach, the behaviour of the damper can be predicted by using different phenomenological models such as Bingham model, Bouc-Wen model, modified Bouc-Wen model, viscoelastic-plastic model and stiffness-viscosity-elasto slide model.

Stanway et al. (1987) used Bingham plastic model to predict the dynamic behaviour of the MR damper and it consists of friction and dashpot elements arranged in parallel as shown in Figure 2.10. This model does not exhibit hysteresis behaviour adequately. Mathematically, the force generated by the Bingham model is given by

$$F_d = f_c \text{sgn}(\dot{x}) + c_0(\dot{x}) + f_0 \quad (2.1)$$

Where, c_0 is the damping coefficient, f_c is the frictional force and f_0 is the offset in the force in order to account for nonzero mean observed in the measured force.

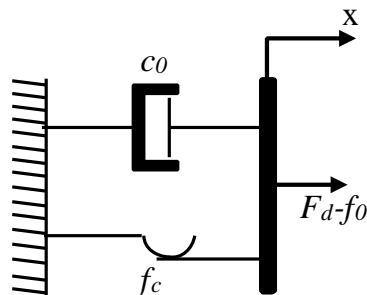


Figure 2.10 Bingham model

Gamota and Filisko (1991) proposed an extended Bingham model (Figure 2.11) to predict the behaviour of the damper in pre-yield and post yield region. The extended Bingham model consists of a set of linear elements connected in series with Bingham model.

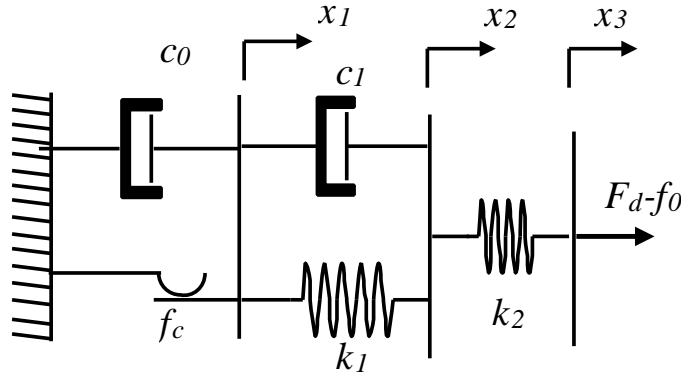


Figure 2.11 Gamota – Filisko model

The force due to Gamota – Filisko model is given by

$$F_d = \begin{cases} k_1 (x_2 - x_1) + c_1(\dot{x}_2 - \dot{x}_1) + f_0 \\ c_0 \dot{x}_1 + f_c \text{sgn}(\dot{x}_1) + f_0 \\ k_2(x_3 - x_2) + f_0 \end{cases} \quad \text{For } |F_d| > f_c \quad (2.2)$$

$$F_d = \begin{cases} k_1 (x_2 - x_1) + c_1(\dot{x}_2 - \dot{x}_1) + f_0 \\ k_2(x_3 - x_2) + f_0 \end{cases} \quad \text{For } |F_d| \leq f_c \quad (2.3)$$

Where, c_0 , f_0 , f_c are the parameters of the Bingham model, k_1 is stiffness, k_2 is the stiffness of the elastic body and c_1 is damping coefficient

Wen (1976) proposed a mathematical model called Bouc-Wen (Figure 2.12) which characterizes the MR damper behavior and it consists of a set of differential equations describing the hysteresis behavior of the MR damper. The damping force developed by Bouc-Wen model is given in the equation (2.4).

$$F_d = c_0 \dot{x} + k_0 x + \alpha z \quad (2.4)$$

Where,

$$\dot{z} = \delta \dot{x} - \beta \dot{x} |z|^n - \gamma z |\dot{x}| |z|^{n-1}$$

Where, F_d is damper force, k_0 is the stiffness, c_0 is the viscous coefficient, α , β , δ , γ and n are the parameters of the Bouc-Wen model that need to be adjusted in order to control shape of the hysteretic curve

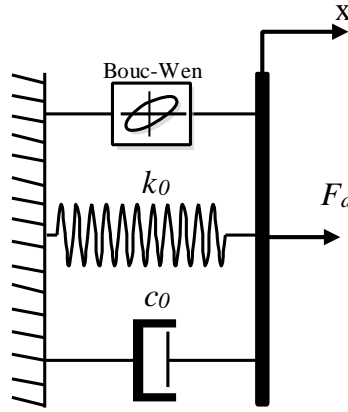


Figure 2.12 Bouc-Wen model

Spencer et al. (1997) reviewed several idealized mechanical models for controllable fluid dampers and also proposed a new model which describes the behavior of a typical MR damper more effectively called modified Bouc-Wen model. The schematic of modified Bouc-Wen model is illustrated in Figure 2.13 and it consists of a linear viscous damper with damping coefficient in series and a spring connected in parallel with a Bouc-Wen model. The damper force developed by the modified Bouc-Wen model is expressed as

$$F_d = c_1 \dot{y} + k_1 (x - x_0) \quad (2.5)$$

Where,

$$\dot{y} = \frac{1}{c_0 + c_1} [\alpha z + c_0 \dot{x} + k_0 (x - y)]$$

$$\dot{z} = \gamma|\dot{x} - \dot{y}|z|z|^{(n-1)} - \beta(\dot{x} - \dot{y})|z|^n + \delta(\dot{x} - \dot{y})$$

In the above equation α , γ , β , δ , k_0 , k_1 , c_0 , c_1 and n are the parameters to be evaluated by optimization technique. The shape of the hysteresis curve can be controlled by parameters α , γ and parameters β , δ is the restoring amplitude, n is the parameter representing the smoothness of transition from elastic to plastic response.

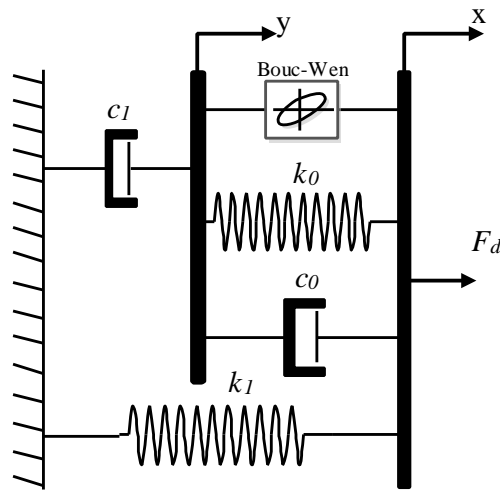


Figure 2.13 Modified Bouc-Wen model

Ikhouane and Dyke (2007) used Viscous Dhal model to predict the dynamic behaviour of the MR damper operating in share mode. The proposed model is validated with experimental results.

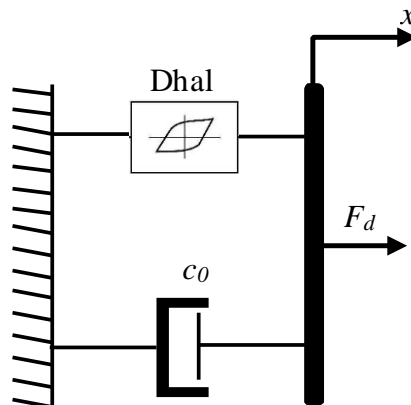


Figure 2.14 Viscous Dhal model

The Viscous Dhal model is given in Figure 2.14 and it consist of first-order nonlinear differential equation,

$$F_d = c_0 \dot{x} + \alpha z \quad (2.6)$$

$$\dot{z} = \rho(\dot{x} - |\dot{x}|z) \quad (2.7)$$

Where, c_0 is the viscous damping coefficient, z is the nondimensional hysteresis variable and α and ρ are the parameters of the Dhal model

Li et al. (2000) studied the effect of excitation amplitude, operating frequency and magnetic field on the damper force and equivalent damping capabilities of MR damper. They also proposed visco-plastic model to predict the hysteresis behaviour of MR damper. In viscoelastic–plastic model, the MR damper operates in rheological domain, namely pre-yield and post-yield as shown in Figure 2.15. According to this model, in the pre yield region, deformations are viscoelastic and in the post yield region, the deformations are viscoplastic.

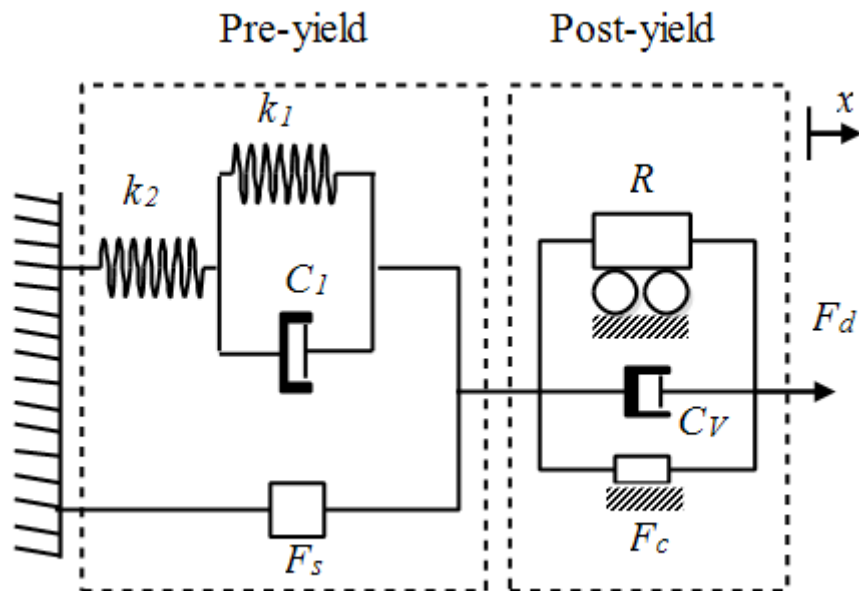


Figure 2.15 Viscoelastic–plastic model

The governing equation given by

$$F_d = F_{ve} + F_s, \quad |F_d| \leq F_c, \text{preyield} \quad (2.8)$$

$$F_d = C_v \dot{x} + R\ddot{x} + F_c \text{sgn}(\dot{x}), \quad |F_d| > F_c, \text{postyield}$$

Where, F_c is the yield force, C_v is the viscous damping coefficient, R is the equivalent inertial mass and F_{ve} is the viscoplastic force determined separately by using viscoplastic theory.

Hu and Wereley (2008) proposed stiffness-viscosity-elasto slide (SVES) model to predict the behaviour of MR damper and compare the results with experimental investigations. The schematic of SVES is illustrated in Figure 2.16. The model consist of linear and nonlinear elements and the force developed from this model is given by

$$F_d = k_1 x + Cx + f_{es} \quad (2.9)$$

Where k_1 is the stiffness, C viscous damping coefficient and f_{es} force due to elasto slide model with sliding displacement of x_s

$$f_{es} = k_2 x_s \quad (2.10)$$

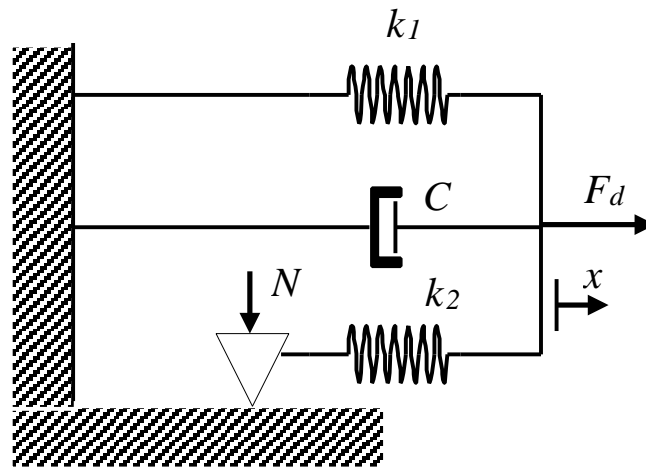


Figure 2.16 Stiffness-viscosity-elasto slide model

Kwok et al. (2007) and Giuclea et al. (2004) conducted experiments on MR damper and they have considered Bouc-Wen model to characterize the MR damper. The parameters of Bouc-Wen model were evaluated by using genetic algorithm and the proposed model was validated with experimental results. Cesmeci and Engin (2010) carried out experimental and theoretical study to predict dynamic behavior of MR damper and the Bingham plastic model is considered for theoretical study. Butz et al. (2002) provided an over-view of properties of electro and magneto-rheological fluids and their applications. They have also discussed various phenomenological models of ER and MR devices. Bodgen and Jacek (2003) analyzed different parametric models such as Bingham model, Bouc-Wen model, Spencer Model, Gornowicz-Filisko model and Li model for modeling MR dampers. They have considered various behavior characteristics such as visco-plastic, visco-elasto-plastic and visco-elastic with a hysteresis. They have chosen different damper parameters based on experimental identifications. Aguirre et al. (2010) studied the parametric identification of a small scale MR damper using the Viscous Dhal model and compared theoretical results with experimental results. They have reported that, both theoretical and experimental results have good agreement. Yao et al. (2002) designed an MR damper working in flow mode and evaluated its performance. They have adopted Bouc-Wen model to characterize MR damper behavior. They have formulated quarter car model with MR damper and also reported comparative study between passive and MR based suspension system. Linder and Wereley (2003) proposed non-linear quasi-steady ER and MR damper model using an idealized Bingham plastic shear flow mechanism for the flow mode of damper operation with leakage effect and validated the results with experimental studies. Wereley and Pang (1998) developed non-linear quasi-steady ER and MR damper models using an idealized Bingham plastic share flow mechanism. Different flow modes like shear mode, flow mode and mixed mode of both models have been considered for analysis.

2.5.2. Non-parametric model

Non-parametric model is also used to predict the behaviour of MR damper and it can be described by combining the analytical expressions that try to give close result to the actual scenario. Non-parametric model can be formulated by using either (1) interpolation technique, or (2) neural based methods. Choi et al. (2001) considered polynomial model to predict the behaviour of ER/MR damper at particular current value and validated results with experimental results. Force developed by this model can be described as

$$F_d = \sum_{i=0}^n a_i v^i \quad (2.11)$$

Where, a_i is the coefficient of polynomial, n is the order of the polynomial and v is the velocity associated with external excitation and in this model force can be evaluated as a function of velocity.

Ehrgott and Masri (1992) presented mathematical model for MR damper based on non-parametric approach, by using two dimensional orthogonal Chebyshev polynomials to estimate the damper force based on the damper velocity and acceleration data. Gavin et al. (1996) also used Chebyshev polynomials model to approximate the MR damper behaviour but they have considered three dimensional orthogonal Chebyshev polynomial function based on the displacement, velocity and electric field strength.

Metered et al. (2010) carried out experimentation to study the dynamic characteristics of an MR damper and used feed forward neural network method to predict the behavior of MR damper and validated the results with experimental findings. Figure 2.17 illustrates multi-layer neural network structure used for prediction of damper force.

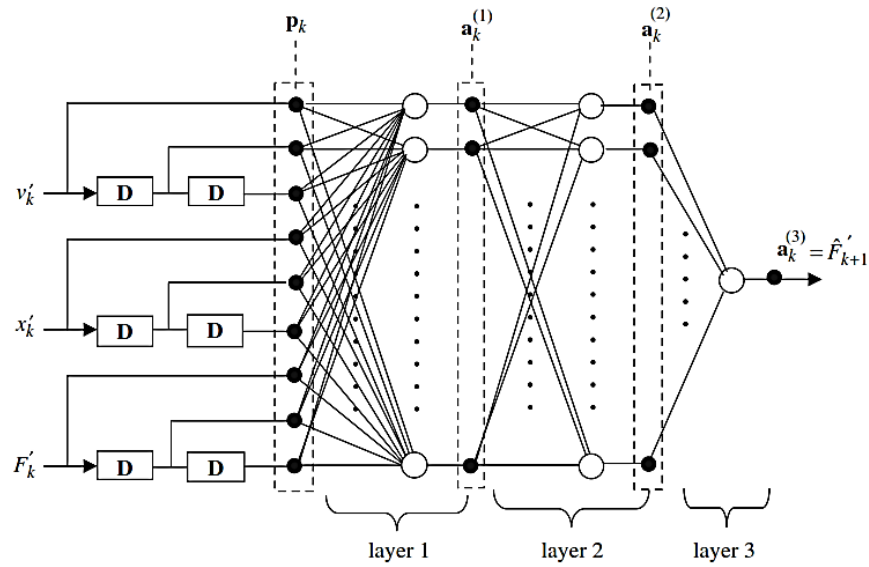


Figure 2.17 Neural network MR damper model (Courtesy: - Metered et al., 2010)

Where P_k is the input for the first layer, $a_k^{(1)}$ is the output of first layer, $a_k^{(2)}$ is the output of second layer and $a_k^{(3)}$ is the output of third layer.

Wang and Liao (2004) proposed both forward and inverse recurrent neural networks model to predict the damper force. In forward model, the damper force is predicted from the applied voltage and in the inverse model, the applied voltage is predicted from the output damper force. Schurter and Roschke (2000) predicted damper force by neuro- fuzzy model based on the behavior of a set of non-linear differential equations of an MR damper. They have adopted the adaptive neuro-fuzzy inference system (ANFIS) to determine the parameters necessary for developing the damper model. Boada et al. (2011) presented dynamic analysis of an MR damper under sinusoidal excitation. They used recursive lazy learning method to predict the response of MR damper. Ekkachai and Nilkhamhang (2012) proposed a novel method to study the hysteresis behavior of MR damper by using elementary hysteresis model (EHM) and feed forward neural network (FNN). Atray and Roschke (2003) designed, developed and characterized the MR damper for controlling the vibration of the railcar. The neuro-fuzzy model based on the displacement, velocity and voltage has been adopted to predict the behaviour of the MR damper. This model predicts the damper force by utilizing 24 fuzzy rules.

Nitin et al. (2013) conducted experiments on prototype MR damper under cyclic excitation and a nonparametric model has been proposed to predict MR damper behavior. Guan et al. (2009) presented finite element analysis and multi objective optimization (genetic algorithm) for MR damper. They have considered fifth order polynomial to relate the shear stress and magnetic flux density. Turnip et al. (2010) investigated the numerical aspect of sensitivity control of an MR damper. They have modelled an MR damper by using nonparametric approach using sixth order polynomial. Song et al. (2005) studied the non-parametric modelling approach to model the MR damper and they used series of continuous and differentiable mathematical functions to represent the characteristics of the physical damper. They have also described force saturation with the help of polynomial function. Spaggiari et al. (2012) conducted experimental study on MR damper at low frequency and polynomial model has been used to predict the behavior of MR damper. Savaresi et al. (2005) conducted experimental study on MR damper and developed a black-box model based on nonlinear autoregressive exogenous (NARX) structure to predict the behaviour of MR damper.

2.6. ACTIVE VIBRATION CONTROL OF VEHICLES

In active suspension system, hydraulic actuator is additionally added to the passive suspension components in which the reactions to the applied loads are positively supplied by automatically controlled powered actuators.

Rao and Prahlad (1997) proposed fuzzy-logic controller for active vibration control of quarter car suspension system in order to enhance ride comfort of the vehicle under pseudo-random road profile. The effective control action can be achieved by tuning the linguistic variable of the fuzzy membership function. Ting et al (1995) developed sliding model fuzzy logic controller to improve the ride comfort and stability of quarter car active suspension system. The fuzzy rules to reduce the vibration of vehicle are constructed by self-tuning method instead of human knowledge.

Eski and Yildirim (2009) designed the neural network based controller to control the vibration of seven degrees of freedom (DOF) active full car model subjected to random road roughness. The neural network control system consists of robust controller and feed forward neural network predictive controller. They have also evaluated the performance of active suspension system by using proportional integral derivative (PID) controller and compared results between them. Priyandoka et al (2009) developed hybrid controller to isolate the vibration of active quarter car suspension system. Hybrid controller comprises of two different controllers such as sky-hook and adaptive neuro active force controller (SANAC). The performances of the active quarter car suspension system with SANAC controller are evaluated experimentally as well as mathematically and results were compared. Amato and Viassolo (2000) developed controller for active suspension system to improve the passenger ride comfort. Control system consists of inner loop and outer loop controller. The inner loop controller reduces the actuator nonlinearity and outer loop controller controls hydraulic actuator to achieve the desirable force to provide better performance. Fateh and Alavi (2009) developed impedance control strategy for controlling the vibration of active suspension system. In this control, an impedance rule prescribes the desired behaviour of the suspension system in the form of second order linear system. Sharkawy (2005) used the adaptive fuzzy control (AFC) and fuzzy logic control (FLC) for active suspension system to provide better ride comfort and road holding qualities. They also evaluated the responses of the active suspension system with linear quadratic regulator (LQR) control and compared the results with passive suspension system. Yeh and Tsao (1994) proposed fuzzy preview controller to control the vibration of active suspension system. In this, control action is achieved by sensing the road irregularities ahead of vehicle and control signal is provided to the actuator to develop required force to isolate the vibration of a vehicle system. Narayanan and Raju (1990) investigated an active suspension system to control the non-stationary response of a single DOF vehicle model with variable velocity over a rough road. They optimized suspension with respect to ride comfort and road handling using stochastic optimal control theory. Alleyne et al. (1993) conducted comparative study between sliding mode and PID controlled active suspensions system by using quarter car model. Campos et al. (1999) designed an active controller

based on the time scale separation and input decoupling transformation to improve the ride quality of four DOF vehicle model. The controller system consists of inner loop and outer loop control. The inner loop control is used to eliminate the terrain disturbance and outer loop is used to stabilize the pitch and heave motion. They used adaptive fuzzy logic controller in eight DOF active suspension system to provide continuous improvement of ride comfort under different traffic conditions. They also tuned different parameters of the fuzzy controller according to different traffic conditions using multi-objective pareto-optimal solution. Huang and Lin (2003) used a quarter car active suspension system to improve ride comfort over passive suspension system. They developed a self-organized fuzzy controller for active suspension system to control the position and acceleration amplitude of the sprung mass. Lin (2009) designed a fuzzy sliding mode controller to control the nonlinear active suspension system in order to improve ride comfort and road holding performance of vehicles.

Active suspension system possesses inherent drawbacks as it requires large power to activate the actuator. The cost of suspension system is high and complex in design, therefore difficulties arise in implementation of control hardware.

2.7. SEMI-ACTIVE VIBRATION CONTROL OF VEHICLES

In semi-active suspension system, passive damper is replaced by adjustable damper and it combines the advantage of the active suspension system in terms of improved vehicle performance and robustness of the passive suspension system, without requiring large power source and the amount of damping can be tuned in real time. In semi-active suspension system, if the control system fails, it works as passive suspension system (Yao et al. (2002)).

2.7.1. Quarter car model

The quarter car suspension system consists of $\frac{1}{4}$ th mass of the vehicle body and single suspension system. The suspension system is connected between sprung mass and

unsprung mass and in quarter car model, only vertical dynamic analysis is considered. The quarter car model is as given in Figure 2.18.

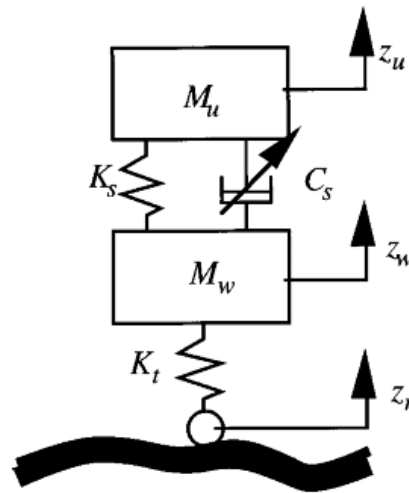


Figure 2.18 Quarter car model (Courtesy: - Nakai et al, 2000)

Where, M_u is sprung mass, M_w is unsprung mass, K_s is spring stiffness, K_t is the tire stiffness and C_s is the suspension damping coefficient.

Rao et al. (2010) conducted the ride comfort analysis of off-road vehicles by replacing the normal passive damper with controllable, two-state, semi-active damper and compared it with passive suspension system. Alexandru and Alexandru (2011) compared passive suspension and active suspension of motor vehicle subjected to road bump. Havelka and Musil (2012) studied the performance of quarter car model under random road condition with non-linear adaptive model of MR damper. Sireteanu and Stoia (2003) optimized the system nonlinear damping characteristics for passive and semi-active suspension with respect to ride comfort criterion. Prabakar et al. (2013) conducted dynamic response analysis of quarter car model with MR damper based suspension system subjected to stationary random road profile. They have considered modified Bouc-Wen MR damper model as a suspension element. Georgiou et al. (2007) found optimum value of suspension stiffness and damping for better ride comfort, suspension travel and road holding of vehicle. Naik et al. (2009) analytically derived the condition for chaotic motion and investigated the chaotic vibration response of single DOF quarter car model.

Holdmann and Holle (1999) studied different control algorithms for a semi-active suspension to improve the driving safety and ride comfort of a vehicle. Lam et al. (2002) proposed a semi active control for quarter car suspension with MR damper. They have used PID controller for system control and also analysed the performance of the quarter car model subjected to road bump as excitation. Jeon et al. (1999) studied the vibration isolation performance of a MR damper with on-off skyhook control strategy. Chen (2009) proposed skyhook surface sliding mode control method to semi-active vehicle suspension system for its ride comfort enhancement. Gopala and Narayanan (2009) reported dynamic response studies of two degree freedom quarter car model with nonlinear passive elements traversing a rough road with sky-hook control strategy. Dutta et al. (2013) evaluated the performance of the sky-hook control strategy in modified Bouc-Wen model of a quarter car model equipped with the MR damper under random and sinusoidal excitation. Ahmadian and Pare (2000) studied different semi-active control strategies such as sky-hook, ground hook and hybrid controller for nonlinear quarter car model. Kurczyk and Pawełczyk (2013) studied semi-active control of suspension of an all-terrain vehicle by using fuzzy control compared with skyhook control. Yoshimura et al. (2001) developed an active suspension system for a quarter car model using the concept of sliding mode control. Balamurugan et al. (2014) conducted experimental study of an MR damper and evaluated the performance of quarter car model by incorporating MR damper with sky-hook sliding mode control strategy. They have considered modified algebraic model as MR damper model. Khiavi et al. (2013) proposed optimal nonlinear control strategy for a semi-active suspension system with MR damper in order to improve the ride quality and stability of the vehicle. Non-parametric (polynomial) model has been used to represent the MR damper in semi-active suspension system.

Yue et al. (1989) applied linear quadratic regulator (LQR) and linear quadratic Gaussian (LQG) controller to a quarter car model. Dong et al. (2010) studied and compared the different semi-active control strategy such as skyhook control, hybrid control, LQG, sliding mode control and the fuzzy logic controllers with the help of quarter car model with MR damper. Agharkakli et al. (2012) studied the quarter car suspension system with LQR control technique under different road conditions and

compared the results with passive suspension system. Du et al. (2005) used H-infinity control strategy for vehicle suspension system of a quarter car model equipped with MR damper. Nugroho et al. (2013) proposed adaptive neuro fuzzy inference system (ANFIS) technique to control quarter car suspension system with MR damper and modified Bouc-Wen model has been used to represent MR damper. They evaluated the performance of the semi-active quarter car suspension system subjected to road bump and compared the results with passive suspension system. Nguyen et al. (2015) developed neuro-fuzzy controller (NFC) based on the ANFIS for controlling the vibration of quarter car suspension system. They also analysed the performance of quarter car suspension with sky-hook control strategy and compared the results between them.

2.7.2. Half car model

In half car model, the pitch and bounce degrees of freedom are studied and it is illustrated in Figure 2.19. Prabakar et al. (2009) studied the optimal preview control of half car model with MR damper under random road excitation, MR damper has been modelled using modified Bouc-Wen model.

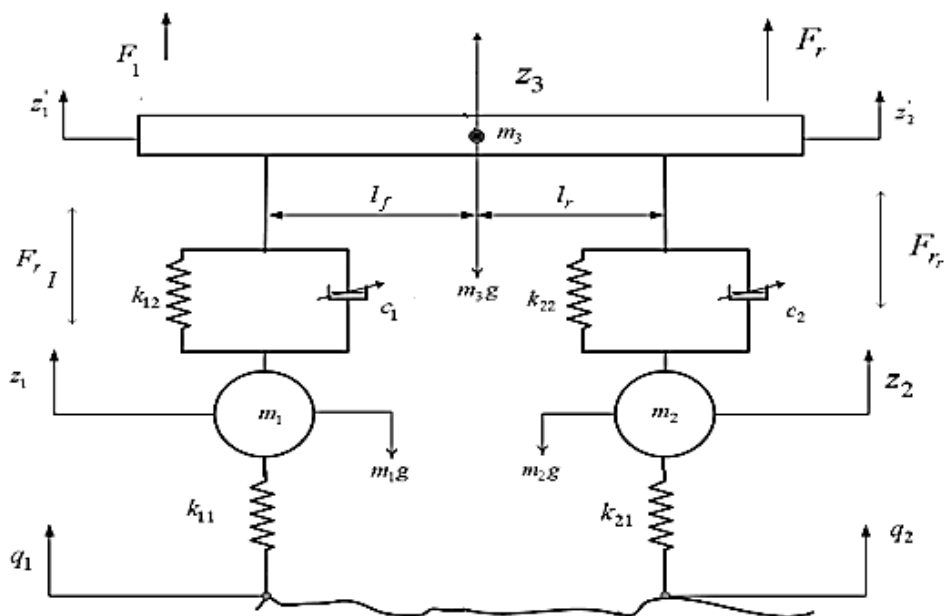


Figure 2.19 Half car model (Courtesy: - Kamalakkannan et al, 2013)

Rossi and Lucente (2004) used H-infinity control strategy to quarter car and half car semi-active suspension system in order to improve the ride comfort and road handling performance. Eltantawie (2012) developed decentralized neuro-fuzzy controller to improve the ride and stability of half car model with MR damper. They evaluated the performance of half car model under two different road conditions (road bump and random road undulations) as inputs. They also compared the obtained results with passive suspension system. Karkoub et al. (2006) conducted analytical study to evaluate the effectiveness of the MR damper in reduction of vibration by using half car model with optimal control strategy. Kasprzyk et al. (2014) evaluated the performance of semi-active half car model with sky-hook and LMS control algorithms and compared the results between them. Hrovat (1993) compared the performances of active and passive suspension systems on quarter, half and full car models using linear quadratic optimal control. Talib et al. (2013) evaluated the performance of the half car active suspension system with self-tuning PID controller under different road conditions.

2.7.3. Full car model

The suspension systems are connected between sprung mass and four unsprung masses. The full car model is as shown in the Figure 2.20.

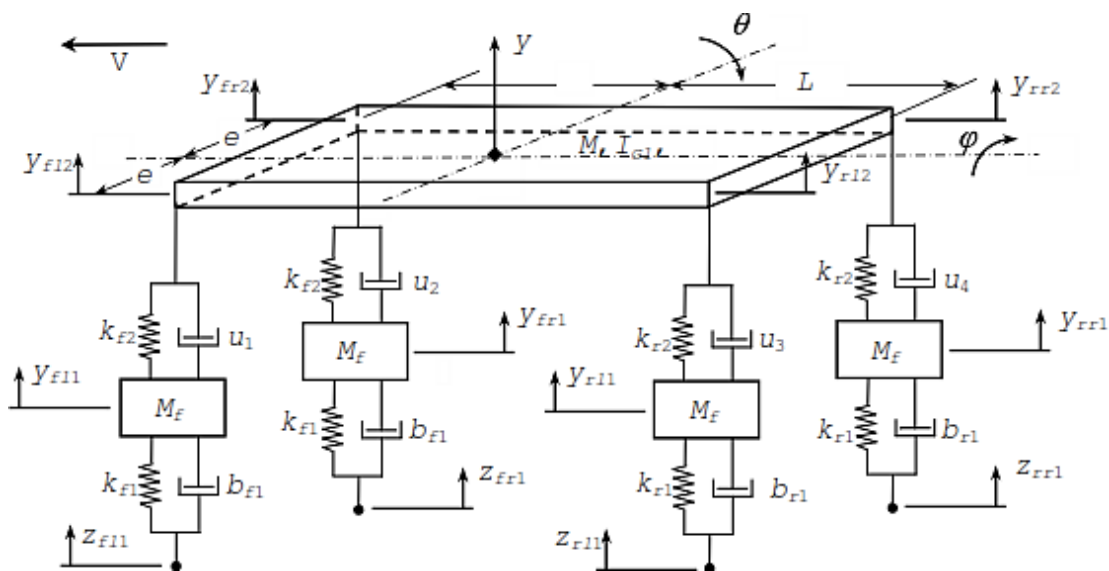


Figure 2.20 Full car model (Courtesy: - Ercan, 2009)

Where, M is sprung mass, M_f is unsprung mass, θ is pitch angle, ϕ is the roll angle, k_{f1} and k_{r1} are tire stiffness, k_{f2} and k_{r2} are the spring stiffness, u_1 , u_2 , u_3 and u_4 are the suspension damping coefficient, b_{f1} , b_{f2} , b_{f3} and b_{f4} are the tire damping coefficient and y_{f11} , y_{r11} , y_{f12} and y_{r12} are the vertical displacement of unsprung and sprung mass.

Guclu (2005) studied the dynamic behavior of eight degrees of freedom full car vehicle model having active suspension system with fuzzy controller. Fang et al. (2011) developed double loop control for full car semi-active suspension system to provide better ride comfort and stability. The double loop controller consists of inner loop control and outer loop control. The inner loop controller isolates the force transmitted from unsprung mass. The outer loop controller stabilizes the sprung mass deflection by linear control. Jahromi and Zabihollah (2010) designed linear quadratic regulator (LQR) and fuzzy logic controller for full car model with MR damper in order to reduce the amplitude of the sprung mass and compared the results with passive suspension system. Paksoy et al. (2014) developed intelligent controllers using self-tuning fuzzy logic controller as a semi-active control strategy in a full car vehicle model with MR damper to reduce the vibration of the vehicle. The performances of full car model with these controllers are evaluated under road bump as input and compared the results between them. Zhang et al. (2013) studied the dynamic behaviour of MR damper based on full car vehicle model with sky-hook control strategy. They have considered modified Bouc-Wen model for representing MR damper.

2.8. SCOPE AND OBJECTIVES

The main scope of the thesis is to investigate the performance of MR damper used as semi-active suspension element in vehicle models to improve ride comfort and road holding performance of vehicle subjected to random road irregularities. Significant research work has been carried out in the field of experimental analysis of MR damper. Based on the experimental work, many mathematical models have been proposed to represent the MR damper analysis. Some of the areas needed to be investigated to improve the performance of the MR damper are given below.

- Better performance of MR damper depends on correct proportions of the MR fluid constituents. Many investigations are still possible for finding optimal proportions of the MR fluid constituents.
- There are many literatures when it comes to modelling of MR damper based on parametric approach, but few researchers have focused on nonparametric approach.
- Comparative study of performance in terms of ride comfort and road holding of a vehicle with conventional passive dampers and a vehicle equipped with MR damper.

2.8.1. Objectives

1. To design and develop a prototype magnetorheological (MR) damper
2. To analyze the variation of magnetic flux density in the fluid flow gap with electromagnetic circuit parameters by using Finite Element Analysis (FEA).
3. To find the optimum proportion of MR fluid constituent on damper performance and to study dynamic behaviour of MR damper with optimum proportion of constituent in MR fluid
4. To develop mathematical model to predict the behaviour of MR damper and to validate with experimentation
5. To develop a mathematical model of the vehicle with MR damper as suspension element and to conduct dynamic response analysis of vehicle subjected to road irregularities.

2.9.SUMMARY

This chapter presented an elaborated review on MR fluid and its application. Literature was basically classified into MR fluid, MR fluid applications, MR damper and its application in vibration isolation, MR damper model, active vibration control and semi-active vibration control in vehicle suspension system.

CHAPTER-3

METHODOLOGY AND EXPERIMENTAL SETUP

3.1. INTRODUCTION

Semi-active control device offers reliability comparable to that of passive device, versatility and adaptability of fully active system, without requiring large power source. In semi-active suspension, the amount of damping can be tuned in real time. The variation of damping may be achieved by introducing solenoid valves (electro-hydraulic dampers), or by the use of fluids which may vary their viscosity, if subject to an electric or magnetic field. MR damper is a semi-active control device that uses MR fluids to produce controllable damping force. This chapter presents detailed research methodology and experimental setup involved in the research work.

3.2. METHODOLOGY

The research work mainly focused on performance evaluation of MR damper for vehicular application. Figure 3.1 illustrates overall research methodology involved in this research work. Initially, design of MR damper was carried out and found the optimum fluid flow gap for the effective performance of MR damper with help of design optimization technique. Different proportions of MR fluids were prepared and the optimum proportion of MR fluid was found by statistical optimization technique. The dynamic behaviour of designed MR damper with optimum proportion of fluid is studied experimentally by using damper testing machine.

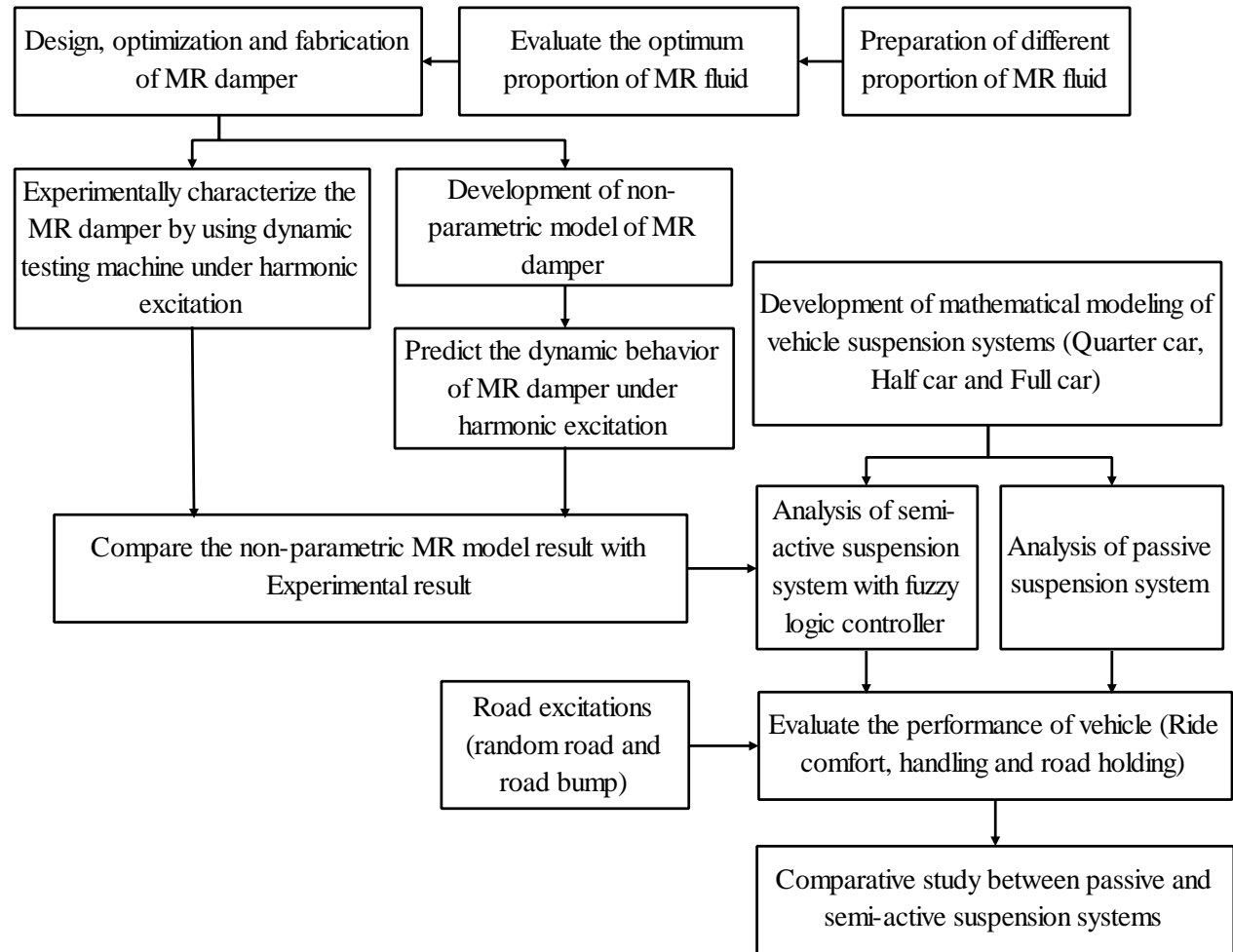


Figure 3.1 Research methodology

Nonparametric model was developed to predict the behaviour of the MR damper and validated with experimental results. Computationally, ride comfort and road holding performance of vehicle was carried out under random road conditions by incorporating developed nonparametric model in semi-active suspension system. Then, the results were compared with passive suspension system.

3.2.1. Design of MR damper

The design of the MR damper is just similar to the conventional hydraulic damper design with necessary modification. In MR damper, the piston having the electromagnetic coil capable of delivering the magnetic field in the fluid flow gap provided around the piston. In MR dampers, the damping forces are controlled by the action of magnetic field on the MR fluid. This allows the damping characteristics of the shock absorber to be continuously controlled by varying the magnetic field. The detail of design of MR damper is described in chapter-4.

3.2.2. Optimization of MR damper

To maximize the effectiveness of the MR damper, controllable force range should be as large as possible, therefore small gap size is required. A small fluid flow gap size will increase the controllable force range, but when the fluid flow gap size is very small, the viscous force increases much faster than the controllable force and the dynamic range decreases. If the gap size is large, both viscous force and controllable forces decrease. Hence optimal fluid flow gap size will be selected to maximize the dynamic range. The design optimization of MR damper is studied in chapter-4.

3.2.3. Preparation of MR fluid

Initially, the silicone oil and grease are taken in a container and stirred continuously until the grease is dissolved completely in the silicon oil, then carbonyl iron particles are added to the mixture of silicon oil and grease.

3.2.4. Evaluation of optimum proportion of MR fluid

Better performance of MR damper depends on precise proportions of the MR fluid constituents. The constituent of MR fluid varies from 20-40% volume fraction of magnetizable particles in carrier fluid based on different applications. Hence, it is necessary to find optimal proportions of MR fluid on damper performance. The procedure involved in finding the optimum proportion of MR fluid is deliberated in chapter-5.

3.2.5. Dynamic characterization of MR damper

MR damper is considered to be a continuously controllable semi-active device, in which variable damping force can be achieved in real time with minimal power consumption. The dynamic behaviour of the MR damper can be studied by using force versus displacement characteristic curve. The energy dissipation of MR damper can be found from the area enclosed under the force versus displacement curve and stiffness can be represented by the slope of the curve for a particular current input, excitation frequency and amplitude. The dynamic behaviour of MR damper is discussed in chapter-5.

3.2.6. Development of nonparametric model of MR damper

Non-parametric approach employs analytical expression to describe the characteristics of modelled device and it is highly useful for studying the linear/nonlinear behavior of a system. The advantage of the non-parametric modelling methods is that, they can avoid the pitfalls of parametric approaches while being robust and applicable to linear system/ nonlinear system/ hysteresis system (Gangrou, 2011). The novel approach for developing nonparametric model is discussed in chapter-6.

3.2.7. Ride comfort and road holding analysis of a vehicle

Mathematical model of a quarter car, half car and full car vehicle model with MR damper was formulated. Dynamic response analysis of the vehicle having MR damper based suspension system with suitable control strategy was carried out under random

road irregularities and road bump as inputs. Comparative study was conducted between passive and semi-active suspension system. Development of mathematical modeling of vehicle is conferred in chapter-7.

3.3. EXPERIMENTAL SETUP

To study the dynamic behavior of MR damper, experimentation was carried out using a custom built damper testing machine. The damper testing machine mainly consists of an electro-dynamic shaker, power amplifier, linear variable differential transducer (LVDT), force transducer and a data acquisition system. The Figure 3.2 shows the schematic representation of the damper testing machine.

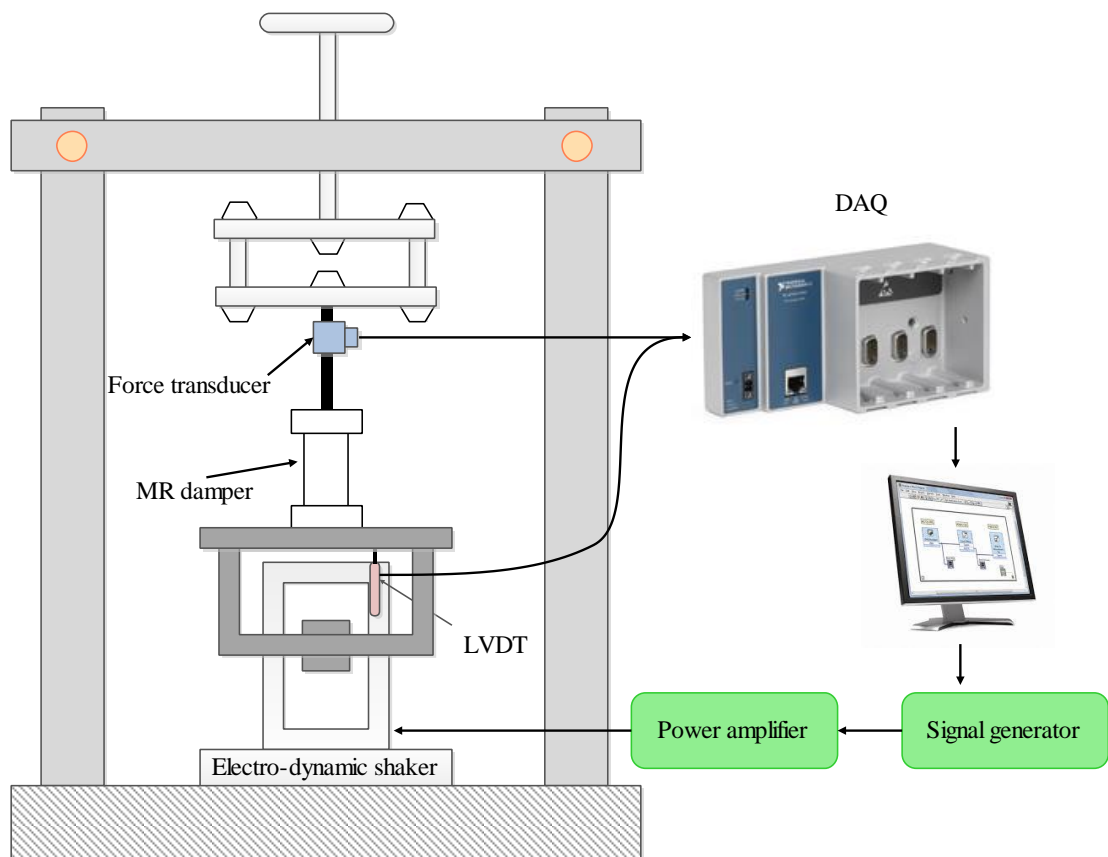


Figure 3.2 Schematic representation of damper testing machine

3.3.1. APS 420 electro-dynamic shaker

The APS 420 ELECTRO-SEIS shaker is a long stroke, electro-dynamic force generator specifically designed to be used alone or in arrays for studying dynamic response characteristics of various structures as shown in Figure 3.3. It is used in modal excitation of complex structures, particularly when low frequencies are required. Furthermore, it can be used for low frequency vibration testing of components and assemblies. Specification of APS 420 shaker is given in Table 3.1.



Figure 3.3 APS 420 electro-dynamic shaker

Table 3.1 Specification of APS 420 shaker

Parameters	Specifications
Force (Sine Peak)	900 N (200 lbf)
Velocity (Sine Peak)	1,000 mm/s (39 inch/s)
Stroke (Peak - Peak)	150 mm (5.9 inch)
Frequency Range	DC ... 200 Hz
Operation	horizontal or vertical
DC Coil Resistance	1.1 ohms

3.3.2. APS-145 power amplifier

The APS-145 dual mode (voltage mode and current mode) power amplifier (Figure 3.4) is specially designed to drive power for electro-dynamic shakers. It can be operated in the voltage mode in order to produce constant velocity. The amplifier has

rated AC output is around 810 VA into 2.5 ohm to exciter or resistive load and it can be used as voltage generator with low output impedance and a flat voltage frequency response or as a current generator with high output impedance and flat current frequency response. Specification of APS 145 amplifier given in Table 3.2.



Figure 3.4 APS 145 power amplifier

Table 3.2 Specification of APS 145 amplifier

Parameters	Specifications
Power Output, Max.	810 VA into a 2.5 Ohm exciter or resistive load, at 25°C, at 1 kHz and nominal mains voltage.
Voltage Output, Max.	45 V RMS, DC ... 15 kHz
Current Output, Max.	4 A DC 15 A RMS > 0.1 Hz, Z = 1.5 Ohm 18 A RMS > 0.1 Hz, Z = 2.5 Ohm – optimal impedance
Frequency Range	0.1 Hz ... 10 kHz full power DC ... 50 kHz small signal voltage (-20 dB)
Input Voltage, Max.	10 V RMS

3.3.3. Signal Generator

The signal generator (Figure 3.5) is a device used to generate different types of electrical wave form over a wide range of frequency. Some of the most common wave forms produced by signal generators are as follows:

- 20 MHz sine and square waveforms
- Ramp, triangle, noise, pulse generation with variable edge, and DC waveforms
- 14-bit, 50 MS/s, 64 K point arbitrary waveforms
- AM, FM, PM, FSK, and PWM Modulation, Linear and logarithmic sweeps and burst all standard



Figure 3.5 Signal generator

3.3.4. Data acquisition using LabVIEW

The data acquisition system (DAQ) consists of hardware unit and an application programming interface. The real time analog signals obtained from the sensor are sent to the hardware unit. The hardware unit performs the conditioning of the signals to increase the signal-to-noise ratio. This conditioned analog signal is sent to data acquisition card which converts analog signal to digital signal and send the data to the computer for further processing.

3.3.4.1. Displacement transducer (Honeywell-LVDT)

The displacement transducer is fixed between the side of the shaker housing and vibrating plate. It is a long stroke displacement transducer used to measure the static and dynamic displacement. Figure 3.6 shows the displacement transducer (LVDT) and specification of the sensor is provided in Table 3.3.

Table 3.3 Specification of displacement transducer (Honeywell-LVDT)

Parameter	Specification
Stroke range	± 1 in
Non-linearity	$\pm 0.25\%$ full scale
Temperature range	-50° C to 125° C
Input supply	1V to 7V

3.3.4.2. Force transducer

Kistler force transducer is used in the experimental setup and it is fitted at the end of the piston rod. Force transducer offers a wide selection of force measurement ranges for compression and tension. Figure 3.7 shows the force transducer and specification of the sensor is provided in Table 3.4.

Table 3.4 Specification of force transducer (KISTLER)

Parameter	VALUE
Measuring direction	Tension/compression
Measuring range	-220 to 220 N
Number of axes	1
Measuring mode	Direct
Operating temperature range	-50 to 120° C



Figure 3.6 Displacement transducer



Figure 3.7 Force transducer

3.3.4.3. NI-DAQ system

The NI-9234 (Figure 3.8) and NI-9215 (Figure 3.9) are the DAQ system used to acquire force and displacement signals. Specifications of NI-9234 and 9215 are given in Table 3.5. The output of force transducer and LVDT are connected to DAQ via Bayonet Neill–Concelman (BNC) cables and from there it is connected to a computer. The acquired signals were analyzed using LabVIEW software from National Instruments (NI).



Figure 3.8 NI-9234 module



Figure 3.9 NI-9215 module

Table 3.5 Specification of NI-9234 and NI-9215

Parameter	Specification	
	NI-9234	NI-9215
Number of channels	4 analog input channels	4 analog input channels
ADC resolution	24 bits	16 bits
Types of ADC	Delta-Sigma	Successive approximation register(SAR)
Sampling mode	Simultaneous Sampling	Simultaneous Sampling
Input voltage	± 5 V	± 10 V

3.3.5. Software interface

A Virtual Instrument (VI) program was developed to acquire and analyze vibration data for these experiments. Figure 3.10 shows the graphical block diagram of the VI program. The acquired data were saved in the preferred location for further analysis.

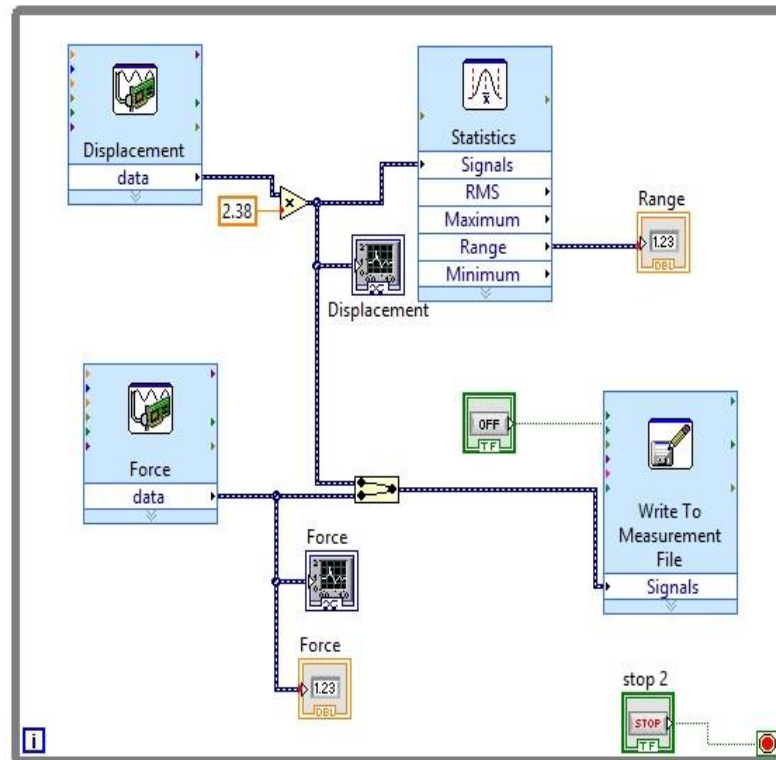


Figure 3.10 VI Block diagram for data acquisition

3.4. SUMMARY

This chapter started with a conceptual overview of research methodology, which includes design of MR damper and experimental set up used for research work. Later sections describe the data acquisition systems and sensors used for the experimentation. In the subsequent chapters, above said methods have been applied to study dynamic behavior of MR damper.

CHAPTER-4

DESIGN, FABRICATION AND OPTIMIZATION STUDY OF MR DAMPER

4.1. INTRODUCTION

The performance of the MR damper significantly depends on the magnetic flux density induced in the fluid flow gap from the electromagnetic circuit incorporated into it and the variation of damper force with variation of magnetic flux density due to applied current. Hence, optimization study has been adopted in this chapter in order to study the variation of magnetic flux density in the fluid flow gap with respect to the various electromagnetic circuit parameters such as current magnitude, number of turns in a coil, coil core length, fluid flow gap and flange length by using finite element analysis (FEA).

4.2. DESIGN OF MR DAMPER

The design of the MR damper has been carried out just similar to the conventional hydraulic damper design with necessary modification. In MR damper, piston having the electromagnetic coil capable of delivering the magnetic field in the fluid flow gap is provided around the piston. Piston made up of magnetic steel material and piston rod with non-magnetic stainless steel having lower permeability is used to avoid flux leakage through the coil. Figure 4.1 illustrates the free-body diagram of the piston and the applied forces due to the damper movement, external force (F_{damper}), generated pressure difference in compression chamber and extension chamber given by the following equation.

$$F_{damper} = F_{compression} - F_{extension} \quad (4.1)$$

$$F_{compression} = P_c A_p \quad (4.2)$$

$$F_{extension} = P_E (A_p - A_r) \quad (4.3)$$

Where, P_c is compression chamber pressure, P_E is extension chamber pressure, A_p is the area of piston and A_r is area of piston rod

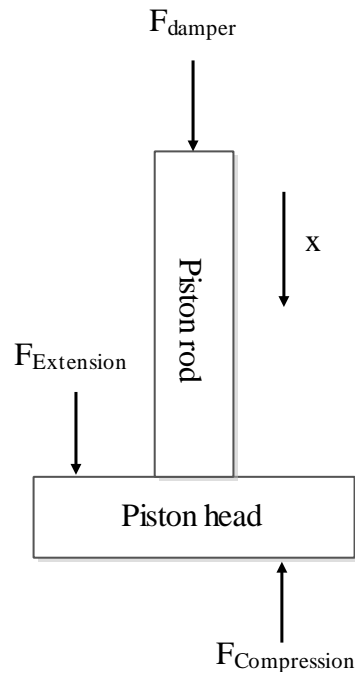


Figure 4.1 Free body diagram of piston

The schematic diagram of twin tube damper is as shown in Figure 4.2. In twin tube damper, there are two different fluid passages. Due to the movement of piston, part of the fluid flows from compression chamber to extension chamber through the flow gap provided around the piston. Part of the fluid flows from compression chamber to the reservoir and this flow compresses the trapped gas in the gas chamber. The pressure in the gas chamber can be calculated as follows

$$P_g = P_0 \left(\frac{V_0}{V_0 + A_r x} \right)^{1.4} \quad (4.4)$$

Where, P_0 is the initial pressure of gas chamber, V_0 is initial volume of gas chamber and x is the piston movement.

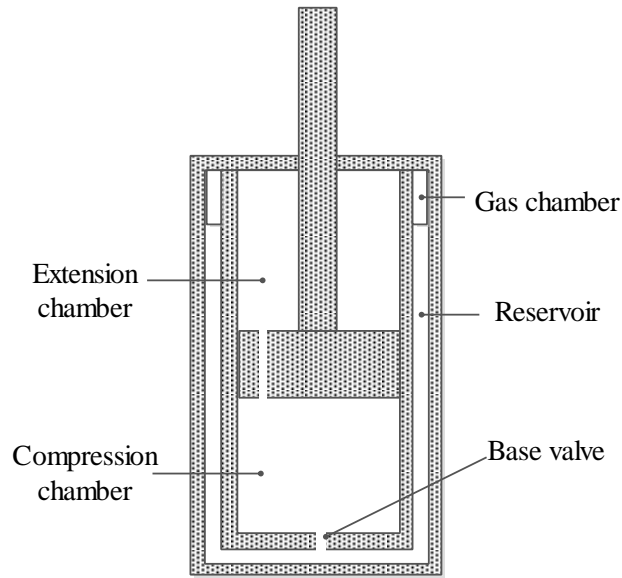


Figure 4.2 Schematic representation of twin tube damper

The pressure exerted by the gas chamber is opposed directly by the fluid pressure in the reservoir. Therefore, the reservoir pressure (P_R) is assumed equal to the gas pressure (P_g).

$$P_R = P_g \quad (4.5)$$

The dynamic range and the controllable force are the two key parameters in the MR damper. The dynamic range is the ratio of controllable force to uncontrollable force, where uncontrollable force includes fluid viscosity force and friction force. To provide a wide control range of the MR damper, a large value of the dynamic range is desired. The dynamic range of MR damper can be described by equation (4.6).

$$D = 1 + \frac{F_\tau}{F_\eta + F_f} \quad (4.6)$$

Where, F_τ is controllable force due to the field-induced stress (τ_y), F_η is fluid viscosity force and F_f is friction force.

$$F_{\tau} = \frac{c\tau_y L A_p}{g} \text{sgn}(v_p) \quad (4.7)$$

$$F_{\eta} = \left(A_p v_p + \frac{w g v_p}{2} \right) \frac{12 \eta L A_p}{w g^3} \quad (4.8)$$

Where, A_p is the area of piston, v_p is the piston velocity, τ_y is the field dependent yield stress, η is the viscosity of fluid and L , w , g are the length, width, gap of the fluid flow channel.

To maximize the effectiveness of the MR damper, controllable force range should be as large as possible, therefore small gap size is required. A small fluid flow gap size will increase the controllable force range, but when the fluid flow gap size is very small, the viscous force increases much faster than the controllable force and the dynamic range D decreases. If the gap size is large, both viscous force and controllable force decreases. Hence optimal fluid flow gap size has been selected to maximize the dynamic range. Exhaustive literature is found on the MR damper optimization of fluid flow gap to get maximum magnetic flux density and these are discussed in chapter-2. In the present study based on past literature, 1.5 mm fluid flow gap has been considered between piston and cylinder of the MR damper (Yao et al. 2002; Sternberg et al. 2014 and Choi et al. 2012) for analysis.

The flow of magnetic field depends upon the magnetic permeability of the material. According to the magnetic Ohm's law, the magnetic potential is given as follows

$$NI = \oint R_m \quad (4.9)$$

$$\oint = B A \quad (4.10)$$

Where, \oint is the magnetic flux, R_m is total reluctance of the magnetic circuit, I is the applied current, N is the number of turns in a coil, B is the magnetic flux density and A is cross sectional area magnetic circuit.

The magnetic circuit of MR damper is as shown in Figure 4.3. The magnetic circuits mainly consist of magnetic core, yoke, cylinder and annular flow path. The total reluctance of the electromagnetic circuit is composed of magnetic core reluctance (R_{core}), yoke reluctance (R_y), cylinder reluctance (R_c) and annular flow path reluctance (R_g).

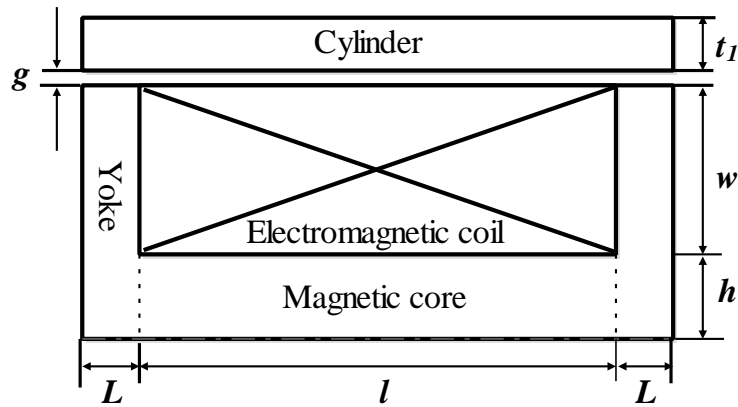


Figure 4.3 Electromagnetic circuit structure

$$R_m = R_{core} + R_y + R_c + R_g \quad (4.11)$$

$$N = \frac{\Phi (R_{core} + R_y + R_c + R_g)}{I} \quad (4.12)$$

The designed dimension of twin tube MR damper is given in the Table 4.1.

Table 4.1 Dimension of twin tube MR damper

Parameters	Dimensions (mm)
Inner diameter of inner cylinder	28
Thickness of inner cylinder (t_1)	5
Inner diameter of the outside cylinder	46
Thickness of outer cylinder (t_2)	9
Distance between poles (l)	21
Flange length (L)	2
Radial distance from piston rod to coil width (h)	7.5
Coil width (w)	5

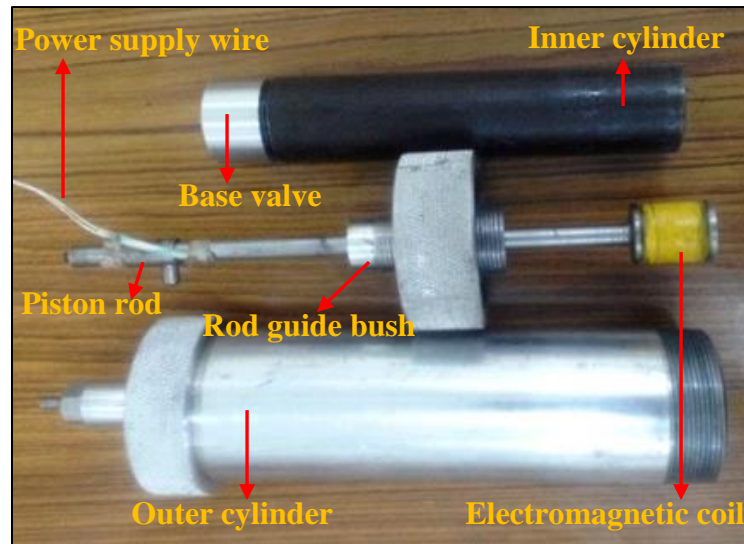


Figure 4.4 Components of MR damper

Figure 1.11 shows the schematic representation of twin tube MR damper. Twin tube MR damper consists of inner cylinder, outer cylinder, piston rod iron core, electromagnetic coil, road guide bush and base valve. The different components of fabricated twin tube MR damper are as shown in Figure 4.4. The base valve is attached at the end of the inner cylinder and it allows the fluid flow from inner cylinder to outer cylinder and from outer to inner cylinder during compression and extension stroke. The electromagnetic coil is wound on the piston head and lead of wire from the coil is passed through the inclined hole in the piston rod, which is just above the iron core and it is taken out through the other hole located at the top end of the piston.

4.3. MAGNETIC FIELD ANALYSIS

The flow of magnetic field depends upon the magnetic permeability of the material. The relative permeability of the MR fluid is little bit higher than air, while magnetic core and inner cylinder block are ferromagnetic media, their relative permeabilities are very high. Therefore, according to the fundamental properties of electromagnetic field theory, the magnetic induction line is almost parallel at the interface between boundaries of air, MR fluid, piston and cylinder block. The magnetic lines of force

leaked outside are little. Ohm's law can be used to analyze the relationship of magnetic flux and magneto-motive force in the circuit (Bakshi, (2009)).

$$\Phi = \frac{NI}{R_m} \quad (4.13)$$

Where, Φ is magnetic flux in a circuit, NI is magneto-motive force of whole magnetic circuit, R_m is magneto-resistive of the whole magnetic circuit ($R_m = \frac{l}{\mu A}$), μ is magnetic permeability and A is cross sectional area of magnetic circuit.

And current density applied to the coil is

$$J = \frac{NI}{A} \quad (4.14)$$

Where, N is number of turns in a coil and I is current through coil.

The purpose of modeling MR fluid based device is to find relation between input electric power (usually the current applied to the coil) and output mechanical power (damping force for MR damper). In order to deal with modeling of MR based devices, firstly the magnetic circuit of the MR based devices should be solved. In general, the magnetic circuit can be analyzed using the magnetic Kirchoff's law as follows

$$\sum Hl = NI \quad (4.15)$$

Where, H is the magnetic field intensity of the circuit and l is the overall effective length.

The magnetic flux conservation rule of the circuit can be stated as

$$\Phi = BA \quad (4.16)$$

Where, Φ magnetic flux of the circuit, A and B are the cross sectional area and magnetic flux density respectively.

At low magnetic field, the magnetic flux density (B) increase in proportion to the magnetic field intensity (H) as follows

$$B = \mu_0\mu_r H \quad (4.17)$$

Where, μ_0 is magnetic permeability of free space ($4\pi 10^{-7}$ Tm/A) and μ_r is the relative permeability of material.

As magnetic field become large, its ability to polarize the magnetic material diminishes and the material is almost magnetically saturated. According to magnetic flux conservation rule of magnetic circuit, the relation between magnetic field intensity in the MR fluid and the applied current can be approximated as (Nguyen et al. (2009)).

$$H_{MR} = \frac{NI}{2g} \quad (4.18)$$

The magnetic flux density developed in the fluid flow gap is given as

$$B = \frac{\mu_0\mu_{MR}NI}{2g} \quad (4.19)$$

Where, g is fluid flow gap and μ_{MR} is relative permeability of MR fluid.

4.4. OPTIMIZATION OF MR DAMPER

For design optimization, a finite element method integrated with an optimization tool is used to obtain optimal geometric dimensions of the MR damper to maximize an objective function (magnetic flux density in the fluid flow gap). In vehicle suspension design, the ride comfort and stability are the two conflicting performance indexes to be considered. In order to avoid the force being transmitted from road surface to the vehicle body, high damping force is required. The damping force produced by an MR damper depends mainly on the magnetic field induced in the fluid flow gap provided in between piston and cylinder (Li et al (2003)).

In the optimization technique, an objective function should be proposed, which is dependent on the purpose of the optimal design and the application of the devices. It is noted that, the objective function is always minimized. Therefore, if the purpose of the optimization is to maximize an objective function of the devices, then

the function should be transformed to equivalent objective function. The equivalent objective function is the function, when it minimized, corresponding performance function is maximized. The objective function is given by

$$OBJ = \alpha_f \frac{B_{g,r}}{B_g} \quad (4.20)$$

Where, α_f is the weight factor, B_g is the magnetic flux density in the fluid flow gap and $B_{g,r}$ reference magnetic flux density.

The reference magnetic flux density is obtained from the FEA analysis of the MR damper at initial values of design parameters. After the preliminary FE analysis for initial value of parameters, the variables to be optimized are constrained. The geometric dimensions of the electromagnetic circuit are varied during the optimization process, so that the mesh size is specified by the number of elements per line rather than element size and the magnetic field intensity is not constant along the pole length. Therefore, it is necessary to define paths along the MR active volume where magnetic flux passes. The average magnetic field intensity across the fluid flow gap is evaluated by integrating the field intensity along the defined path and dividing it by the pole length (w). Thus the magnetic flux density can be calculated by below equation ((Nguyen, (2009))

$$B_{MR} = \frac{\int_0^t B_{MR}(s) ds}{w} \quad (4.21)$$

Where, $B_{MR}(s)$ is the magnetic flux density at each nodal point located on the defined path.

In the analysis, the first order method implemented in the FEA optimization tool is used to find the optimal solution. The procedure to achieve optimal design parameters of the MR damper using the first order method of FEA optimization tool is shown in Figure 4.5. Starting with initial value of design variables, by executing the FE analysis, magnetic flux density is calculated. Then the FEA optimization tool transforms the optimization problem with constrained design variables to unconstrained ones via penalty functions.

$$f(x) = \frac{OBJ}{OBJ_0} + \sum_{i=1}^n P_{x_i}(x_i) \quad (4.22)$$

Where, OBJ_0 is the reference objective function value that is taken from the present group of design set, P_{x_i} is the exterior penalty function for the design variable x_i .

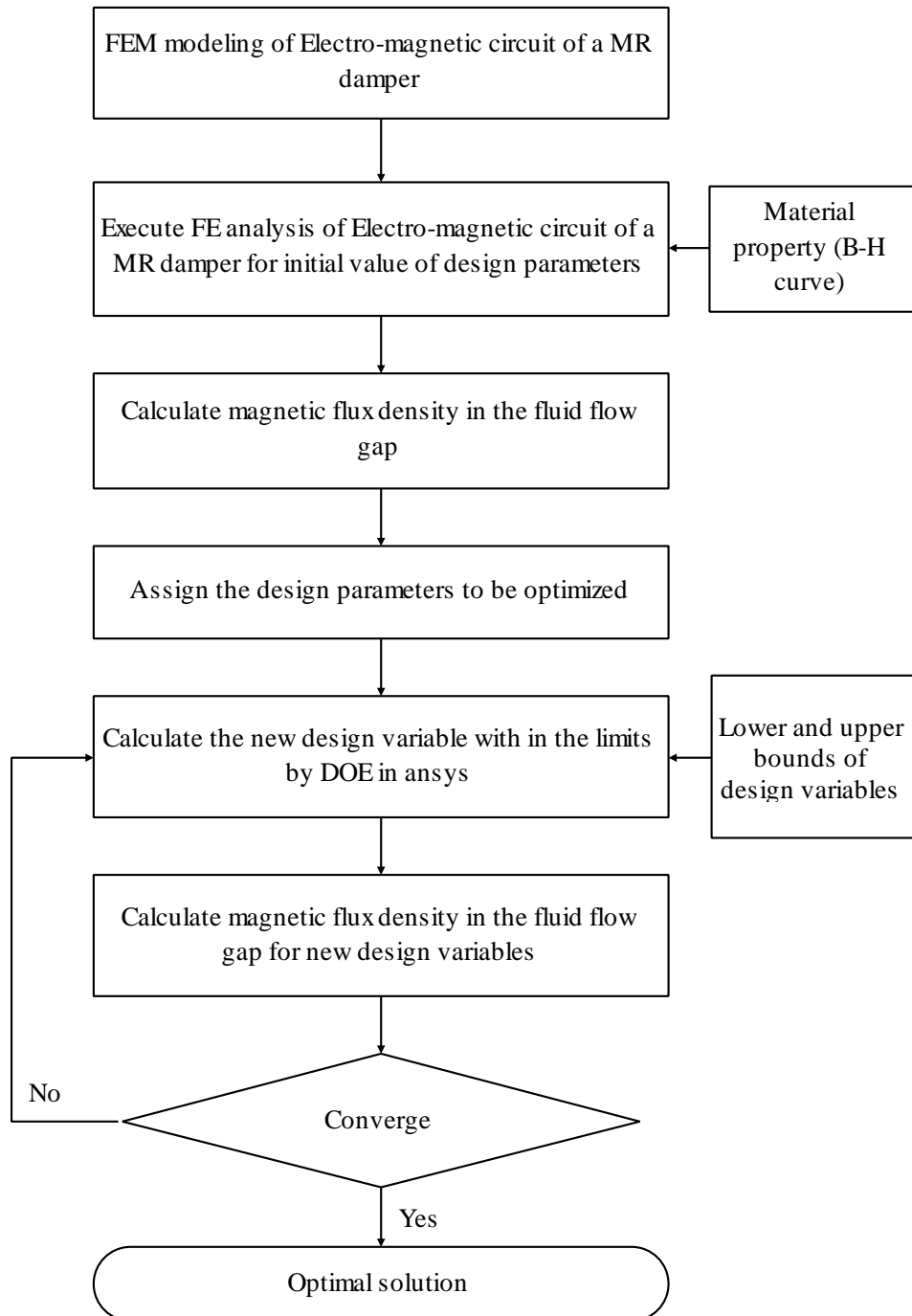


Figure 4.5 Methodology for optimization of MR damper using FEA

For initial iteration ($j=0$), the search direction of design variables is assumed to be the negative of the gradient of the unconstrained objective function, then the value of design variables in the next iteration ($j+1$) is obtained from the following equation

$$x^{(j+1)} = x^j + s_j d^j \quad (4.23)$$

Where, the line search parameter s_j is evaluated by using a combination of golden section algorithm and local quadratic fitting technique. Then the FE analysis is executed with the new values of design variables and the convergence of the objective function is checked. If the convergence occurs, the values of the design variables at this iteration are optimum. If not converging, the subsequent iterations will be performed.

4.4.1. Finite element modeling of MR damper

Twin tube MR damper consists of inner tube, outer tube, piston over which electromagnetic coil is wound and base valve as shown in the Figure 4.4. The fluid flow gap of 1.5mm provided in between piston and its inner housing is mentioned in Figure 4.6. The finite element model of twin tube MR damper is built and analyzed by using FEA. Because of symmetrical geometry, only one fourth of computational domain is constructed for the analysis. The finite element model of twin tube MR damper is as shown in Figure 4.7.

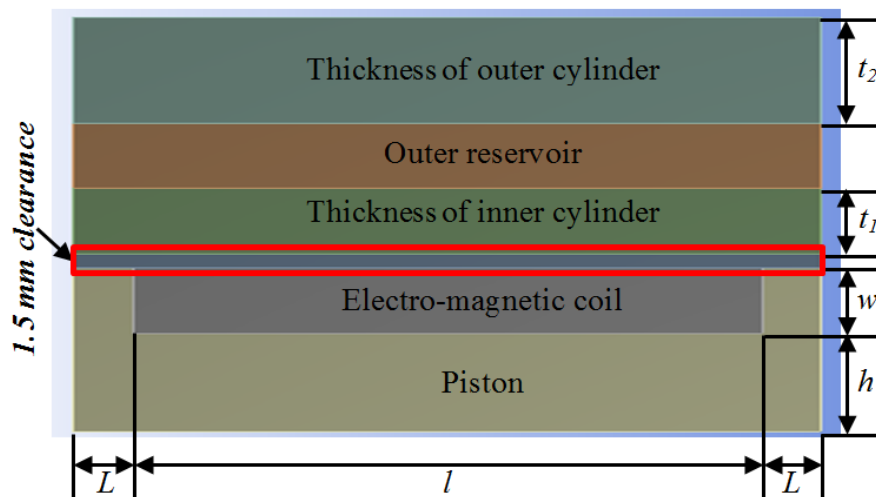


Figure 4.6 MR valve of twin tube MR damper

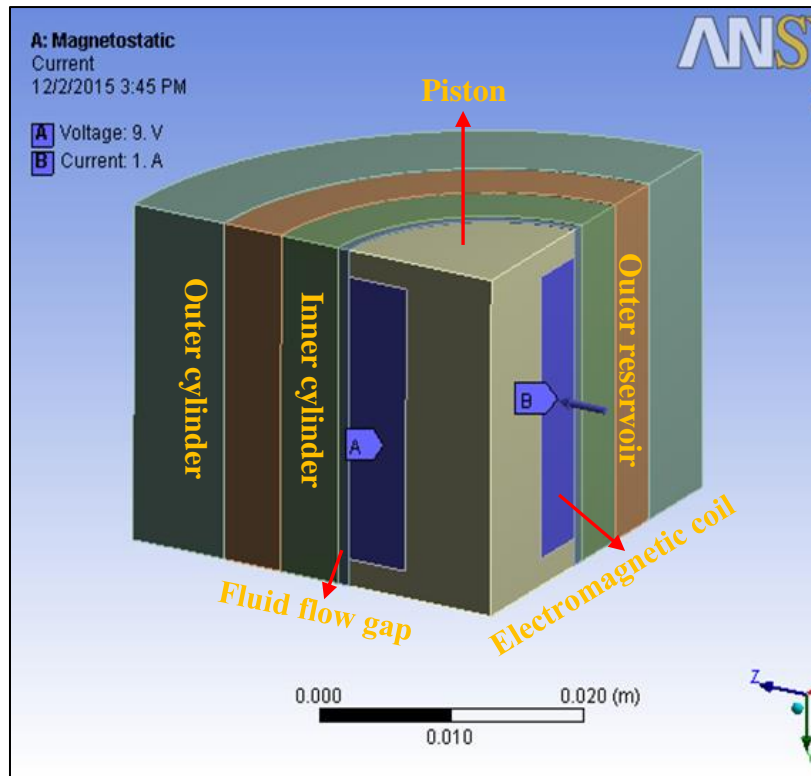


Figure 4.7 Finite element model of MR damper

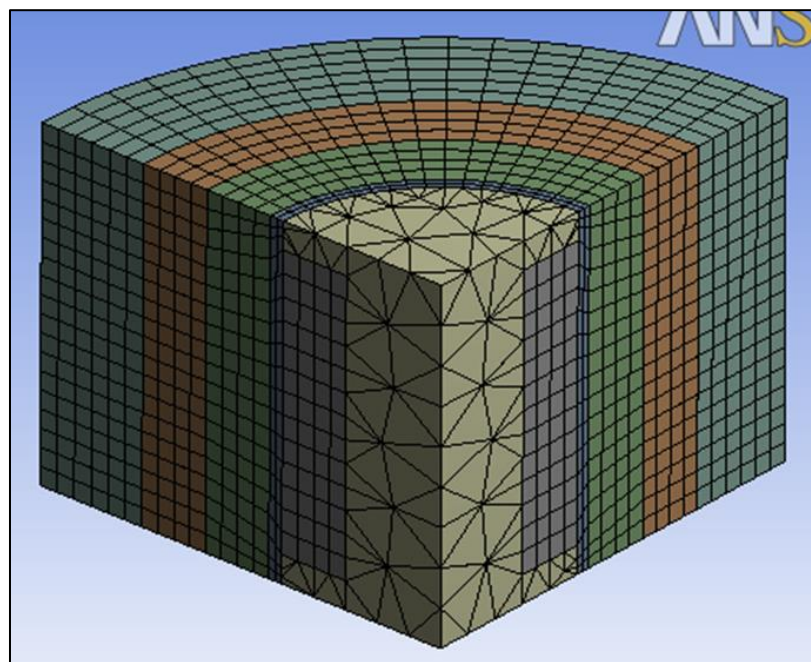


Figure 4.8 Mesh FE model of MR damper

4.4.1.1. FEA Assumptions and model details

During the magnetostatic analysis, it is assumed that the flux leakage out of the outer cylinder is small enough to be negligible. The flux lines are parallel to the surface and it is imposed by “Flux Parallel” boundary condition. The geometries of MR damper are meshed by using auto mesh technique and it consists of 21,321 combinations of hexahedral and tetrahedral elements, 50,990 nodes in that the fluid flow gap consist of 648 elements and 4,063 nodes. The meshed geometries FEA model is as shown in Figure 4.8.

4.4.1.2. Boundary conditions

In this FEM analysis, the piston and inner cylinder is taken as steel and the outer cylinder considered as aluminum alloy. The properties of MR damper component is given in Table 4.2. The permeability of free space is taken as $\mu_0=4\pi\times 10^{-7}$ H/m. The electromagnetic circuit in the piston consists of 1000 number of turns and it is subjected to a maximum current up to 1A and 9V electric potential and the boundary conditions are also mentioned in Figure 4.7.

Table 4.2 Magnetic properties of MR damper

Material	Relative permeability
Steel (SA1008)	B-H curve (Figure 4.9)
Copper	1
MR Fluid (MRF132-DG)	B-H curve (Figure 4.10)
Aluminum alloy	1

Figures 4.9 and 4.10 depict the typical magnetic properties of steel and MR fluid respectively and it signifies the saturation of the material. In saturable materials, permeability is not constant and it depends on magnetic field strength. The magnetic flux density increase is proportional to magnetic field strength up to certain limit, there after the magnetic flux density will not increase.

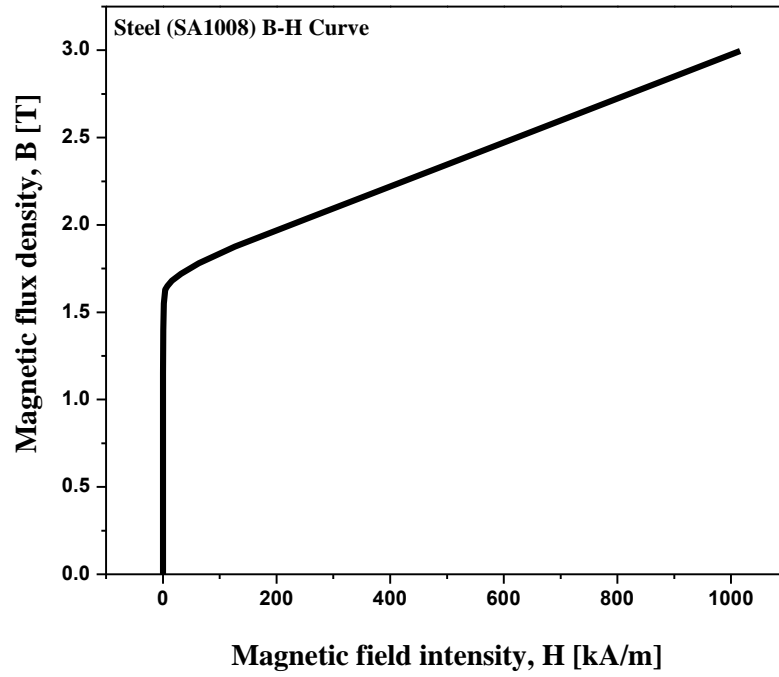


Figure 4.9 B-H curve of steel

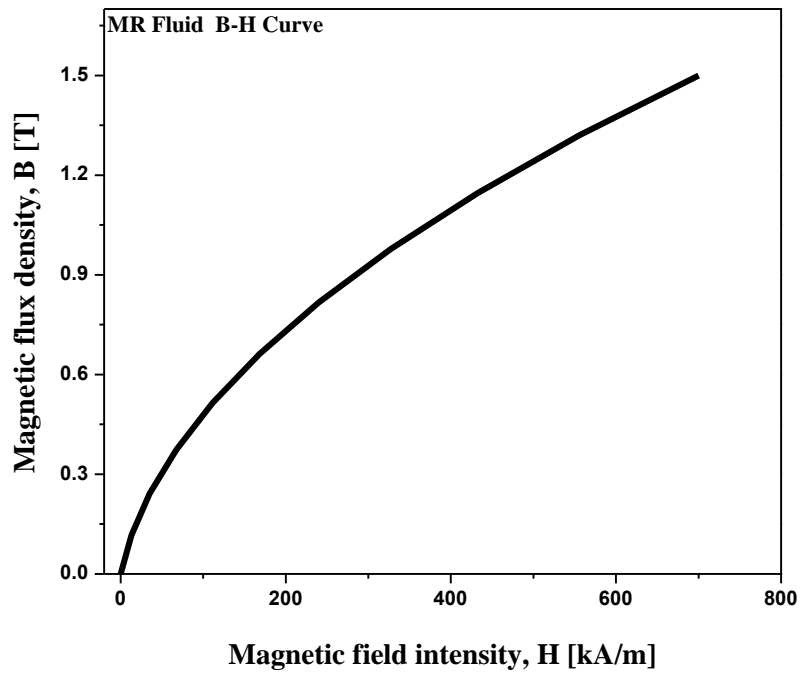


Fig.4.10 B-H curve of MR fluid (LORD MRF132-DG)

Current density for the applied current can be calculated by using Kirchoff's law as,

$$J = \frac{N_c I}{A} \quad (4.24)$$

Where, N_c is number of turns in the coil, I is applied current in Ampere and A is coil area in m^2 .

The variations of magnetic flux density in the fluid flow gap observed in between lower and upper boundaries are given in the Table 4.3.

Table 4.3 lower and upper boundaries of the parameters.

Parameters	Lower bound	Upper bound
Core length (l)	18mm	22mm
pole length (L)	2mm	5mm
Fluid flow gap (g)	0.5mm	2mm
Number of turns in a coil (N)	500	1000
Current magnitude (I)	0.1A	1A

4.5. RESULTS AND DISCUSSION

Parametric studies were conducted to investigate the effect of parameters on magnetic flux density. The variables are varied between lower and upper bounds as given in Table 4.3. In the analysis, the current is varied from 0.1A to 1A. The analysis result shows that, magnetic flux density increases with increase in current applied to the coil of an MR damper (Figure 4.11). From the Figure 4.11 it is observed that the magnetic flux density increases linearly with increase in current up to 0.5A, however this rising decays gradually between 0.5A to 1A, due to saturation.

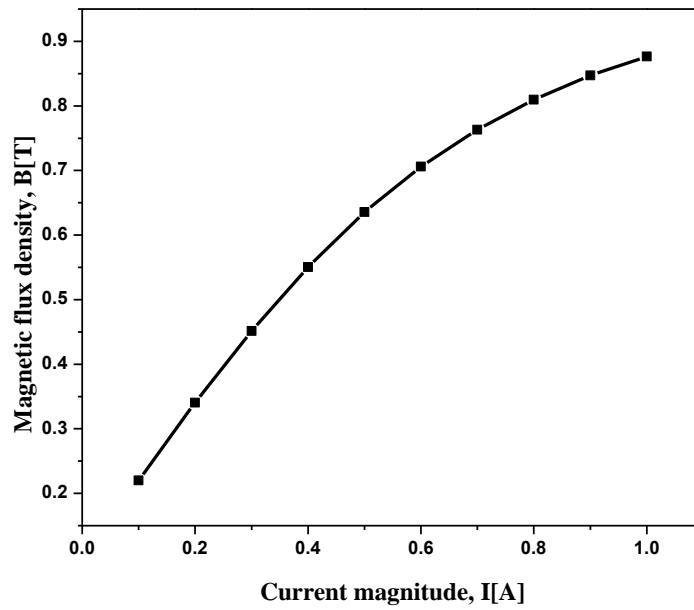


Figure 4.11 Magnetic flux density v/s Current magnitudes

The number of turns in a coil greatly influences the inductance. The inductance of the coil is due to magnetic flux around it. Stronger the magnetic flux for a given value of current, greater will be the inductance. Hence magnetic flux density increases proportional to the number of turns (Figure 4.12).

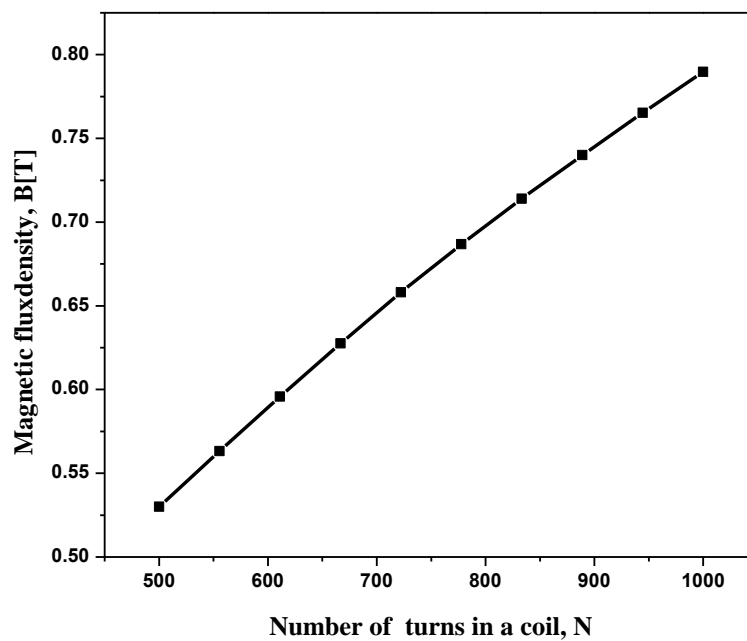


Figure 4.12 Magnetic flux density v/s numbers of turns in the coil

Magnetic flux density increases by increasing the core diameter or increasing the core length. In both cases, more wire is required to construct the coil, thus more lines of force exists to produce the required back emf. Hence the magnetic flux density increases gradually with increase of core length (Figure 4.13).

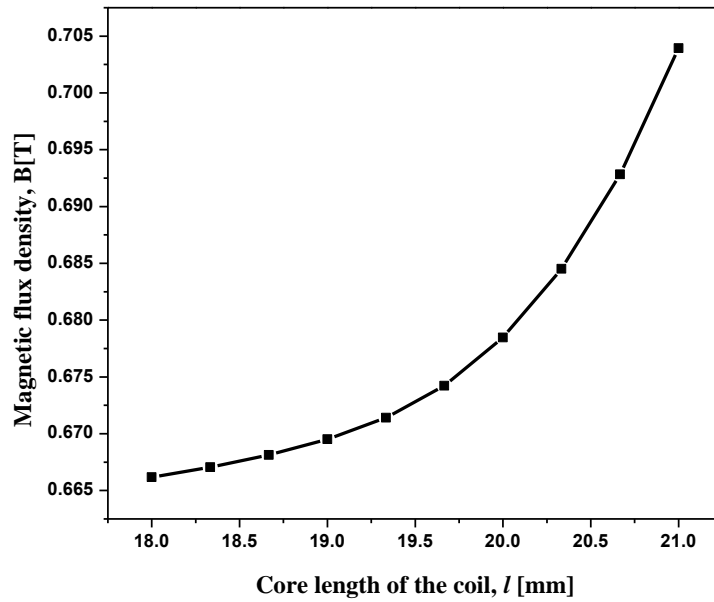


Figure 4.13 Magnetic flux density v/s Core length of coil

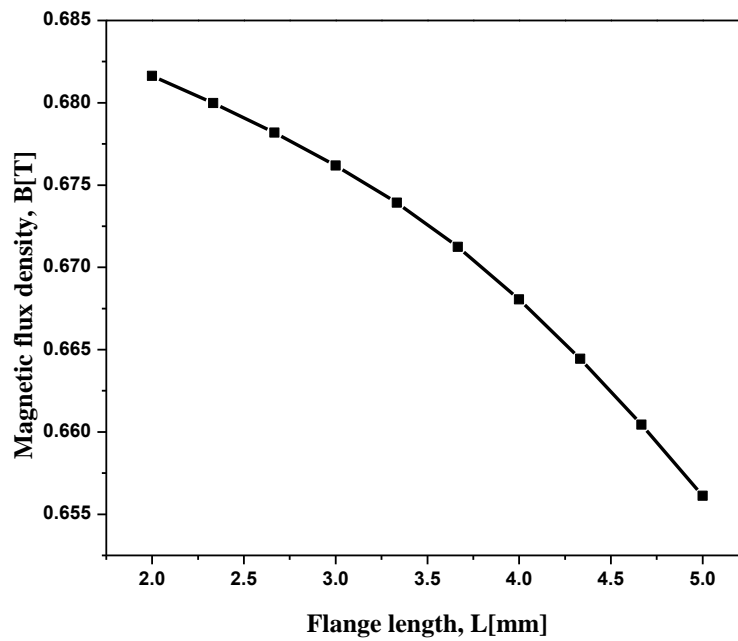


Figure 4.14 Magnetic flux density v/s Flange length

Magnetic flux density passing perpendicular to the flow direction through the flange length, develops field dependent resistance on MR fluid flow. Any magnitude of magnetic field has to pass through smaller flange length that causes bigger magnetic flux density in the MR fluid flow gap (Figure 4.14). Figure 4.15 illustrates magnetic flux density v/s fluid low gap. Increase in flow gap leads to more flux leakage, which results in decrease of magnetic flux density.

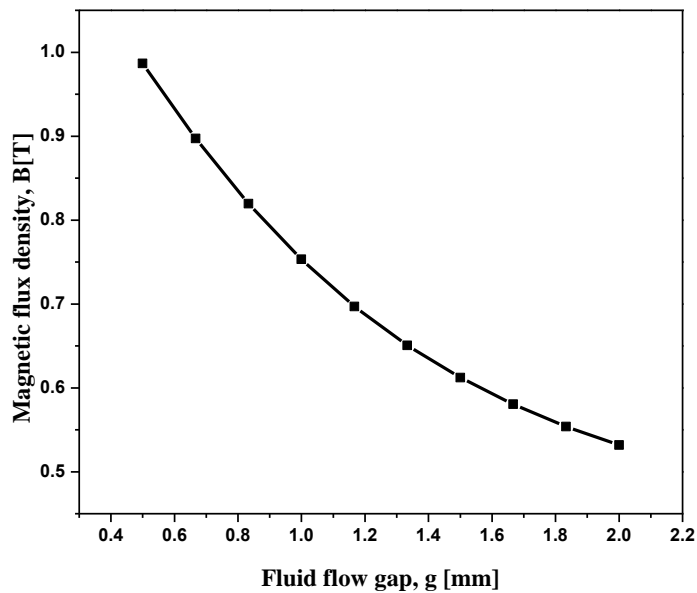


Figure 4.15 Magnetic flux density v/s Fluid flow gap

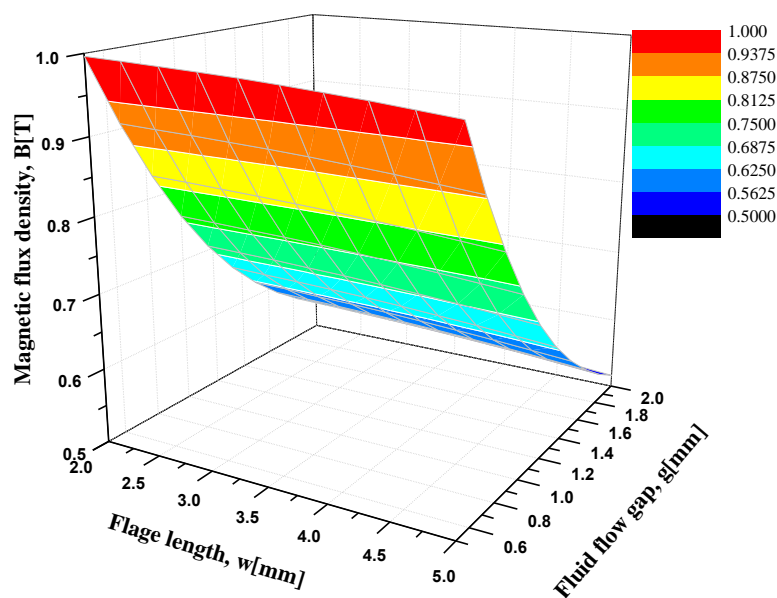


Figure 4.16 Surface plot of Magnetic flux density v/s fluid flow gap and flange length

Figure 4.16 represents the response surface, which is plotted with design variable (flange length and fluid flow gap) v/s response (magnetic flux density). The surface plotted will make it easy to understand the variation of magnetic flux density along with design variables.

Optimal parameter of MR damper provides targeted maximum magnetic flux density, which is obtained from the FEA optimization as three candidates as shown in Table 4.4. To maximize the performance of MR damper, the dynamic range should be kept high. When the fluid flow gap size is very small, the dynamic range decreases. Hence, candidate-C has been chosen for fabrication of prototype MR damper.

Table 4.4 optimal parameters obtained from FEA

Parameters	Flange length, w[mm]	Fluid flow gap, g[mm]	Core length, l[mm]	Current magnitude, I[mA]	Number of turns (N)	Magnetic flux density, B[T]
Candidate A	3.41	0.66	19.54	630.37	758	0.963
Candidate B	3.52	0.87	19.56	682.21	810	0.922
Candidate C	3.79	1.12	19.39	811.81	732	0.839

4.6. SUMMARY

Optimization of electromagnetic circuit of an MR damper has been carried out to study the variation of magnetic flux density induced in the fluid flow gap with respect to the various electromagnetic circuit parameters such as current magnitude, number of turns in a coil, coil core length, fluid flow gap and flange length. Finite element optimization method has been adopted for the analysis. Results shows significant increase of magnetic flux density in the fluid flow gap with increase of applied current, number of turns in a coil, coil core length and it decreases with increase of fluid flow gap and flange length. Optimization study suggested that the fluid flow gap size less than 1.12 mm can result in significant increase of magnetic flux density.

CHAPTER-5

EVALUATION OF OPTIMAL LEVEL OF PARAMETERS ON THE PERFORMANCE OF MR DAMPER

5.1. INTRODUCTION

This chapter discusses the evaluation of optimum level of parameters such as proportion of MR fluid, operating frequency and applied current on the performance of the MR damper by using Taguchi design of experiment. Previous chapter discussed the variation of magnetic flux density in the fluid flow gap with electromagnetic circuit parameters. Along with these parameters, other parameters such as proportion of MR fluid, operating frequencies and applied current also have influence on the damper performance. Hence, it is necessary to evaluate these parameters too on damper performance. After evaluating optimum parameters, experiments were conducted to analyze the dynamic behaviour of MR damper with these optimum levels of parameters.

5.2. CONSTITUENTS OF MR FLUID

The magnetorheological fluid is a smart fluid, whose rheological property varies within short time (milliseconds) to the external stimulus. When the magnetic field is applied, particles in the fluid get aligned in to chain like structure in the direction of applied magnetic field and the chain is broken by hydrodynamic drag, as they are subjected to the shear force (Choi et al. (2006)). The change in properties of the fluid is completely reversible, when applied magnetic field is removed. A typical magnetorheological (MR) fluid consists of 20% to 40% percent by volume of relatively pure (3-10 micron diameter size) magnetizable particles, suspended in a carrier fluid. Figure 5.1 shows constituents of MR fluid.

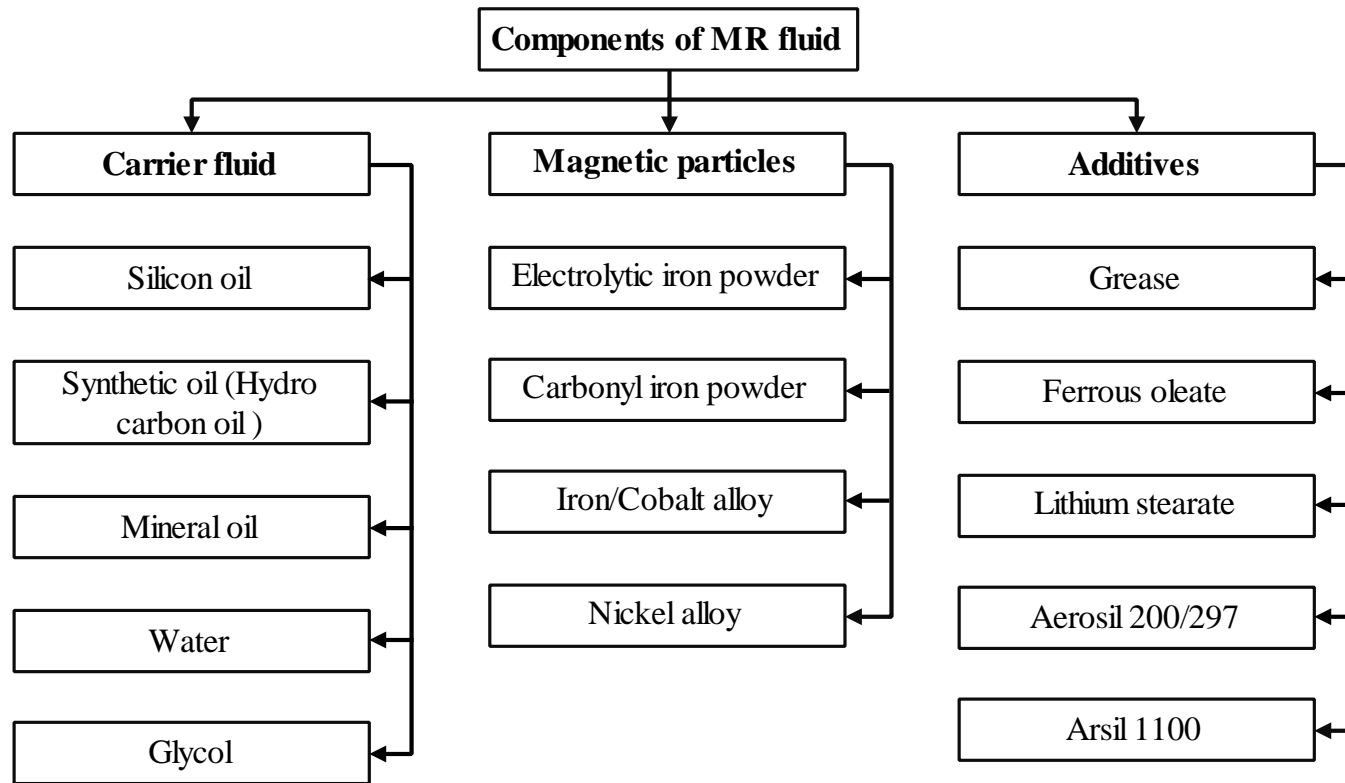


Figure 5.1 Constituents of MR Fluid

5.2.1. Carrier fluid

Carrier fluid is the major constituent of MR fluids. MR fluid viscosity substantially depends on the composition and chemistry of the carrier oil. Viscosity of the carrier fluid must be low in order to achieve the maximum MR effect (Olabi and Grunwald (2007)). Carrier fluid can be either polar or non-polar liquid, but it should be temperature independent.

The rate of change of viscosity with respect to the temperature is more in case of mineral oil. Hence, this is the drawback of the use of mineral oils as a carrier fluid in MR fluid for low temperature applications. Synthetic oil possess some important properties like higher flash point, high shear strength and high viscosity index, but it does not solidify at high temperatures.

Silicone oil has good temperature-stability, good heat-transfer characteristics, oxidation resistance, very low vapor pressure and high flash points. There is a little change in physical properties over a wide temperature span and a relative flat viscosity temperature slope and serviceability from -40°C to 204°C . The different properties of these carrier fluids are given in Table 5.1.

Table 5.1 The different properties of carrier fluids (Kumbhar et al. (2014))

Properties	Mineral oil	Synthetic oil	Silicone oil
Viscosity at 400°C (Pa-s)	0.028	0.1068	0.11
Flash point $^{\circ}\text{C}$	171-185	230	>300
Fire point $^{\circ}\text{C}$	260-330	350	~ 500
Specific gravity	0.818-0.95	0.817	0.9124
Density at 25°C (Kg/m^3)	825	873-894	760

5.2.2. Magnetizable particles and additive materials

For maximum MR effect, the magnetic particles with lowest coercivity and highest saturation magnetization are preferred. Because, when magnetic field is taken off, MR fluid should come to its demagnetized state in short time (milliseconds). Due to its

low coercivity and high saturation magnetization. Pure carbonyl iron powder appears to be the main magnetic phase of most practical MR fluid compositions. This is because carbonyl iron is chemically pure and the particles are meso-scale and spherical in nature in order to eliminate the shape anisotropy (Muhammad et al. (2006)).

Viscosity of the MR fluid is affected by magnetic field and concentration of the magnetizable particles. Higher concentration of the magnetizable particles in the carrier fluid leads to higher viscosity of the MR fluid in the absence of magnetic field and it is undesirable. Lower the viscosity of MR fluid leads to instability and sedimentation problem (Shibayama, (2002)). Hence, optimum concentration of magnetizable particles is used to get the maximum MR effect.

High viscous material like grease is used as additives to improve the settling stability and also enhance lubricity, modifies the fluid thickness or viscosity, keeps the particles suspended in the liquid, and slows down the gravitational setting of the iron particles.

5.3. MR FLUID PREPARATION

Magnetorheological (MR) fluid consists of 20-40 percent by volume of relatively pure (3-10 micron diameter size) magnetizable particles (electrolytic iron powder, carbonyl iron powder, iron/cobalt alloys and nickel alloys), suspended in a carrier fluid (mineral oil, synthetic oil, silicon oil, hydrocarbon oil, water and glycol). In this study, five different proportions of silicon oil and carbonyl iron powder based MR fluid are prepared, they are

- 20 % carbonyl iron powder and 80 % silicone oil
- 25 % carbonyl iron powder and 75 % silicone oil
- 30 % carbonyl iron powder and 70 % silicone oil
- 35 % carbonyl iron powder and 65 % silicone oil and
- 40 % carbonyl iron powder and 60 % silicone oil

Primarily, the silicon oil and grease (stabilizer) (Kolekar et al. (2014)) are taken in a container and the mixture is stirred continuously with the help of mechanical stirrer until grease is dissolved in the silicone oil. Then the carbonyl iron particles are added to the mixture of silicone oil and grease. This mixture is again stirred continuously at constant speed in order to get uniform distribution of carbonyl iron particle in silicone oil (Figure 5.2).



Figure 5.2 Preparation of MR fluids

5.4. EXPERIMENTAL ANALYSIS OF MR DAMPER

To study the performance of MR damper, experiments were carried out using a custom built damper testing machine as shown in Figure 5.3. The main components of the damper testing machine are electrodynamic shaker, linear variable differential transformer (LVDT), force transducer and a data acquisition system. The APS 420 ELECTRO-SEIS electrodynamic shaker is used for exciting the MR damper. The shaker has a rated sine peak force of 900 N with frequency range of 1 to 200 Hz. The rated peak to peak amplitude/displacement is 150 mm. It can be operated manually or by using PC based control mode and compatible with PC based data actuation. APS 145 power amplifier is used in the voltage mode in order to produce constant velocity.

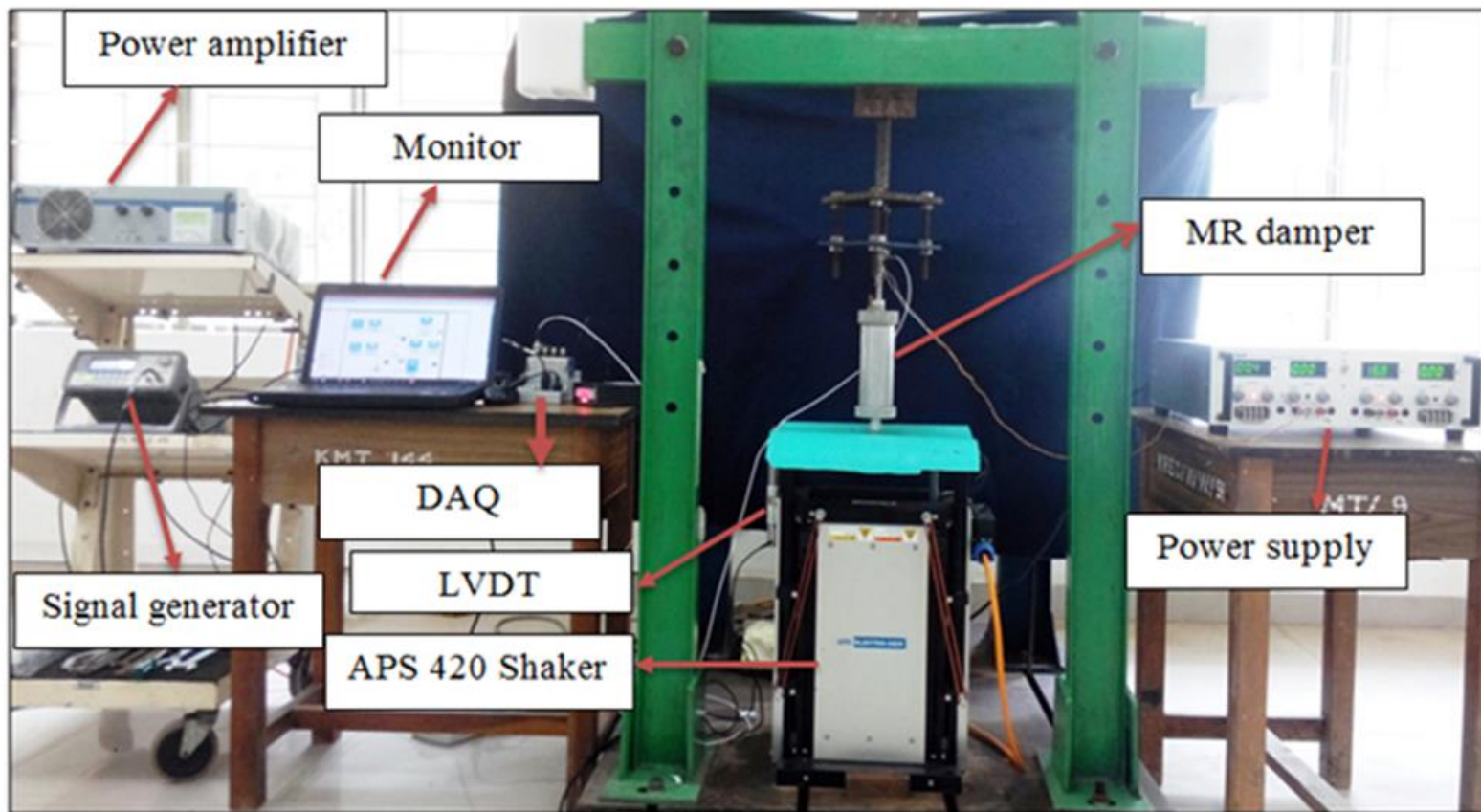


Figure 5.3 MR damper test set up

The damper test was performed at 1.5 Hz and 2 Hz frequencies for different current values. Current varied from 0.1 A to 0.4 A (increment of 0.1 A) with a sinusoidal signal of +/-0.005 m amplitude. The current was monitored and supplied through DC power supply (0-64 V/5A Max.). The damping force experienced by the piston rod is sensed by a force transducer fitted at the top of the piston rod and the displacement was measured through LVDT. The evaluated damper performance (damper force) with different proportion of MR fluid has been used to find the optimum parameters which influences to provide better performance of MR damper with help of Taguchi design of experiments.

5.5. TAGUCHI METHOD DESIGN OF EXPERIMENTS

Taguchi design of experiment is a standardized effective statistical method for optimization of design of experiments for performance quality of a product. The traditional experimental design methods are too complex and difficult to use and large number of experiments have been carried out, when the parameters increase (Shaji and Radhakrishnan, (2003)). To solve this problem Taguchi method uses certain standard orthogonal array by which the simultaneous and independent evaluation of two or more parameters for their ability to affect the variability of a particular product or process characteristics can be done in a minimum number of experiments (Yang and Tarn, (1998)). Figure 5.4 illustrates experimental detail of Taguchi method.

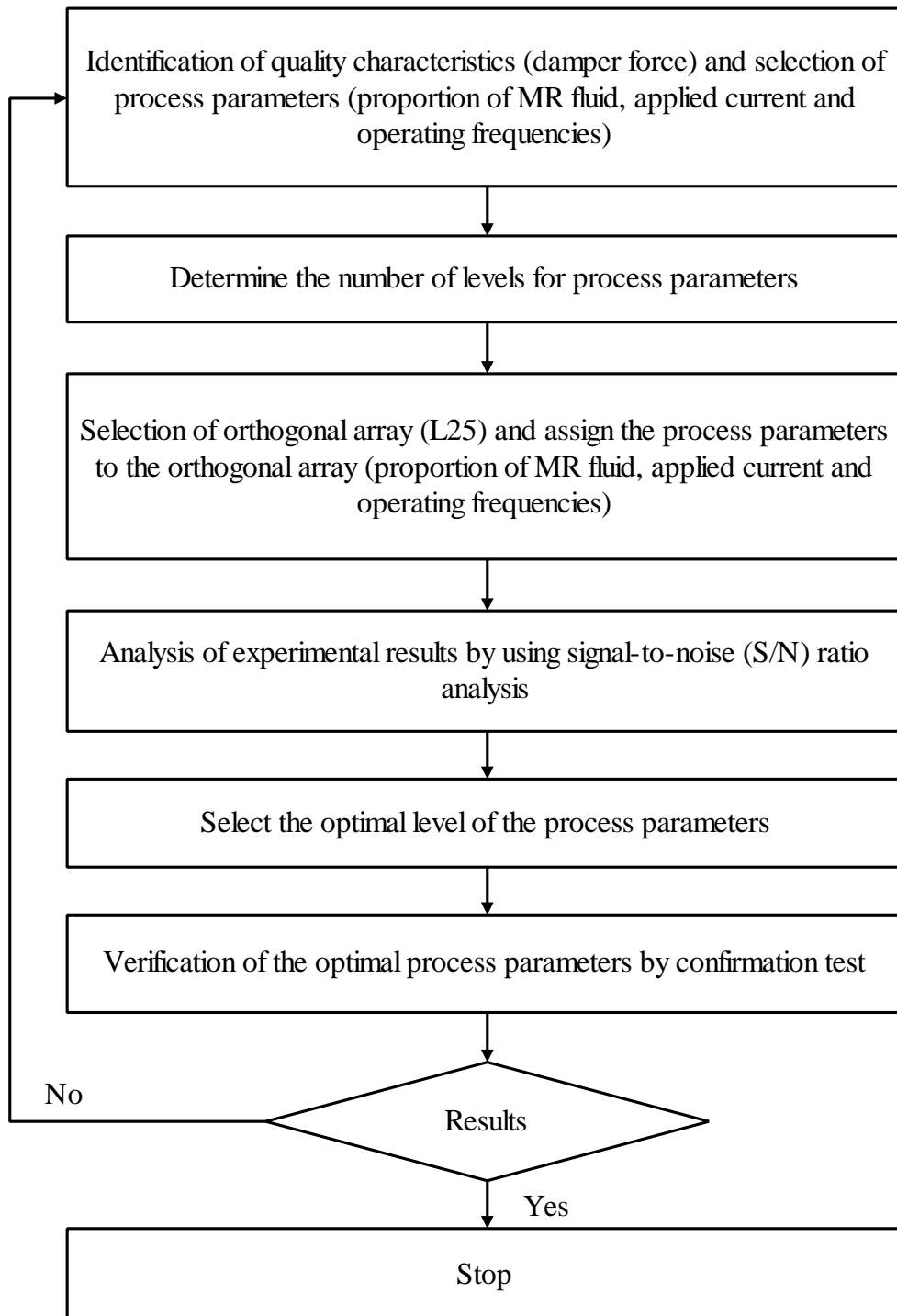


Figure 5.4 Detail procedure of Taguchi design of experiment

5.5.1. Selection of process parameters and their levels

The proportion of MR fluid, operating frequency and applied current are the input parameters chosen on the performance of MR damper (damper force). The proportion of MR fluid and applied current has each five levels, while operating frequency has two levels. The chosen parameters and their levels are given in Table.5.2.

Table 5.2 Parameters and their levels

No. of Factors	Name	Levels
1	Proportion of MR fluid	A, B, C, D, E
2	Frequency (Hz)	1.5, 2, 1.5, 2, 1.5
3	Current (A)	0, 0.1, 0.2, 0.3, 0.4

5.5.2. Orthogonal array

Classical experimental design methods are too complex and are not easy to use. A large number of experiments have to be carried out when the number of the process parameters increases. To solve this problem, Taguchi method uses a special design of orthogonal arrays to study the entire parameter space with only a small number of experiments. To select the appropriate orthogonal array for the experiments, total degrees of freedom need to be computed and then choose the appropriate orthogonal array to fit the specific task. In this study, L_{25} orthogonal array is considered and consists of 25 set of experiments in 5 levels with 3 factors. The experimental layout of the L_{25} orthogonal array is given in Table 5.3.

Table 5.3 Experimental design layout of L₂₅ orthogonal array

No. of Experiments	Proportion of MR fluid	Frequency (Hz)	Current (A)
1	1	1	1
2	1	2	2
3	1	3	3
4	1	4	4
5	1	5	5
6	2	1	2
7	2	2	3
8	2	3	4
9	2	4	5
10	2	5	1
11	3	1	3
12	3	2	4
13	3	3	5
14	3	4	1
15	3	5	2
16	4	1	4
17	4	2	5
18	4	3	1
19	4	4	2
20	4	5	3
21	5	1	5
22	5	2	1
23	5	3	2
24	5	4	3
25	5	5	4

5.5.3 Signal-Noise (S/N) ratio analysis

Taguchi method uses S/N ratio to measure the variations of the experimental design. The S/N ratio represents the ratio of the mean (desirable value) to the standard deviation (undesirable value) for the output characteristics. The quality characteristics deviating from the desired values are measured by using S/N ratio. Generally there are three categories of quality characteristics in the analysis of S/N ratio, they are maximization, minimization of output and target the design output to predefined nominal value. The S/N ratio for each level of process parameter is computed based on the S/N analysis. Therefore, to obtain optimum parameter on MR damper performance (damper force), maximization ratio is selected. The S/N ratios of each type of quality characteristics can be evaluated by using following equations (Hascalık and Caydaş, (2008)).

Nominal is the best

$$S/N_{NB} = 10 \log \left(\frac{\bar{y}}{s_y^2} \right) \quad (5.1)$$

Maximization of output

$$S/N_{LB} = -10 \log \left(\frac{1}{n} \sum_{i=1}^n \frac{1}{y_i^2} \right) \quad (5.2)$$

Minimization of output

$$S/N_{SB} = -10 \log \left(\frac{1}{n} \sum_{i=1}^n y_i^2 \right) \quad (5.3)$$

Where, y is the observed data, \bar{y} is the average of the observed data, s_y^2 is the variance of the y and n is the number of observation.

Regardless of the category of the performance characteristics, larger S/N ratio corresponds to better performance characteristics. Therefore, optimal level of the process parameter is the level with highest S/N ratio (Nalbant et al. (2007)).

5.5.4. Confirmation test

The purpose of the confirmation test is to validate the conclusion drawn during analysis phase (Tosun et al. (2004)). Once the optimal level of parameters is selected, final step is to predict and verify the improvement of the performance characteristics using the optimal level of process parameters. The predicted S/N ratio $\hat{\eta}$ using the optimal level of parameters can be calculated by using equation (5.4) (Lin (2002), Nalbant et al. (2007)).

$$\hat{\eta} = \eta_m + \sum_{i=1}^q (\bar{\eta}_m - \eta_m) \quad (5.4)$$

Where, η_m is the mean of the S/N ratio, $\bar{\eta}_m$ is mean of the S/N ratio at the optimal level and q is the number of process parameters that significantly affect the performance characteristics.

5.6. RESULTS AND DISCUSSION

From the S/N ratio analysis, optimal combination of the process parameter can be predicted and finally, confirmation experiment conducted to verify the optimal process parameters obtained from the design of experiments. Table 5.4 depicts the experimental results for damper force and corresponding S/N ratios. S/N ratios for the output characteristics are calculated by using equation (5.2).

Table 5.4 Factors assigned to L₂₅ orthogonal array and experimental result.

No. of Experiments	Proportion of MR fluid	Frequency (Hz)	Current (A)	Damper force (N)	S/N ratio for Damper force
1	A (20-80%)	1.5	0	25.702	28.199
2	A	2	0.1	47.872	33.601
3	A	1.5	0.2	54.2	34.680
4	A	2	0.3	67.492	36.585
5	A	1.5	0.4	71.073	37.034
6	B (25-75%)	1.5	0.1	58.271	35.309
7	B	2	0.2	81.472	38.220
8	B	1.5	0.3	96.53	39.693
9	B	2	0.4	103.789	40.323
10	B	1.5	0	38.749	31.765
11	C (30-70%)	1.5	0.2	83.826	38.467
12	C	2	0.3	107.419	40.621
13	C	1.5	0.4	113.845	41.126
14	C	2	0	51.698	34.269
15	C	1.5	0.1	63.47	36.051
16	D (35-65%)	1.5	0.3	94.176	39.478
17	D	2	0.4	112.913	41.054
18	D	1.5	0	42.526	32.573
19	D	2	0.1	63.323	36.031
20	D	1.5	0.2	77.646	37.802
21	E (40-60%)	1.5	0.4	110.754	40.887
22	E	2	0	36.149	31.162
23	E	1.5	0.1	56.947	35.109
24	E	2	0.2	83.483	38.431
25	E	1.5	0.3	96.628	39.702

Figure 5.5 illustrates the plots of three control parameters studied at five levels for MR damper performance. S/N ratio corresponds to the larger variance of the output characteristics around the desired value.

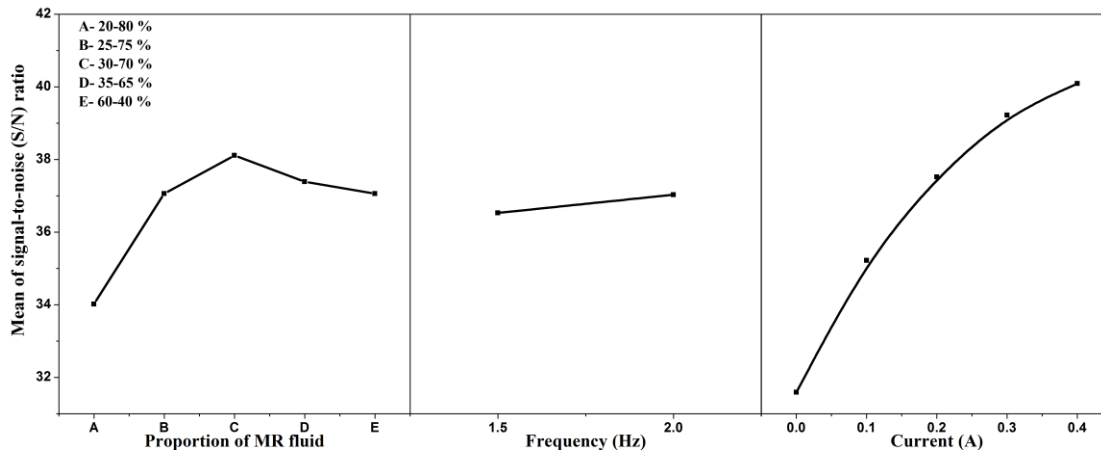


Figure 5.5 S/N ratio v/s variations in parameters

The mean S/N ratios for each level of parameters which effects on the damper force are computed in a similar manner and shown in Table 5.5.

Table 5.5 Response table for mean S/N ratios for damper force

Parameters	Mean of S/N ratios					
	Level-1	Level-2	Level-3	Level-4	Level-5	Delta
Proportion of MR fluid	34.02	37.06	38.11*	37.39	37.06	4.09
Current (A)	31.59	35.22	37.52	39.22	40.09*	8.49
Frequency (Hz)	36.53	37.03*	-	-	-	0.50
(* Optimal level)						

Based on the data presented in Table 5.5, optimal parameters for damper performance are obtained by 30-70% (Level-3) proportion of MR fluid at 2Hz (Level-2) frequency.

5.6.1. Experimental results

Dynamic behavior of an MR damper with 30-70% proportion of MR fluid at 2 Hz frequency is analyzed by using force v/s displacement curve as shown in Figure 5.6. Observation shows that the damping force increases with the increase in input current. Also the slope of the curve increases with increase in current, which indicate increase in stiffness. Bucinskas et al. (2016) and Zhou et al. (2009) reported similar behavior in their experimental analysis. The effective field dependent stiffness (K_{eff}) can be evaluated by using equation (5.5).

$$K_{eff} = \frac{F_{Max} - F_{min}}{X_{max} - X_{min}} \quad (5.5)$$

Where, F_{Max} and F_{min} are the maximum and minimum damper force, X_{max} and X_{min} are the maximum and minimum excitation displacement.

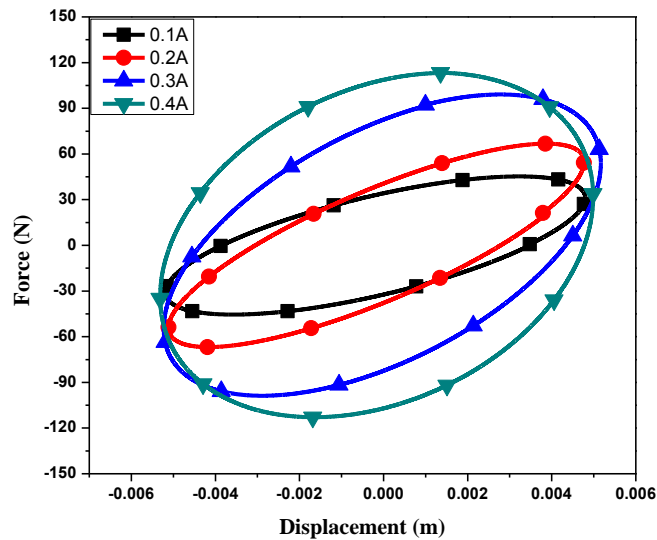


Figure 5.6 Force v/s displacement curve

The energy dissipation of MR damper can be found from the area enclosed under the force v/s displacement curve for a particular current input, excitation frequency and amplitude. The variation of stiffness and energy dissipation with current is illustrated in Figure 5.7 and it can be noted that the stiffness and energy dissipation increases significantly with increase in current.

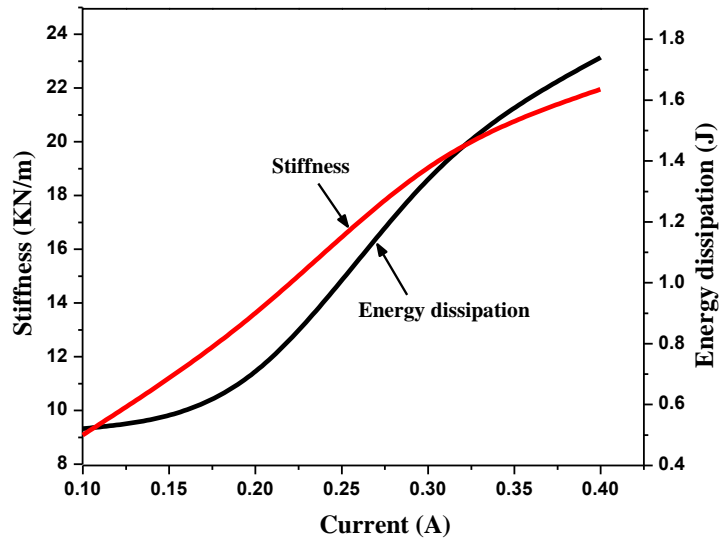


Figure 5.7 Variation of stiffness and energy dissipation v/s current

In MR damper, damping factor is a function of current because as current increases the damping coefficient also increases. The equivalent field dependent damping coefficient at various magnetic fields can be evaluated by using equation (5.6).

$$C_{eq} = \frac{w_d}{\pi\omega X^2} \quad (5.6)$$

Where, w_d is the energy dissipated in each cycle, ω is frequency and X is the amplitude.

The equivalent damping coefficient at different current value is given in Table 5.6

Table 5.6 Equivalent damping at different current value

Current (A)	Damping coefficient (N.s/m)
0.1	529.32
0.2	735.66
0.3	1255.02
0.4	1662.57

Field dependent damping coefficient and the applied current can be related by first order exponential function as given in equation (5.7)

$$C_{eq}(I) = a * \exp(b * I) \quad (5.7)$$

Where, I is the applied current, a and b are the coefficients of the equation and it can be determined by curve fitting method ($a = 370.2$ and $b = 3.807$).

5.7. SUMMARY

This chapter discussed the evaluation of optimal parameters such as proportion of MR fluid and operating frequencies on the damper performance. Taguchi design of experiments is adopted for finding the optimum parameters. The characterization of MR damper is carried out at 1.5 Hz and 2 Hz frequencies with different proportion of MR fluid under varying current. Current is varied from 0.1 A to 0.4 A with an increment of 0.1 A. Then the set of experimental result is converted into signal-to-noise (S/N) ratio. Based on the mean S/N ratios of the output characteristics, it can be concluded that, 30 % carbonyl iron powder and 70 % silicone oil proportion of MR fluid and 2 Hz frequencies are optimal for damper performance.

The dynamic behavior of MR damper with 30-70% proportion of MR fluid at 2Hz frequency for different current values has been conducted. The result shows that, both slope and area enclosed by the force v/s displacement curves are increases with increase of current. It demonstrates the developed MR damper has capability to vary both stiffness and damping by an external magnetic field.

CHAPTER-6

DEVELOPMENT OF NON-PARAMETRIC MR DAMPER MODEL

6.1. INTRODUCTION

In the previous chapter, the optimum proportion of MR fluid and optimum level of operating frequency are evaluated based on the damper performance using Taguchi design of experiments. The dynamic behaviour of MR damper was also studied experimentally with these optimum parameters at different current values. This chapter discusses the development of a novel non-parametric MR damper model based on the magnetic flux density induced in the fluid flow gap to predict the MR damper behaviour analytically and also compare the performance between developed non-parametric MR damper model with existing standard Bouc-Wen MR damper model. The parameters of the Bouc-Wen MR model have been evaluated by NSGA-II optimization technique. The results of both the models are validated with experimental investigations.

6.2. DEVELOPMENT OF NONPARAMETRIC MODELING

Non-parametric approach employs analytical expression to describe the characteristics of modelled device and it is highly useful for studying the linear/nonlinear behavior of a system. The advantage of non-parametric modelling methods is that they can avoid the pitfalls of parametric approaches while being robust and applicable to linear system/ nonlinear system/ hysteresis system (Gangrou, 2011). This study presents a novel approach to study the nonparametric modelling of an MR damper. The detail procedure of development of nonparametric model of a magnetorheological damper is given in Figure 6.1.

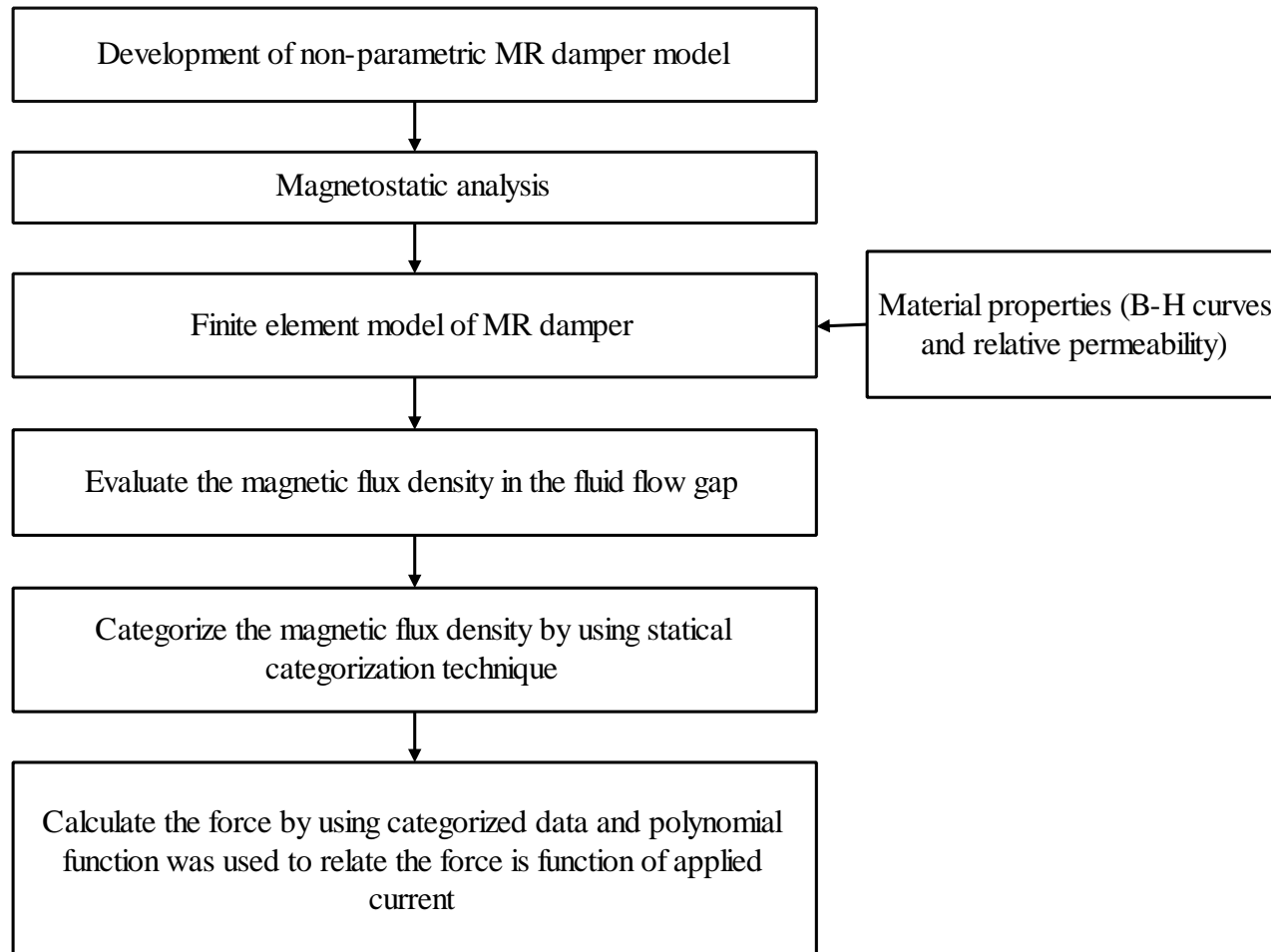


Figure 6.1 Detail procedure for development of nonparametric model

6.2.1. Magnetostatic analysis

Magnetostatic analysis is used to find the magnetic field and its related quantities such as magnetic flux density, field intensity, inductance and flux linkage due to application of electric current. It is also used to verify the risks of magnetic saturation in the devices, which could limit the performance of the devices. In the present study, the magnetostatic analysis of MR damper has been carried out. Based on the magnetostatic result, non-parametric model has been developed. The finite element model of twin tube MR damper has been built and analyzed by using FEA. The finite element model of twin tube MR damper model is shown in Figure 6.2. Taking the advantage of geometrical symmetry, only one fourth of computational domain has been constructed for the analysis. The assumptions made in finite element analysis, model details and boundary conditions are given in section - 4.4 of chapter - 4.

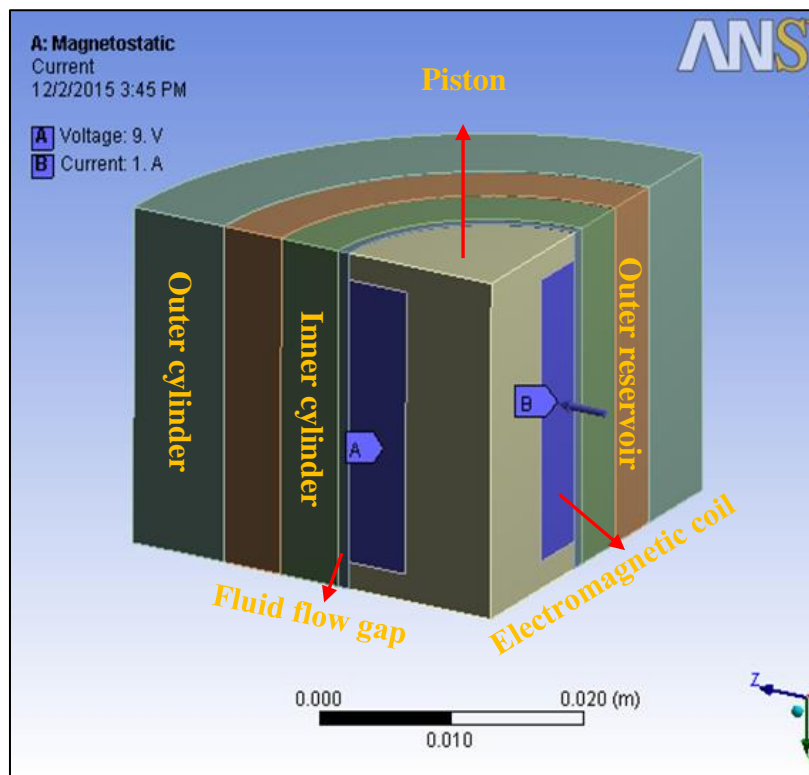


Figure 6.2 Finite element model of MR damper piston

The magnetostatic analysis of MR damper provides the nodal solution at the clearance space (fluid flow gap) between the piston and cylinder of MR damper under its magnetic induction. The total magnetic flux density of MR damper at fluid flow gap is as shown in Figure 6.3.

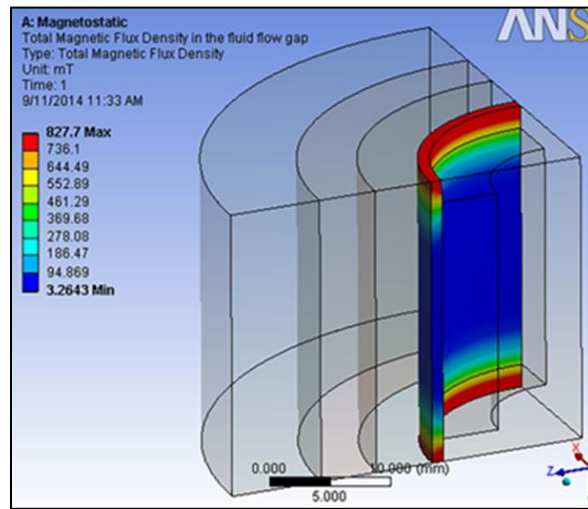


Figure 6.3 Total magnetic flux density in the fluid flow gap

The magnetic flux density obtained from the magnetostatic analysis of MR damper for different values of current is categorized by using the statistical data categorizing technique. Hence, the magnetic flux density in the fluid flow gap is divided into five categories based on the maximum and minimum total magnetic flux density for corresponding current value. In this classification method, each class consists of an equal data interval. The step length is calculated by using following formula,

$$\text{Step length} = \frac{\text{Range of data}}{\text{Number of categories required}}$$

$$= \frac{\text{Max. total magnetic flux density} - \text{Min. total magnetic flux density}}{\text{Number of categories required}}$$

The categorized data are given in Table 6.1. The summation of average total magnetic flux density obtained from categorization technique is used to find the force.

Table 6.1 Categorized data

Current(A)	Average total magnetic flux density (mT)	Percentage of exposure	Average total magnetic flux density (mT)	Percentage of exposure	Average total magnetic flux density (mT)	Percentage of exposure	Average total magnetic flux density (mT)	Percentage of exposure	Average total magnetic flux density (mT)	Percentage of exposure
0.1	8.76	59.44%	96.93	4.63%	157.34	6.45%	221.30	3.69%	285.24	25.79%
0.2	17.15	59.44%	163.77	4.63%	244.03	4.63%	334.18	5.51%	450.67	25.79%
0.3	25.20	59.44%	180.33	1.87%	292.45	7.38%	433.00	5.51%	576.82	25.79%
0.4	31.11	59.44%	207.72	1.87%	332.35	7.38%	487.35	5.51%	645.03	25.79%
0.5	35.54	59.44%	223.21	1.87%	353.92	7.38%	516.04	5.51%	680.58	25.79%
0.6	36.22	57.62%	194.80	3.69%	372.63	7.38%	540.68	5.51%	710.91	25.79%
0.7	40.15	57.62%	206.10	3.69%	389.71	7.38%	561.88	5.41%	737.80	25.89%
0.8	43.98	57.62%	216.54	3.69%	404.66	7.33%	569.36	4.63%	758.53	26.73%
0.9	47.73	57.62%	226.26	3.69%	407.81	6.45%	572.90	5.51%	780.43	26.73%
1	49.41	56.68%	228.74	4.63%	420.69	6.45%	588.97	5.51%	800.49	26.73%

The damping force due to applied magnetic field can be calculated for particular current value by using equation (6.2).

$$F_d = \frac{A \sum (B_i^2 \times n_i)}{2\pi\mu_0\mu_r}, i=1, 2, 3 \dots \quad (6.2)$$

Where, F_d is the force in Newton, B_i is the magnetic field in Tesla, n_i is the number of suspended particles, A is the surface area of the suspended particles in m^2 , μ_0 is the permeability of the free space ($4\pi 10^{-7}$ H/m) and μ_r is the relative permeability of MR fluid.

Polynomial model is one of the most commonly used non-parametric models. It is used to describe the force as a function of the current (I) applied to the MR damper.

$$F = \sum_{i=0}^n (\alpha_i I^i) \quad (6.3)$$

Where, n is the order of polynomial and fifth order polynomial function is considered to establish relation between the damping force and applied current.

The hysteresis loop of MR damper is fitted by polynomial with sinusoidal displacement function ($x=a \sin (2\Pi ft)$).

$$F = (\alpha_1 I^5 + \alpha_2 I^4 + \alpha_3 I^3 + \alpha_4 I^2 + \alpha_5 I + \alpha_6)x \quad (6.4)$$

Where, I is the applied current in ‘A’ and coefficient of the equation are constant is determined by curve fitting ($\alpha_1 = -7782, \alpha_2 = 2.126e + 04, \alpha_3 = -2e + 04, \alpha_4 = 6578, \alpha_5 = 849, \alpha_6 = -29.49$).

6.3. DEVELOPMENT OF PARAMETRIC MR MODEL

Parametric MR model is also used to predict the behavior of the MR damper by using different phenomenological models and are briefly described in chapter-2. In the

present study, Bouc-Wen hysteresis model has been used to predict the behavior of MR damper.

6.3.1. Bouc-Wen MR model

Bouc-wen MR model is the most popular model for modelling the hysteretic system. This is more versatile, but also more complicated. Figure 6.4 shows the Bouc-Wen model and it consists of a set of differential equations describing the hysteresis behavior of the MR damper.

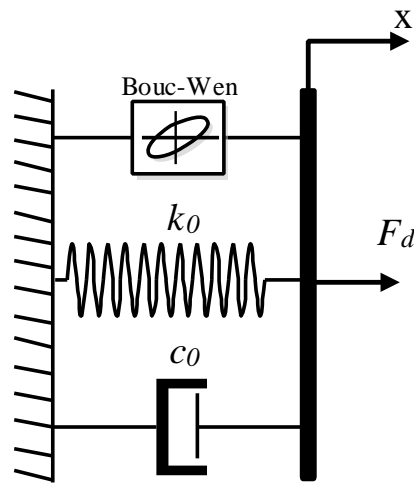


Figure 6.4 Bouc-Wen model

The damping force developed by Bouc-Wen model (Sapinski and Filus, (2003)) is given in the equation (6.5)

$$F_d = c_0 \dot{x} + k_0 x + \alpha z \quad (6.5)$$

Where,

$$\dot{z} = \delta \dot{x} - \beta \dot{x} |z|^n - \gamma z |\dot{x}| |z|^{n-1} \quad (6.6)$$

$$K_0 = K_{0a} I + K_{0b} \quad (6.7)$$

$$C_0 = C_{0a} I + C_{0b} \quad (6.8)$$

Where, F_d is damper force, k_0 is the stiffness, c_0 is the viscous coefficient respectively. $\alpha, \beta, \delta, \gamma$ and n are the parameters that need to be adjusted in order to control shape of the hysteretic curve, z is hysteretic displacement and I is input applied current, K_0 and C_0 are the parameters varying with input applied current.

Nine parameters of Bouc-Wen model ($\alpha, \beta, \delta, \gamma, n, K_{0a}, K_{0b}, C_{0a}$ and C_{0b}) are identified by minimizing the error between Bouc-Wen model force and the experimental force. The objective function used for optimization is given by

$$J = \sum_{i=1}^N (F_{ei} - F_{pi})^2 \quad (6.9)$$

Where, F_e and F_p are the experimental force and predicted force respectively.

The optimum values of the Bouc-Wen parameters are identified by using non-dominated sorting genetic algorithm II (NSGA II) technique (Appendix-I). The optimal parameters of Bouc-Wen model are given in Table 6.2.

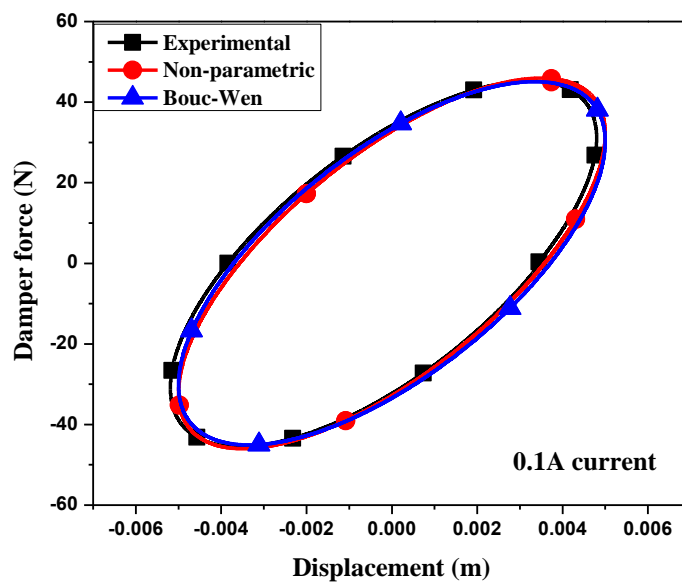
Table 6.2 The optimal parameters of Bouc-Wen MR model

Parameters	Optimum value	Parameters	Optimum value
α	0.0106696	K_{0a}	747
β	1577.0759	K_{0b}	676.3
δ	113.5895	C_{0a}	526.4
γ	1926.2603	C_{0b}	79.73
n	3		

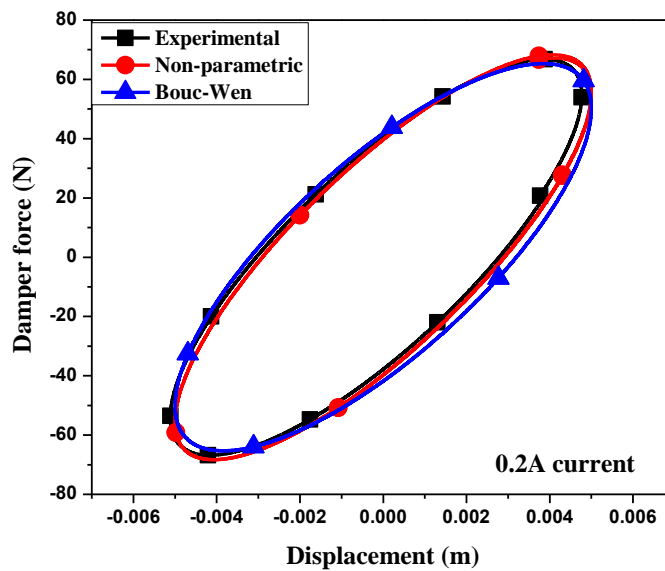
6.3.2. Results and discussion

The dynamic behaviors of MR damper at 2Hz frequency is obtained from experimental investigations, non-parametric MR model and Bouc-Wen MR model and are shown in Figure 6.5. Figures 6.5 (a) to (d) shows characteristic curves of MR damper at 0.1 A to 0.4 A current. A good agreement is observed between MR damper

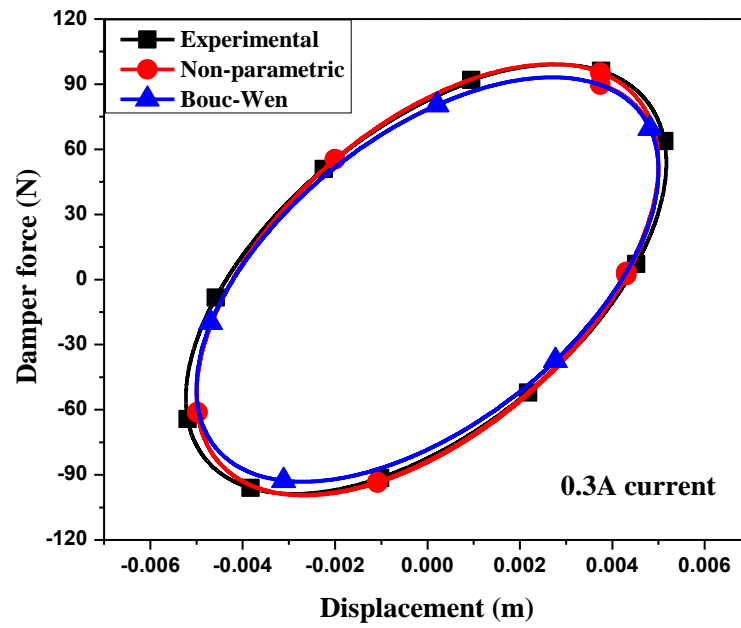
models and experimental results. From the figures 6.5 (a) to (d) it is observed that damper force increases significantly with increase of applied current. Also, the slope and area enclosed by the curve also increases with current. The area enclosed by the characteristic curve of non-parametric MR model as well as Bouc-wen MR model are equivalent to the area enclosed by the experimental characteristic curve. Further study, developed non-parametric MR damper model is used as an element of semi-active suspension system in vehicle.



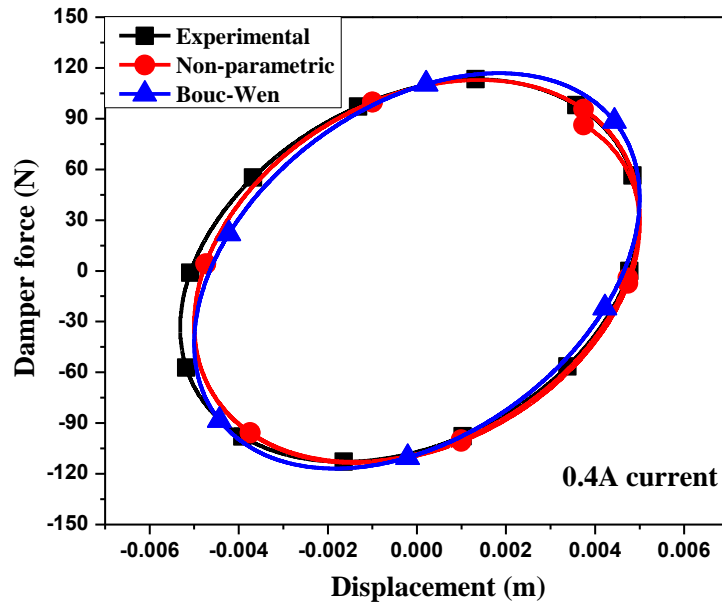
(a) Force v/s displacement curve for 0.1A current



(b) Force v/s displacement curve for 0.2A current



(c) Force v/s displacement curve for 0.3A current



(d) Force v/s displacement curve for 0.4A current

Figure 6.5 Comparison of experimental and MR models results (a) force v/s displacement at 0.1 A, (b) force v/s displacement at 0.2 A, (c) force v/s displacement at 0.3 A and (d) force v/s displacement at 0.4 A

6.4. SUMMARY

This chapter discussed the development of novel non-parametric MR damper model by using magnetic flux density induced in the fluid flow gap. Magnetic flux density obtained from the magneto-static analysis is classified into five categories based on the maximum and minimum magnetic flux density with help of statical data categorizing technique. The average total magnetic flux density from statistical categorization technique is utilized to evaluate the magnetic field dependent damper force which is related to current by using polynomial model. The coefficients of polynomial equation are evaluated by curve fitting method and the hysteresis behaviour of MR damper is predicted. For the purpose of comparison, the standard Bouc-Wen MR damper model is developed and the parameters of the Bouc-Wen model are evaluated by NSGA-II technique. Proposed non-parametric MR damper model and Bouc-Wen MR model have been validated with experimental investigations. The result shows good agreement between them. It is also seen that both the models occupy the same area as that in the experimental results with small variation.

CHAPTER-7

VERTICAL DYNAMIC ANALYSIS OF A VEHICLE WITH MR DAMPER

7.1. INTRODUCTION

In the previous chapter, novel development of non-parametric MR model based on the magnetic flux density induced in the fluid flow gap and standard Bouc-Wen MR model have been developed and validated with experimental results. The parameters of the Bouc-Wen model are found using NSGA-II optimization technique. In the present chapter, developed non-parametric model is incorporated into the vehicle model as a semi-active suspension system. Theoretically conducted ride comfort analysis and road holding performance of the vehicle subjected to random road irregularities and road bump conditions with suitable control strategy.

7.2. ROAD PROFILE

The dynamic behavior of the vehicle model can be evaluated under two types of road condition such as (1) Random road condition and (2) Road bump.

7.2.1. Random road profile model

When a vehicle travels at constant velocity, the road roughness is viewed as stationary process in spatial domain. The power spectral density (PSD) of road roughness in spatial domain can be expressed as (He et al. (2008); Zhang et al. (2002)).

$$G_q(\Omega) = G_q(\Omega_0) \left(\frac{\Omega}{\Omega_0} \right)^{-2} \quad (7.1)$$

Where, $G_q(\Omega)$ is the spatial power spectral density, $G_q(\Omega_0)$ is coefficient of road roughness, Ω is spatial angular frequency and Ω_0 is the reference spatial angular frequency.

The power spectral density (PSD) corresponding to the road excitation being the response of the first order liner filter to white noise excitation and road roughness is given by

$$\dot{Z}_r(t) + 2\pi un_0 Z_r(t) = \sqrt{G_q(\Omega_0)u} w(t) \quad (7.2)$$

Where, $Z_r(t)$ is road roughness amplitude, u is the vehicle forwarded velocity, $w(t)$ is the white noise signal whose power spectral density is unity, ω_o is the lowest cutoff angular frequency and n_0 is reference spatial angular frequency.

Based on the pavement roughness, International Organization for Standardization (ISO-8606) classified roads into 8 classes, indicated by letters A-H. Among those A-D class are for hard surface road and its roughness values are given in Table 7.1 (Tyan et al. (2009); Barbosa (2011)).

Table 7.1 Road roughness detail

Degree of road roughness $G_q(\Omega_0)$ ($10^{-6}\text{m}^2/(\text{cycle}/\text{min})$)	
Road classes	Geometric mean
A (very good road)	16
B (Good road)	64
C (Average road)	256
D (Poor road)	1024
E (Very poor road)	4096

In this research work, average road (C-level road) is considered to evaluate the performance of vehicle models. Figure 7.1 shows the random road roughness profile in time domain and its PSD, when vehicle speed is at 25 m/s on C level road.

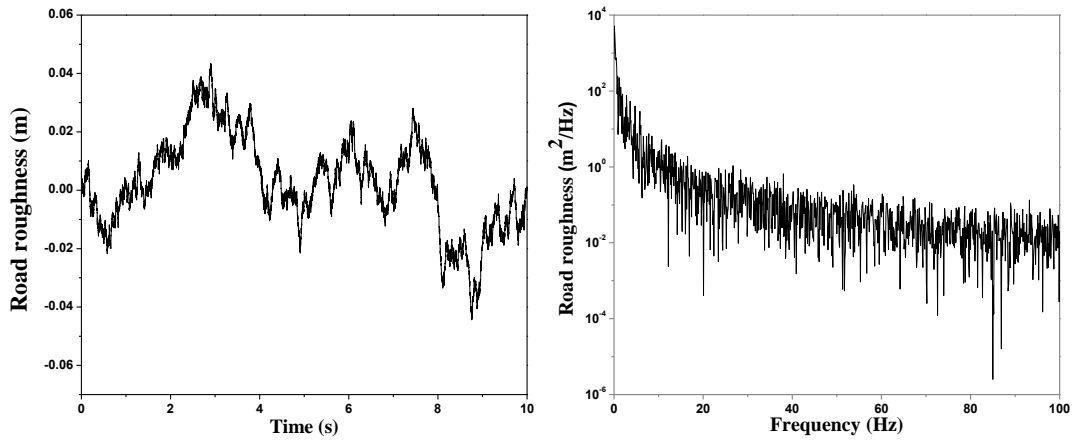


Figure 7.1 Random road roughness in time domain and its PSD

7.2.2. Road bump profile

The performance of the vehicle model is also evaluated under road bump disturbance with bump height of 0.11m. The road bump input can be considered as half-sine wave and is described by equation (7.3) (Amato and Viassolo (2000)).

$$z(t) = \begin{cases} \frac{a(1 - \cos(8\pi t))}{2} & \text{if } 0.5 \leq t \leq 0.75 \\ 0 & \text{otherwise} \end{cases} \quad (7.3)$$

Where, a is the amplitude of the bump and the road bump model is as shown in the Figure 7.2.

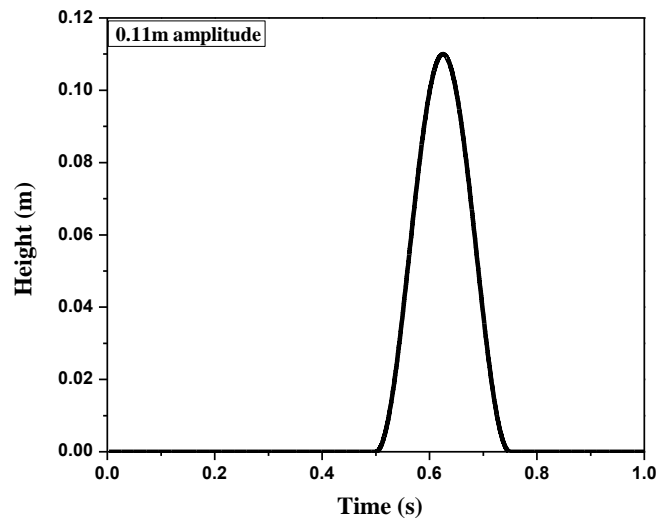


Figure 7.2 Road bump profile

7.2.3. Performance indices

The performance indices help to evaluate the quality of the suspension system and it can be estimated by considering comfort and road holding capabilities of the suspension system. Ride comfort is strongly related to the acceleration of the vehicle body and road holding is directly related to the variation of vertical tyre force. The performance index for comfort and road holding is formulated as follows (Jonasson and Roos, 2008).

$$P_{\text{comfort}} = \frac{|\ddot{x}_{\text{semi-active}}|_{\text{RMS}}}{|\ddot{x}_{\text{Passive}}|_{\text{RMS}}} \quad (7.4)$$

$$P_{\text{Road holding}} = \frac{|F_{t, \text{semi-active}}|_{\text{RMS}}}{|F_{t, \text{Passive}}|_{\text{RMS}}} \quad (7.5)$$

Where, F_t is vertical tyre force and \ddot{x} is sprung mass acceleration.

The performance index $P_{\text{comfort/Roadholding}} < 1$, then the performance of semi-active suspension system is considered to be of superior quality compared with passive suspension system.

7.3. MATHEMATICAL MODELING OF VEHICLE

The performance of MR damper used as a semi-active suspension element with suitable control strategy has been analyzed by using mathematical modelling of vehicles such as quarter car, half car and full car model subjected to stationary random road undulation. Nomenclature and vehicle parameters are given in Table 7.2.

Table 7.2. Nomenclature and vehicle parameters

Parameter	Value
Sprung Mass (M_s)	1583 kg
Roll Axis Moment of Inertia (I_x)	531 kg. m ²
Pitch Axis Moment of Inertia (I_y)	2555 kg. m ²
Front Unsprung Mass (M_u , M_{uf} , M_{u1} and M_{u2})	48 kg
Rear Unsprung Mass (M_{ur} , M_{u3} and M_{u4})	74 kg
Suspension Stiffness (K_s , K_{sf} , K_{sr} , K_{s1} , K_{s2} , K_{s3} and K_{s4})	35000 N/m
Tire stiffness (K_t , K_{tf} , K_{tr} , K_{t1} , K_{t2} , K_{t3} and K_{t4})	220000 N/m
Tire Damping (C_t , C_{tf} , C_{tr} , C_{t1} , C_{t2} , C_{t3} and C_{t4})	700 N.s/m
Distance between front wheels and Center of Gravity (a_1)	1.116 m
Distance between rear wheels and Center of Gravity (a_2)	1.438 m
Distance between left wheels and Center of Gravity (b_1)	0.77 m
Distance between right wheels and Center of Gravity (b_2)	0.765 m

7.3.1. Semi-active control strategies

The performance of the semi-active suspension system is based on type of control strategy used. The main aim of semi-active control strategy is to minimize the acceleration of vehicle body and tire deflection in order to provide safety and ride comfort against road disturbance. In the present research work, comparative study of different control strategies such as sky-hook, proportional integral derivative (PID) and fuzzy logic controllers have been carried out by using quarter car model. Based on the performance, best controller is adopted for studying dynamic response analysis of vehicle models.

7.3.1.1. Sky-hook control strategy

Sky-hook controller is a popular and effective vibration control method because it can dissipate system energy at a higher rate. The sky-hook control can reduce the resonant peak of the sprung mass quite significantly and provide good ride and handling performance of the vehicle. As the name itself indicates, the damper is connected to some inertial reference in the sky as shown in Figure 7.3.

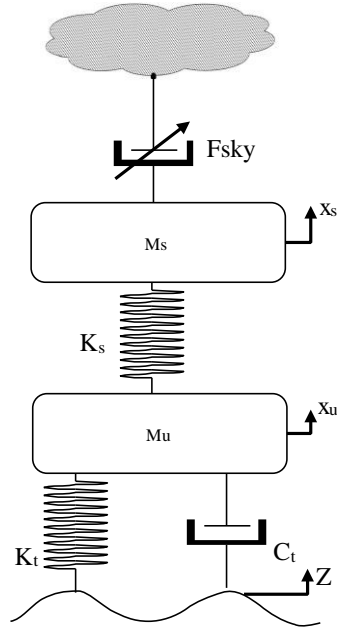


Figure 7.3 Sky-hook control strategy

The main aim of the sky-hook controller is to reduce the RMS acceleration of the sprung mass. The sky-hook control strategy is given in the equation (7.6).

$$F_{sky-hook} = \begin{cases} F_{max}, & \text{if } \dot{x}_s(\dot{x}_s - \dot{x}_u) > 0 \\ F_{min}, & \text{if } \dot{x}_s(\dot{x}_s - \dot{x}_u) \leq 0 \end{cases} \quad (7.6)$$

Where, \dot{x}_s is the sprung mass velocity and \dot{x}_u is unsprung mass velocity

The sky-hook strategy indicates that, if the relative velocity between body and wheel is in the same direction as that of body velocity, then maximum damping force should be applied to reduce the body acceleration. If these two velocities are in the opposite direction, then minimum damping force should be applied.

7.3.1.2. Proportional-Integral-Derivative (PID) control strategy

PID controller is used to increase the ride and road holding performance of the half car model. The PID controller consists of three different parameters such as proportional (P), integral (I) and derivative (D), which are used to decrease the rise time, eliminate the steady state error, decrease the settling time and overshoot of the system. PID controller is a closed loop feedback control system which is used to

minimize the error value between a measured process variable and a desired set point (Gaur and Sheilza, (2013)). The PID control strategy is given in equation (7.7).

$$u(t) = K_p e(t) + K_i \int_0^t e(t) dt + K_d \frac{de(t)}{dt} \quad (7.7)$$

Where, u_i is control signal, K_p is proportional co-efficient, K_i is integral co-efficient, K_d is derivative co-efficient, $e(t)$ is error signal.

The relative displacement between sprung and unsprung is given as input to the PID controller. The control structure for half car model with PID controller is as shown in Figure 7.4.

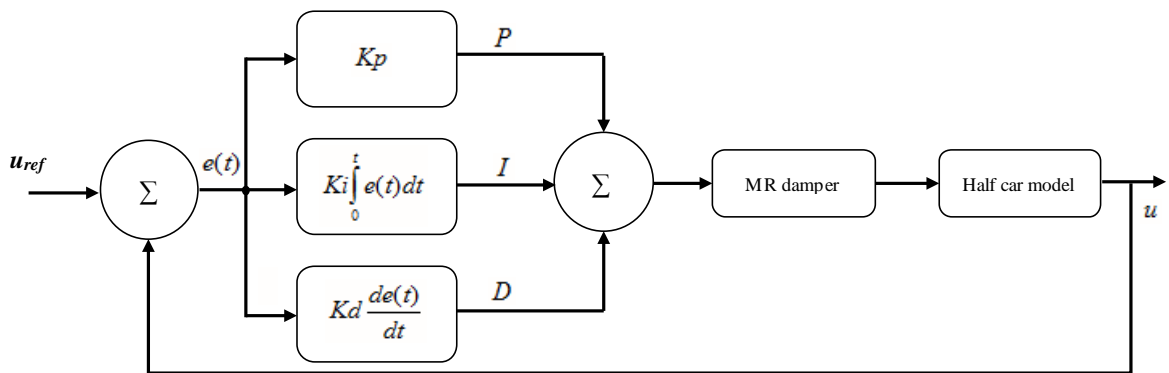


Figure 7.4 Control structure for half car model with PID controller

In PID controller, the better control action on the system can be achieved by tuning the parameters of the controller. Parameters of the PID controller are dependent of each other; if one of the parameter value changes, it affects the other two parameters. The manual tuning method is adapted to getting optimal parameters of PID controller is given in Table 7.3.

Table 7.3 Optimal parameter of PID controller

Parameters	K_p	K_i	K_d
Value	10	0.0008	1

7.3.1.3. Fuzzy logic control strategy

Fuzzy controllers are widely used in the automotive industry. Automatic transmissions, anti-braking system (ABS) and cruise control systems are frequently based on this paradigm of control theory. The idea of fuzzy control is to operate on rules that are human-readable and represent a humans heuristic knowledge about how to control a process (Slaski and Maciejewski (2011)). All rules are represented in a form of fuzzy logic implications. The fuzzy logic controller mainly consists of three stages such as fuzzification, fuzzy inference and defuzzification (Stribrsky et al. (2003)). The control structure for full car model with fuzzy logic controller is as shown in Figure 7.5.

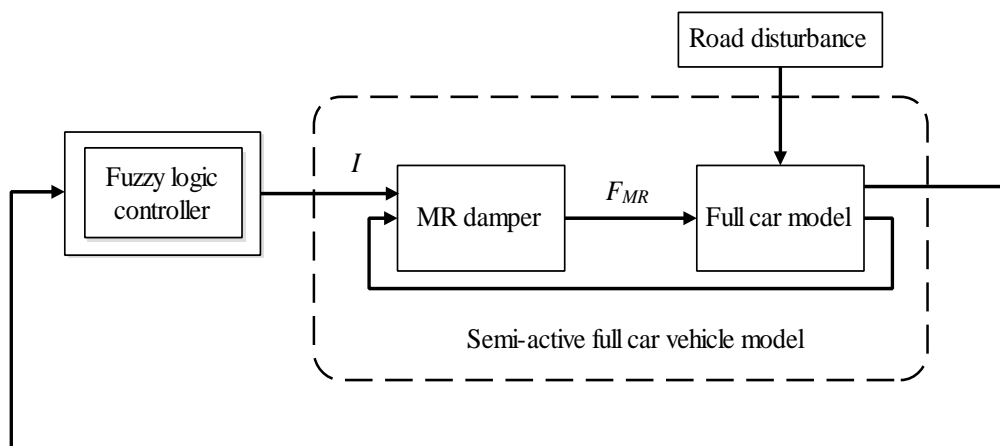


Figure 7.5 Control structure for full car model with fuzzy logic controller

Fuzzification is the process of generating membership value for fuzzy variables by using fuzzy sets. This involves a domain transformation where crisp inputs are transformed into fuzzy inputs. Crisp are exact inputs measured by sensors and passed into control system for processing. The fuzzy interference is formulating the mapping from a given input to an output using fuzzy logic. The mapping then provides a basis from which decision can be made. The fuzzy interference involves all the pieces that are described in membership function, logical operators and If-Then rules. The general form of the rules of the fuzzy logic controller is given below.

$$\text{IF } (\dot{x}_s - \dot{x}_u) \text{ AND } (\dot{x}_s) \text{ AND } (\ddot{x}_s) \text{ THEN } (I)$$

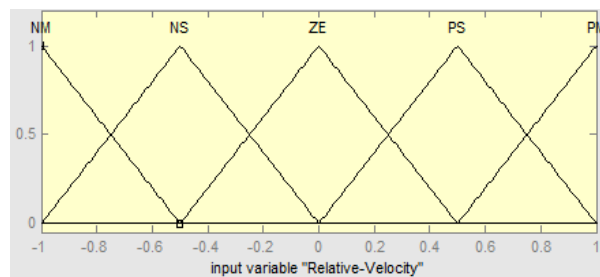
Where, \dot{x}_s is the sprung mass velocity, \dot{x}_u is unsprung mass velocity, \ddot{x}_s is sprung mass acceleration and I is the current output from controller to the MR damper.

The rule base used in the semi-active suspension system for full car model is represented by 75 rules with fuzzy terms derived by modelling the designer's knowledge (Changizi and Rouhani (2011)) and some rules which are used to control the full car model is given in Table 7.4. Finally, the defuzzifier converts the fuzzy inference input into a crisp set of output values. The membership functions are as shown in Figure 7.6.

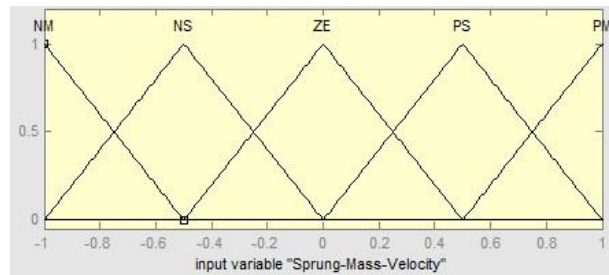
Table 7.4 Fuzzy rules

Rule number	Relative velocity	Sprung mass velocity	Sprung mass acceleration	Current
1	PM	PM	P	ZE
2	PS	PM	P	PM
3	PM	PS	ZE	ZE
4	NM	NS	ZE	ZE
5	NM	NS	P	NS
6	NS	NS	P	NS

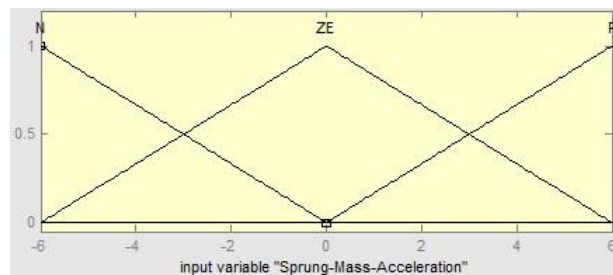
Where, PM- Positive medium, PS- Positive small, P- Positive, ZE- zero, NM- Negative medium, NS- Negative small and N- Negative.



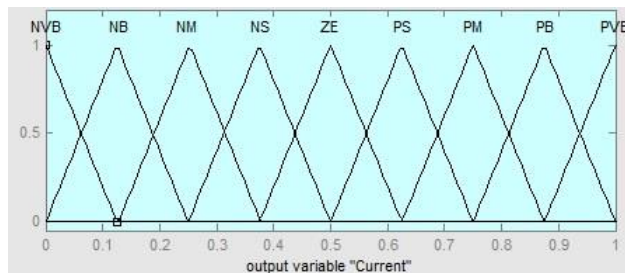
(a)



(b)



(c)



(d)

Figure 7.6 Fuzzy membership functions

7.3.2. Dynamic analysis of quarter car model

A quarter car model with two degree of freedom (DOF) system is analyzed by considering vertical DOF for sprung mass and unsprung mass as shown in Figure 7.7. The vehicle body is represented by sprung mass M_s , the mass due to axel and tire represented by unsprung mass M_u . The spring and damper connected between the sprung mass and unsprung mass represents the vehicle suspension system, K_s is the spring stiffness, F_d is the variable damping force developed by the MR damper.

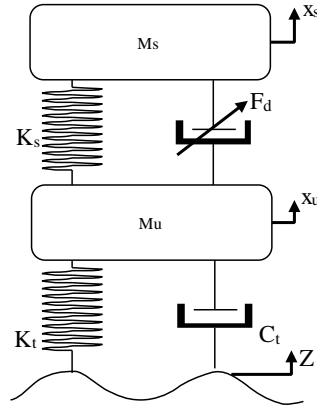


Figure 7.7 Quarter car model with semi-active suspension

Following are the equations of motion for quarter car model

Sprung mass bounce

$$M_s \ddot{x}_s + K_s(x_s - x_u) + F_d = 0 \quad (7.8)$$

Unsprung mass bounce

$$M_u \ddot{x}_u + C_t(\dot{x}_u - \dot{Z}) + K_s(x_u - x_s) + K_t(x_u - Z) - F_d = 0 \quad (7.9)$$

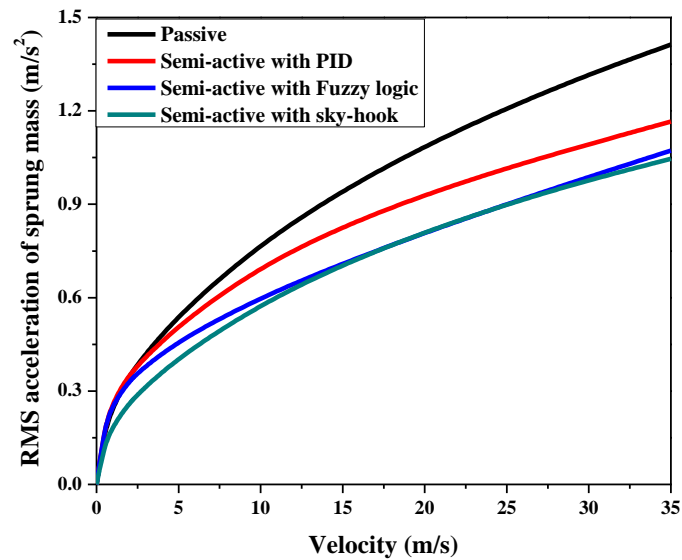
The above equation can be written in the form of state space variables given by

$$\begin{cases} \dot{x} = Ax + Bu \\ y = Cx + Du \end{cases} \quad (7.10)$$

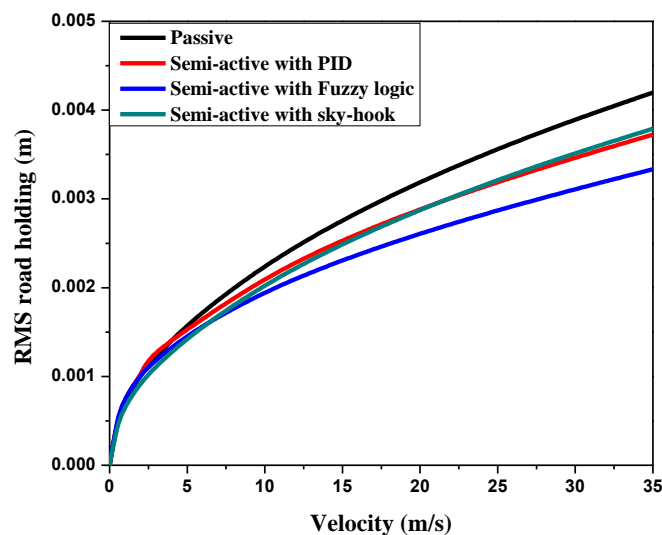
Where,

$$\begin{aligned} x &= [x_s \quad x_u \quad \dot{x}_s \quad \dot{x}_u]^T & u &= [F_d \quad Z \quad \dot{Z}]^T \\ A &= \begin{bmatrix} 0 & 0 & 1 & 0 \\ 0 & 0 & 0 & 1 \\ -\frac{K_s}{M_s} & \frac{K_s}{M_s} & 0 & 0 \\ \frac{K_s}{M_u} & -\left(\frac{K_s+K_t}{M_u}\right) & 0 & \frac{-C_t}{M_u} \end{bmatrix} & B &= \begin{bmatrix} 0 & 0 & 0 \\ 0 & 0 & 0 \\ -\frac{1}{M_s} & 0 & 0 \\ \frac{1}{M_u} & \frac{K_t}{M_u} & \frac{C_t}{M_u} \end{bmatrix} \\ C &= [1 \quad -1 \quad 0 \quad 0] & D &= [0 \quad 0 \quad 0] \end{aligned}$$

The comparative study between different semi-active control strategies has been carried out by using quarter car model subjected to random road irregularities and its responses are as given in Figure 7.8.



(a)



(b)

Figure 7.8 Responses of quarter car model with different control strategies (a) RMS acceleration response and (b) RMS road holding response

Figures 7.8 (a) and (b) shows the RMS acceleration and RMS road holding response of quarter car vehicle with semi-active suspension system respectively under different control strategies. Observation shows that the RMS acceleration semi-active

suspension system with fuzzy logic control strategy closely matches with responses of sky-hook control strategy. But in case of RMS road holding responses, the fuzzy logic control strategy provides considerable improvement than other control strategy.

Hence, fuzzy logic control is adopted to study dynamic response analysis of vehicle models.

7.3.2.1. Dynamic response analysis of quarter car model subjected to random road

The ride comfort and road holding analysis of two degree of freedom quarter car model has been carried out with passive and semi-active (MR damper) suspension system. In semi-active suspension system, MR damper has been modelled by using both non-parametric approach and Bouc-Wen model. Ride comfort in quarter car is mainly affected by vertical movement of the vehicle body.

Dynamic analysis has been carried out by using quarter car model with passive and semi-active suspension system subjected to random road irregularities. The acceleration response and its spectrum of the passive and semi-active quarter car suspension system at constant speed of 35 m/s are illustrated in Figures 7.9. Observation shows that, the semi-active suspension system reduces around 44% of vibration amplitude at resonance frequency of vehicle (Dong et al., 2010) than passive suspension system.

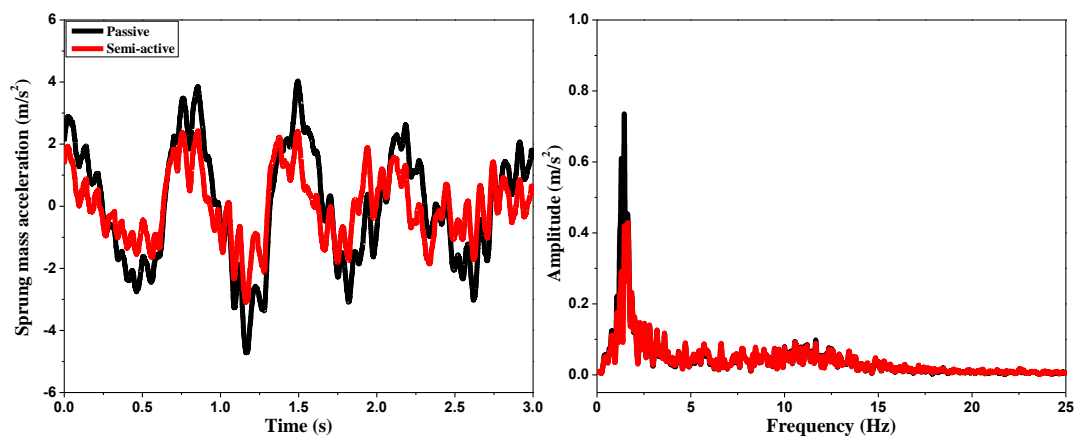


Figure 7.9 Sprung mass acceleration response in time domain and its spectrum

The RMS of the sprung mass acceleration response of both passive and semi-active suspension for different vehicle velocities is shown in Figure 7.10. Observation shows that semi-active suspension system significantly decreases vertical sprung mass acceleration than passive suspension system for all vehicle velocity. This indicates that the semi-active suspension system provides better ride comfort for a vehicle than passive suspension system.

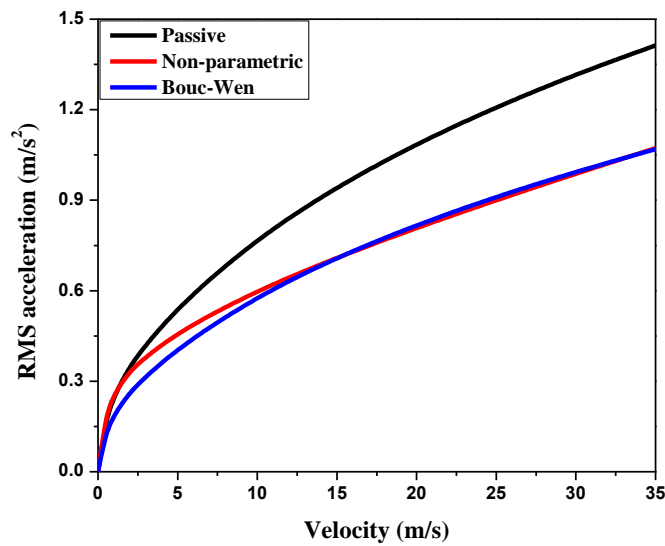


Figure 7.10 RMS acceleration of sprung mass v/s velocity

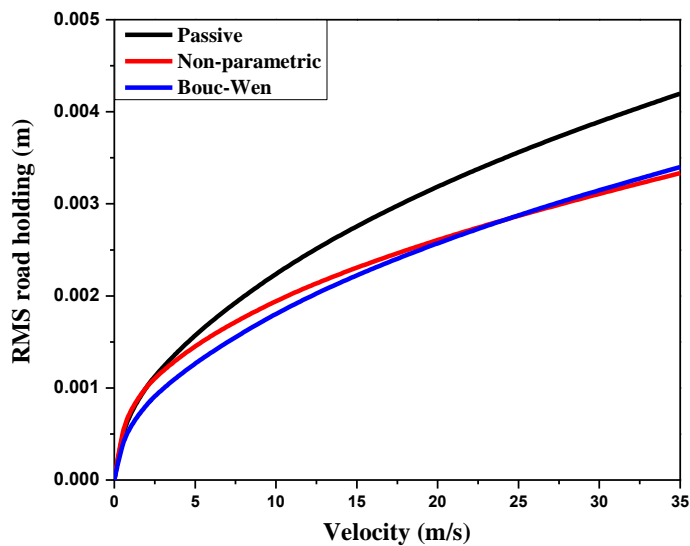


Figure 7.11 RMS road holding v/s velocities

The safety and vehicle stability are affected by firm contact between road surfaces and wheel. Figure 7.11 illustrates the road holding response, which measures the relative displacement between the unsprung mass and road irregularities with respect to different velocities. In this case also, road holding will be better with semi-active suspension than passive suspension for all velocities.

7.3.2.2. Dynamic response analysis of quarter car model subjected to road bump

Figure 7.12 illustrates the acceleration response of quarter car model under road bump profile. The quarter car model with developed non-parametric MR model and Bouc-Wen MR model based suspension system shows around 65% faster settling than passive suspension system. The response of the semi-active suspension system with novel developed non-parametric model is closely matched with the responses of semi-active suspension system with Bouc-Wen MR damper model.

Therefore, developed non-parametric MR damper model will be used as semi-active suspension system element in half car model and also in full car vehicle model.

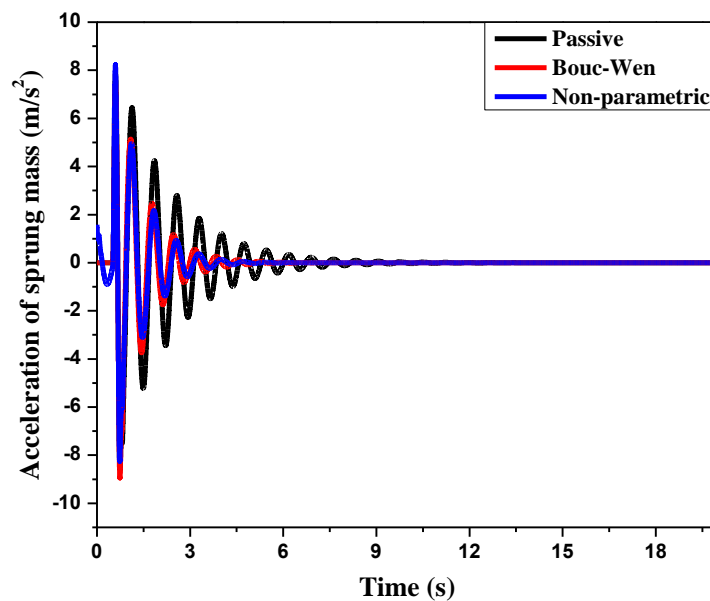


Figure 7.12 Acceleration of vehicle body under road bump

7.3.3. Dynamic analysis of half car model

Half car model with four degree of freedom system (Figure 7.13) is analyzed by considering vertical displacement (x_s) and pitch movement (θ) of vehicle body, vertical displacement of front and rear unsprung masses.

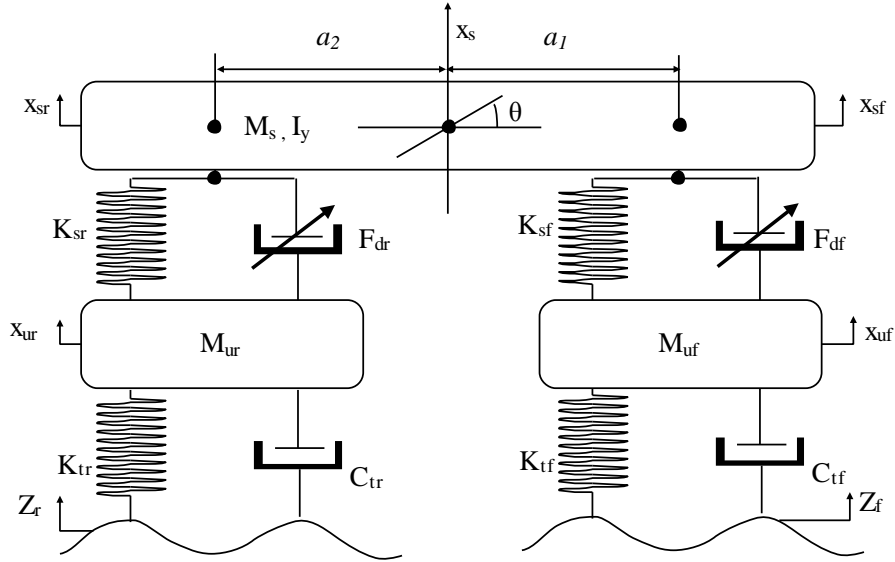


Figure 7.13 Half car model of vehicle

The displacement at each corner of the sprung mass is expressed in terms of bounce, pitch movement.

$$x_{sf} = x_s + a_1\theta \quad (7.11)$$

$$x_{sr} = x_s - a_2\theta \quad (7.12)$$

The equation of motion of a half car model can be described as follows

Sprung mass bounce

$$M_s\ddot{x}_s + K_{sf}(x_{sf} - x_{uf}) + K_{sr}(x_{sr} - x_{ur}) + F_{df} + F_{dr} = 0 \quad (7.13)$$

Sprung mass pitch

$$I_y\ddot{\theta} + a_1K_{sf}(x_{sf} - x_{uf}) - a_2K_{sr}(x_{sr} - x_{ur}) + a_1F_{df} - a_2F_{dr} = 0 \quad (7.14)$$

Unsprung mass bounce

$$M_{uf}\ddot{x}_{uf} + C_{tf}(\dot{x}_{uf} - \dot{h}_f) + K_{tf}(x_{uf} - h_f) - K_{sf}(x_{sf} - x_{uf}) - F_{df} = 0 \quad (7.15)$$

$$M_{ur}\ddot{x}_{ur} + C_{tr}(\dot{x}_{ur} - \dot{h}_r) + K_{tr}(x_{tr} - h_r) - K_{sr}(x_{sr} - x_{ur}) - F_{dr} = 0 \quad (7.16)$$

The above equation can be written in the form of state space variables as given by

$$\begin{cases} \dot{x} = Ax + Bu \\ y = Cx + Du \end{cases}$$

Where,

$$x = [x_s \quad \theta \quad x_{uf} \quad x_{ur} \quad \dot{x}_s \quad \dot{\theta} \quad \dot{x}_{uf} \quad \dot{x}_{ur}]^T$$

$$u = [F_{df} \quad F_{dr} \quad h_f \quad \dot{h}_f \quad h_r \quad \dot{h}_r]^T$$

$$A = \begin{bmatrix} A_{11} & A_{12} \\ A_{21} & A_{22} \end{bmatrix}$$

$$A_{11} = \begin{bmatrix} 0 & 0 & 0 & 0 \\ 0 & 0 & 0 & 0 \\ 0 & 0 & 0 & 0 \\ 0 & 0 & 0 & 0 \end{bmatrix} \quad A_{12} = \begin{bmatrix} 1 & 0 & 0 & 0 \\ 0 & 1 & 0 & 0 \\ 0 & 0 & 1 & 0 \\ 0 & 0 & 0 & 1 \end{bmatrix}$$

$$A_{21} = \begin{bmatrix} -\left(\frac{K_{sf} + K_{sr}}{M_s}\right) & \left(\frac{a_2 K_{sr} - a_1 K_{sf}}{M_s}\right) & \frac{K_{sf}}{M_s} & \frac{K_{sr}}{M_s} \\ \left(\frac{a_2 K_{sr} - a_1 K_{sf}}{I_y}\right) & -\left(\frac{a_1^2 K_{sf} + a_2^2 K_{sr}}{I_y}\right) & \frac{a_1 K_{sf}}{I_y} & \frac{-a_2 K_{sr}}{I_y} \\ \frac{K_{sf}}{M_{uf}} & \frac{a_1 K_{sf}}{M_{uf}} & -\left(\frac{K_{tf} + K_{sf}}{M_{uf}}\right) & 0 \\ \frac{K_{sr}}{M_{ur}} & \frac{-a_2 K_{sr}}{M_{ur}} & 0 & -\left(\frac{K_{sr} + K_{tr}}{M_{ur}}\right) \end{bmatrix}$$

$$A_{22} = \begin{bmatrix} 0 & 0 & 0 & 0 \\ 0 & 0 & 0 & 0 \\ 0 & 0 & \frac{-C_{tf}}{M_{uf}} & 0 \\ 0 & 0 & 0 & \frac{-C_{tr}}{M_{ur}} \end{bmatrix} \quad B = \begin{bmatrix} 0 & 0 & 0 & 0 & 0 & 0 \\ 0 & 0 & 0 & 0 & 0 & 0 \\ 0 & 0 & 0 & 0 & 0 & 0 \\ 0 & 0 & 0 & 0 & 0 & 0 \\ \frac{-1}{M_s} & \frac{-1}{M_s} & 0 & 0 & 0 & 0 \\ \frac{-a_1}{I_y} & \frac{a_2}{I_y} & 0 & 0 & 0 & 0 \\ \frac{1}{M_{uf}} & 0 & \frac{K_{tf}}{M_{uf}} & \frac{C_{tf}}{M_{uf}} & 0 & 0 \\ 0 & \frac{1}{M_{ur}} & 0 & 0 & \frac{K_{tr}}{M_{ur}} & \frac{C_{tr}}{M_{ur}} \end{bmatrix}$$

$$C = \begin{bmatrix} 1 & 0 & 0 & 0 & 0 & 0 & 0 & 0 \\ 0 & 1 & 0 & 0 & 0 & 0 & 0 & 0 \end{bmatrix}$$

$$D = [0 \ 0 \ 0 \ 0 \ 0 \ 0]$$

7.3.3.1. Dynamic response analysis of half car model subjected to random road

Dynamic response analysis of half car model with passive and semi-active suspension system has been carried out under random road irregularities. The acceleration response and pitch rate of the passive and semi-active half car suspension system at constant speed of 35 m/s are illustrated in Figures 7.14 and 7.15. It is observed that sprung mass acceleration and pitch rate are reduced in case of semiactive suspension system than passive suspension system.

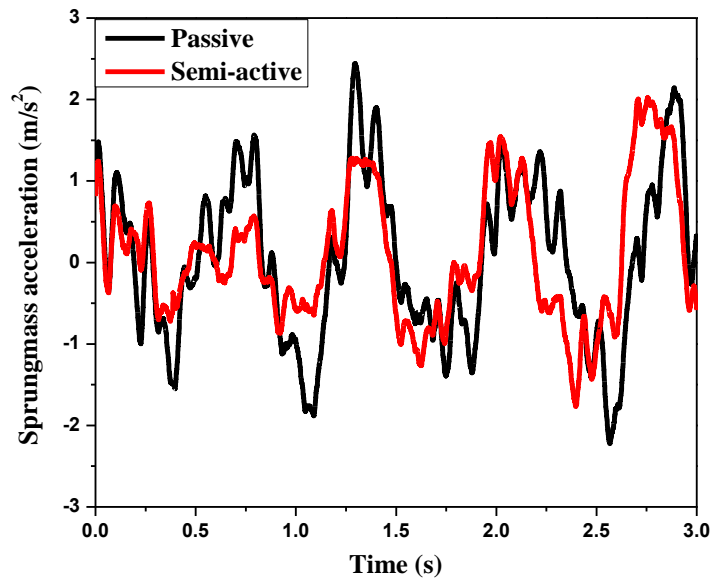


Figure 7.14 Half car sprung mass acceleration in time domain

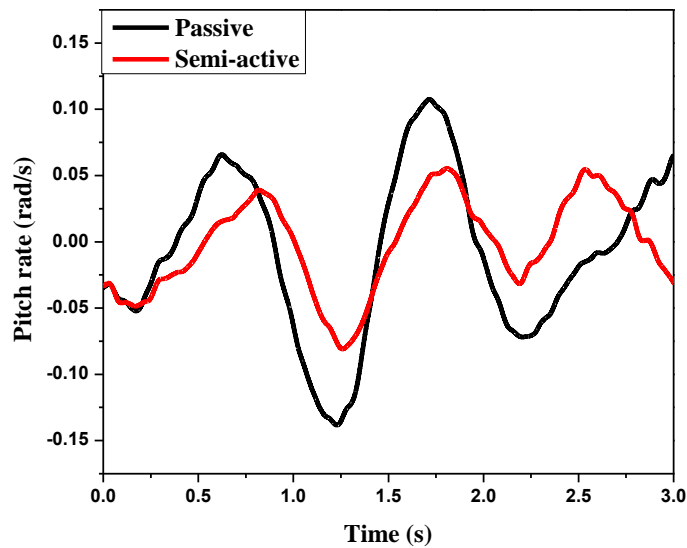


Figure 7.15 Half car pitch rate in time domain

The ride comfort and road holding analysis of half car model with passive and semi-active suspension system has been carried out under random irregularities for different vehicle velocities. Figures 7.16 and 7.17 demonstrate RMS bounce and pitch acceleration responses of sprung mass respectively with different vehicle velocity. It is observed that half car model with developed non-parametric MR based suspension system provides 21% reduction in bounce acceleration and 40% reduction in pitch motion than passive suspension system.

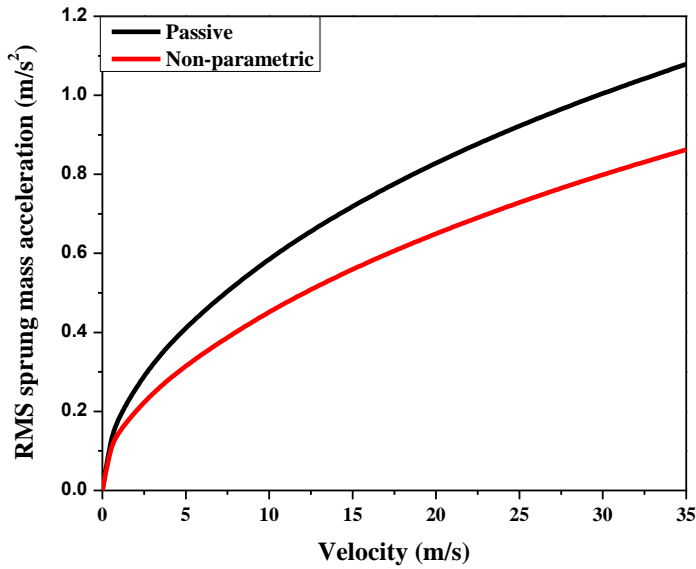


Figure 7.16 Vertical acceleration of Sprung mass

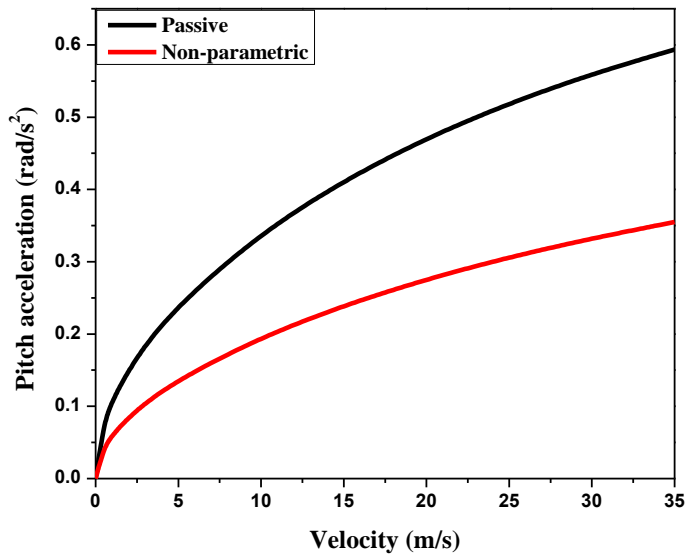


Figure 7.17 Pitch acceleration of Sprung mass

Figures 7.18 and 7.19 depict front and rear road holding (tire deflection) responses of half car model with different vehicle velocity. In this case also, vehicle with MR based suspension system shows around 16% improvement than passive suspension system.

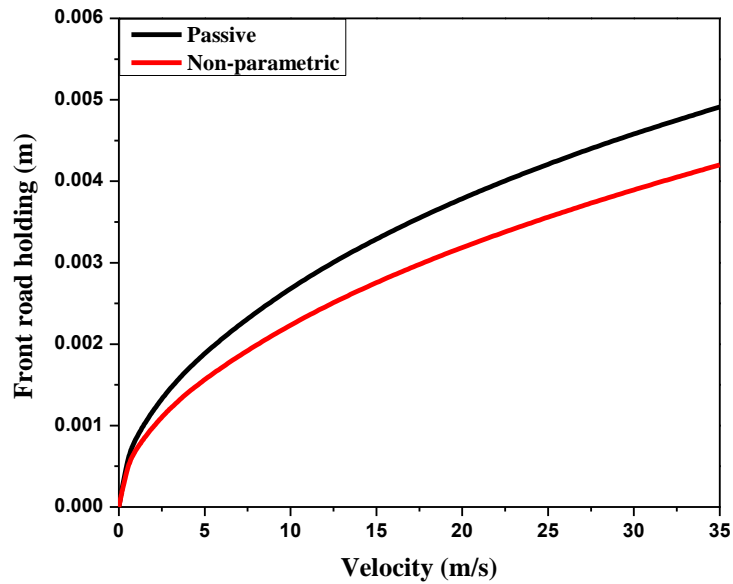


Figure 7.18 Road holding of front wheel

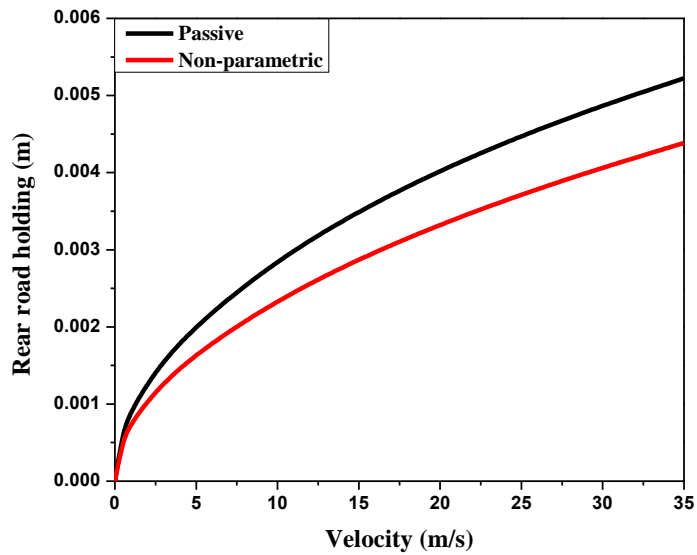


Figure 7.19 Road holding of rear wheel

7.3.3.2. Dynamic response analysis of half car model subjected to road bump

Dynamic response of the half car model subjected to road bump and corresponding responses are given in Figures 7.20 and 7.21 respectively. It can be observed that the MR damper based suspension system shows 13% reduction in peak amplitude and 63% faster settling than passive suspension system.

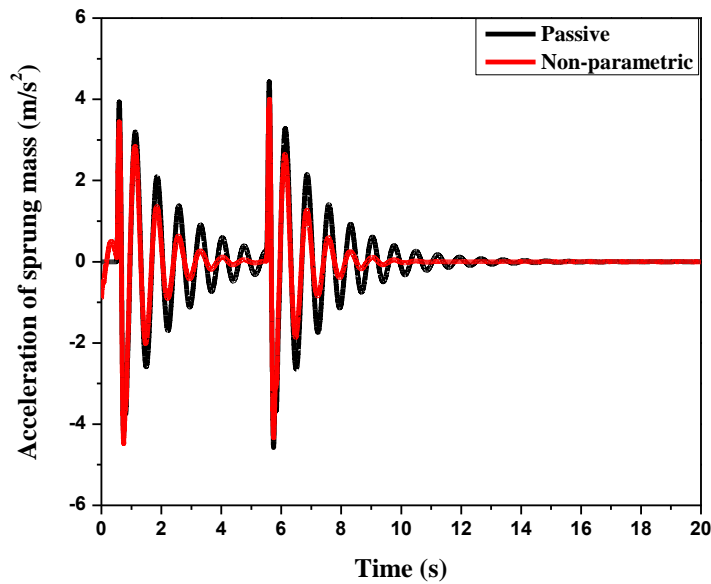


Figure 7.20 Acceleration of vehicle body under road bump

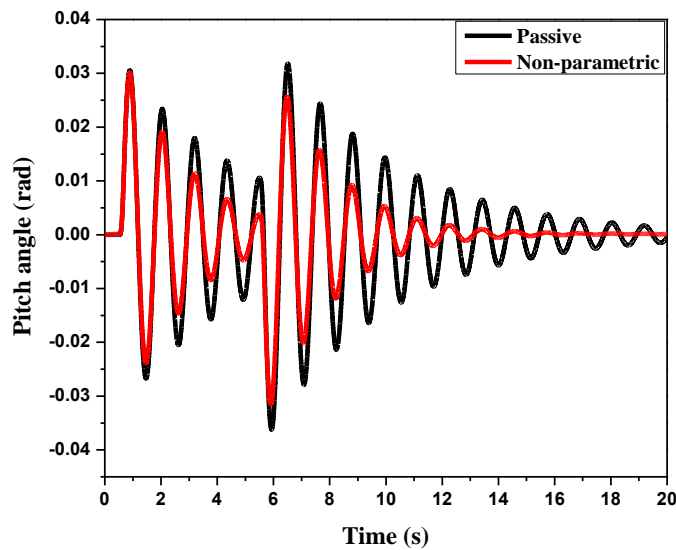


Figure 7.21 Pitch angle of vehicle body under road bump

7.3.4. Dynamic analysis of full car model

The ride comfort and road holding performance of a full car model with seven degrees of freedom system is analyzed by considering vertical movement (x_s), pitch movement (θ), roll movement (ϕ) of vehicle body and four unsprung masses bounce. The full car model is as shown in Figure 7.22.

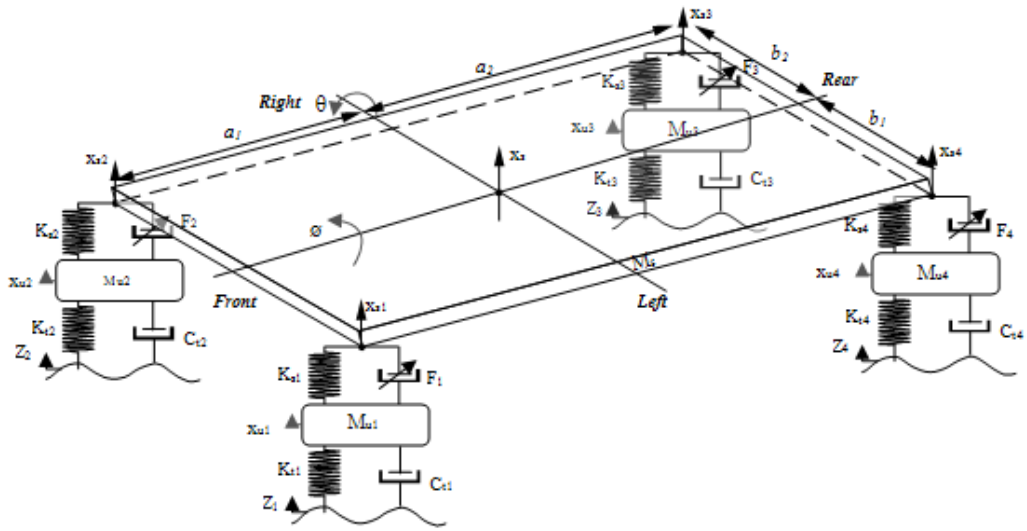


Figure 7.22 Full car vehicle model

The displacement at each corner of the sprung mass is expressed in terms of bounce, pitch and roll movement.

$$x_{s1} = x_s - a_1\theta + b_1\phi \quad (7.17)$$

$$x_{s2} = x_s - a_1\theta - b_2\phi \quad (7.18)$$

$$x_{s3} = x_s + a_2\theta - b_2\phi \quad (7.19)$$

And

$$x_{s4} = x_s + a_2\theta + b_2\phi \quad (7.20)$$

The dynamic equations of full car model are given as follows

Sprung mass bounce

$$M_s\ddot{x}_s + k_{s1}(x_s - a_1\theta + b_1\phi - x_{u1}) + k_{s2}(x_s - a_1\theta - b_2\phi - x_{u2}) + k_{s3}(x_s + a_2\theta - b_2\phi - x_{u3}) + k_{s4}(x_s + a_2\theta + b_1\phi - x_{u4}) + F_1 + F_2 + F_3 + F_4 = 0 \quad (7.21)$$

Sprung mass roll

$$I_x\ddot{\phi} + b_1k_{s1}(x_s - a_1\theta + b_1\phi - x_{u1}) - b_2k_{s2}(x_s - a_1\theta - b_2\phi - x_{u2}) - \quad (7.22)$$

$$b_2 k_{s3}(x_s + a_2 \theta - b_2 \phi - x_{u3}) + b_1 k_{s4}(x_s + a_2 \theta + b_1 \phi - x_{u4}) + b_1 F_1 - b_2 F_2 - b_2 F_3 + b_1 F_4 = 0$$

Sprung mass pitch

$$I_y \ddot{\theta} - a_1 k_{s1}(x_s - a_1 \theta + b_1 \phi - x_{u1}) - a_1 k_{s2}(x_s - a_1 \theta - b_2 \phi - x_{u2}) + a_2 k_{s3}(x_s + a_2 \theta - b_2 \phi - x_{u3}) + a_2 k_{s4}(x_s + a_2 \theta + b_1 \phi - x_{u4}) - a_1 F_1 - a_1 F_2 + a_2 F_3 + a_2 F_4 = 0 \quad (7.23)$$

Unsprung mass bounce

$$M_{u1} \ddot{x}_{u1} + c_{t1}(\dot{x}_{u1} - \dot{Z}_1) + k_{t1}(x_{u1} - Z_1) - k_{s1}(x_s - a_1 \theta + b_1 \phi - x_{u1}) - F_1 = 0 \quad (7.24)$$

$$M_{u2} \ddot{x}_{u2} + c_{t2}(\dot{x}_{u2} - \dot{Z}_2) + k_{t2}(x_{u2} - Z_2) - k_{s2}(x_s - a_1 \theta - b_2 \phi - x_{u2}) - F_2 = 0 \quad (7.25)$$

$$M_{u3} \ddot{x}_{u3} + c_{t3}(\dot{x}_{u3} - \dot{Z}_3) + k_{t3}(x_{u3} - Z_3) - k_{s3}(x_s + a_2 \theta - b_2 \phi - x_{u3}) - F_3 = 0 \quad (7.26)$$

$$M_{u4} \ddot{x}_{u4} + c_{t4}(\dot{x}_{u4} - \dot{Z}_4) + k_{t4}(x_{u4} - Z_4) - k_{s4}(x_s + a_2 \theta + b_1 \phi - x_{u4}) - F_4 = 0 \quad (7.27)$$

The above equation can be written in the form of state space variables given by

$$\begin{cases} \dot{x} = Ax + Bu \\ y = Cx + Du \end{cases}$$

Where,

$$x = [x_s \quad \theta \quad \phi \quad x_{u1} \quad x_{u2} \quad x_{u3} \quad x_{u4} \quad \dot{x}_s \quad \dot{\theta} \quad \dot{\phi} \quad \dot{x}_{u1} \quad \dot{x}_{u2} \quad \dot{x}_{u3} \quad \dot{x}_{u4}]^T$$

$$u = [F_1 \quad F_2 \quad F_3 \quad F_4 \quad Z_1 \quad \dot{Z}_1 \quad Z_2 \quad \dot{Z}_2 \quad Z_3 \quad \dot{Z}_3 \quad Z_4 \quad \dot{Z}_4]^T$$

$$A = \begin{bmatrix} A_{11} & A_{12} \\ A_{21} & A_{22} \end{bmatrix}$$

$$A_{11} = \begin{bmatrix} 0 & 0 & 0 & 0 & 0 & 0 & 0 & 0 \\ 0 & 0 & 0 & 0 & 0 & 0 & 0 & 0 \\ 0 & 0 & 0 & 0 & 0 & 0 & 0 & 0 \\ 0 & 0 & 0 & 0 & 0 & 0 & 0 & 0 \\ 0 & 0 & 0 & 0 & 0 & 0 & 0 & 0 \\ 0 & 0 & 0 & 0 & 0 & 0 & 0 & 0 \\ 0 & 0 & 0 & 0 & 0 & 0 & 0 & 0 \end{bmatrix} \quad A_{12} = \begin{bmatrix} 1 & 0 & 0 & 0 & 0 & 0 & 0 & 0 \\ 0 & 1 & 0 & 0 & 0 & 0 & 0 & 0 \\ 0 & 0 & 1 & 0 & 0 & 0 & 0 & 0 \\ 0 & 0 & 0 & 1 & 0 & 0 & 0 & 0 \\ 0 & 0 & 0 & 0 & 1 & 0 & 0 & 0 \\ 0 & 0 & 0 & 0 & 0 & 1 & 0 & 0 \\ 0 & 0 & 0 & 0 & 0 & 0 & 1 & 0 \\ 0 & 0 & 0 & 0 & 0 & 0 & 0 & 1 \end{bmatrix}$$

$$A_{21} = [A_1 \quad A_2 \quad A_3 \quad A_4 \quad A_5 \quad A_6 \quad A_7]$$

$$A_1 = \begin{bmatrix} -\left(\frac{k_{s1}+k_{s2}+k_{s3}+k_{s4}}{M_s}\right) \\ \left(\frac{a_1k_{s1}+a_1k_{s2}-a_2k_{s3}-a_2k_{s4}}{I_y}\right) \\ \left(\frac{-b_1k_{s1}+b_2k_{s2}+b_2k_{s3}-b_1k_{s4}}{I_x}\right) \\ \frac{k_{s1}}{M_{u1}} \\ \frac{k_{s2}}{M_{u2}} \\ \frac{k_{s3}}{M_{u3}} \\ \frac{k_{s4}}{M_{u4}} \end{bmatrix} \quad A_2 = \begin{bmatrix} \left(\frac{a_1k_{s1}+a_1k_{s2}-a_2k_{s3}-a_2k_{s4}}{M_s}\right) \\ -\left(\frac{a_1^2k_{s1}+a_1^2k_{s2}+a_2^2k_{s3}+a_2^2k_{s4}}{I_y}\right) \\ \left(\frac{a_1b_1k_{s1}-a_1b_2k_{s2}+a_2b_2k_{s3}-a_2b_1k_{s4}}{I_x}\right) \\ \frac{-a_1k_{s1}}{M_{u1}} \\ \frac{-a_1k_{s2}}{M_{u2}} \\ \frac{a_2k_{s3}}{M_{u3}} \\ \frac{a_2k_{s4}}{M_{u4}} \end{bmatrix}$$

$$A_3 = \begin{bmatrix} \left(\frac{-b_1k_{s1}+b_2k_{s2}+b_2k_{s3}-b_1k_{s4}}{M_s}\right) \\ \left(\frac{a_1b_1k_{s1}-a_1b_2k_{s2}+a_2b_2k_{s3}-a_2b_1k_{s4}}{I_y}\right) \\ -\left(\frac{b_1^2k_{s1}+b_2^2k_{s2}+b_2^2k_{s3}+b_1^2k_{s4}}{I_x}\right) \\ \frac{b_1k_{s1}}{M_{u1}} \\ \frac{-b_2k_{s2}}{M_{u2}} \\ \frac{-b_2k_{s3}}{M_{u3}} \\ \frac{b_1k_{s4}}{M_{u4}} \end{bmatrix} \quad A_4 = \begin{bmatrix} \frac{k_{f1}}{M_s} \\ \frac{-a_1k_{s1}}{I_y} \\ \frac{b_1k_{s1}}{I_x} \\ -\left(\frac{k_{t1}+k_{s1}}{M_{u1}}\right) \\ 0 \\ 0 \\ 0 \end{bmatrix}$$

$$A_5 = \begin{bmatrix} \frac{k_{s2}}{M_s} \\ \frac{-a_1k_{s2}}{I_y} \\ \frac{-b_2k_{s2}}{I_x} \\ 0 \\ -\left(\frac{k_{t2}+k_{s2}}{M_{u2}}\right) \\ 0 \\ 0 \end{bmatrix} \quad A_6 = \begin{bmatrix} \frac{k_{s3}}{M_s} \\ \frac{a_2k_{s3}}{I_y} \\ \frac{-b_2k_{s3}}{I_x} \\ 0 \\ 0 \\ -\left(\frac{k_{t3}+k_{s3}}{M_{u3}}\right) \\ 0 \end{bmatrix} \quad A_7 = \begin{bmatrix} \frac{k_{s4}}{M_s} \\ \frac{a_2k_{s4}}{I_y} \\ \frac{b_1k_{s4}}{I_x} \\ 0 \\ 0 \\ -\left(\frac{k_{t4}+k_{s4}}{M_{u4}}\right) \\ 0 \end{bmatrix}$$

$$A_{22} = \begin{bmatrix} 0 & 0 & 0 & 0 & 0 & 0 & 0 & 0 \\ 0 & 0 & 0 & 0 & 0 & 0 & 0 & 0 \\ 0 & 0 & 0 & 0 & 0 & 0 & 0 & 0 \\ 0 & 0 & 0 & \frac{-c_{t1}}{M_{u1}} & 0 & 0 & 0 & 0 \\ 0 & 0 & 0 & 0 & \frac{-c_{t2}}{M_{u2}} & 0 & 0 & 0 \\ 0 & 0 & 0 & 0 & 0 & \frac{-c_{t3}}{M_{u3}} & 0 & 0 \\ 0 & 0 & 0 & 0 & 0 & 0 & 0 & \frac{-c_{t4}}{M_{u4}} \end{bmatrix}$$

$$B = \begin{bmatrix} 0 & 0 & 0 & 0 & 0 & 0 & 0 & 0 & 0 & 0 & 0 & 0 \\ 0 & 0 & 0 & 0 & 0 & 0 & 0 & 0 & 0 & 0 & 0 & 0 \\ 0 & 0 & 0 & 0 & 0 & 0 & 0 & 0 & 0 & 0 & 0 & 0 \\ 0 & 0 & 0 & 0 & 0 & 0 & 0 & 0 & 0 & 0 & 0 & 0 \\ 0 & 0 & 0 & 0 & 0 & 0 & 0 & 0 & 0 & 0 & 0 & 0 \\ 0 & 0 & 0 & 0 & 0 & 0 & 0 & 0 & 0 & 0 & 0 & 0 \\ 0 & 0 & 0 & 0 & 0 & 0 & 0 & 0 & 0 & 0 & 0 & 0 \\ -1 & -1 & -1 & -1 & 0 & 0 & 0 & 0 & 0 & 0 & 0 & 0 \\ \frac{M_s}{a_1} & \frac{M_s}{a_1} & \frac{M_s}{-a_2} & \frac{M_s}{-a_2} & 0 & 0 & 0 & 0 & 0 & 0 & 0 & 0 \\ \frac{I_y}{-b_1} & \frac{I_y}{b_2} & \frac{I_y}{b_2} & \frac{I_y}{-b_1} & 0 & 0 & 0 & 0 & 0 & 0 & 0 & 0 \\ \frac{I_x}{1} & \frac{I_x}{1} & \frac{I_x}{1} & \frac{I_x}{1} & 0 & 0 & 0 & 0 & 0 & 0 & 0 & 0 \\ \frac{1}{M_{u1}} & 0 & 0 & 0 & \frac{k_{t1}}{M_{u1}} & \frac{c_{t1}}{M_{u1}} & 0 & 0 & 0 & 0 & 0 & 0 \\ 0 & \frac{1}{M_{u2}} & 0 & 0 & 0 & 0 & \frac{k_{t2}}{M_{u2}} & \frac{c_{t2}}{M_{u2}} & 0 & 0 & 0 & 0 \\ 0 & 0 & \frac{1}{M_{u3}} & 0 & 0 & 0 & 0 & 0 & \frac{k_{t3}}{M_{u3}} & \frac{c_{t3}}{M_{u3}} & 0 & 0 \\ 0 & 0 & 0 & \frac{1}{M_{u4}} & 0 & 0 & 0 & 0 & 0 & 0 & \frac{k_{t4}}{M_{u4}} & \frac{c_{t4}}{M_{u4}} \end{bmatrix}$$

$$C = \begin{bmatrix} 1 & 0 & 0 & 0 & 0 & 0 & 0 & 0 & 0 & 0 & 0 & 0 & 0 \\ 0 & 1 & 0 & 0 & 0 & 0 & 0 & 0 & 0 & 0 & 0 & 0 & 0 \\ 0 & 0 & 1 & 0 & 0 & 0 & 0 & 0 & 0 & 0 & 0 & 0 & 0 \end{bmatrix}$$

$$D = [0 \ 0 \ 0 \ 0 \ 0 \ 0 \ 0 \ 0 \ 0 \ 0 \ 0 \ 0 \ 0]$$

7.3.4.1. Dynamic response analysis of full car model subjected to random road

Dynamic response analysis of seven DOF full car vehicle model with passive and MR based suspension system has been carried out under random irregularities. The bounce acceleration, pitch rate and roll rate responses at constant speed of 35 m/s are shown in Figures 7.23 to 7.25 respectively.

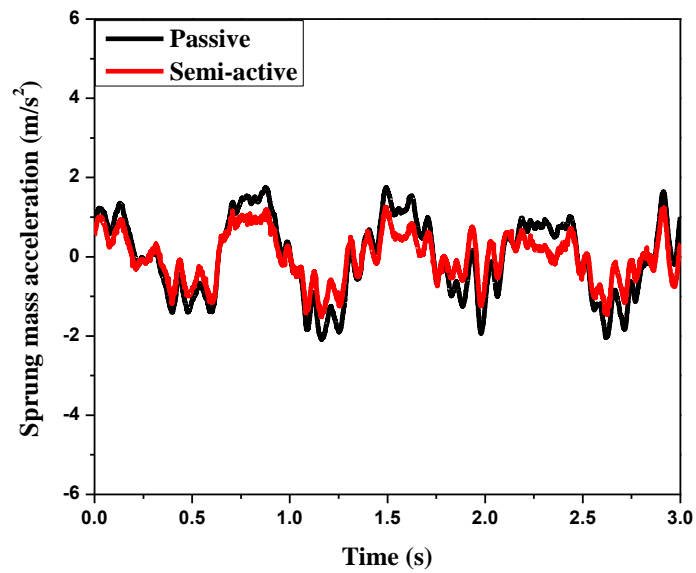


Figure 7.23 Acceleration of sprung mass in time domain

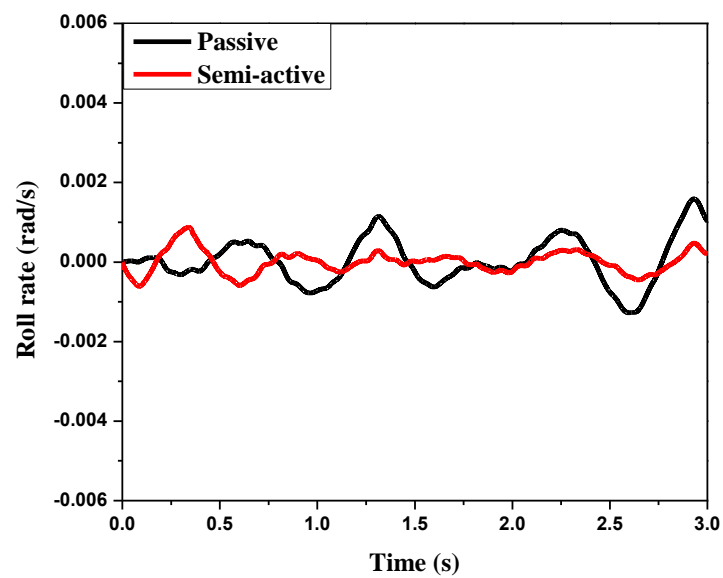


Figure 7.24 Full car roll rate in time domain

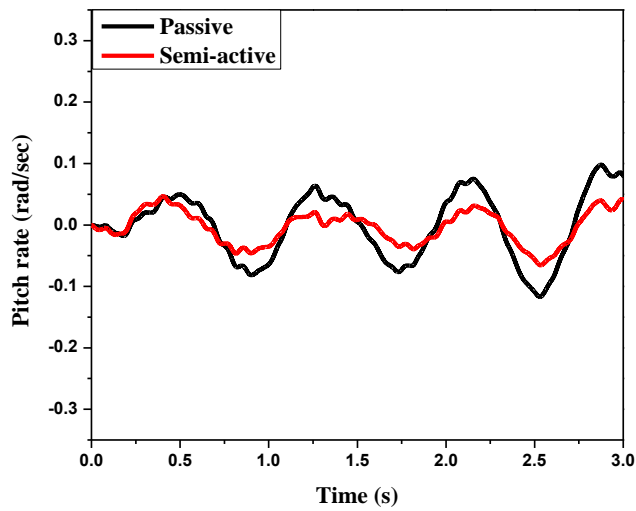


Figure 7.25 Full car pitch rate in time domain

The RMS acceleration, roll acceleration, pitch acceleration and four unsprung mass deflection (road holding) responses are computed for full car vehicle model with passive and MR based suspension system under random road irregularities with different vehicle velocities. The corresponding responses are shown in Figures 7.26-7.28 respectively. It can be observed that developed MR based suspension system performs better than passive suspension system with respect to all vehicle responses for all vehicle velocity.

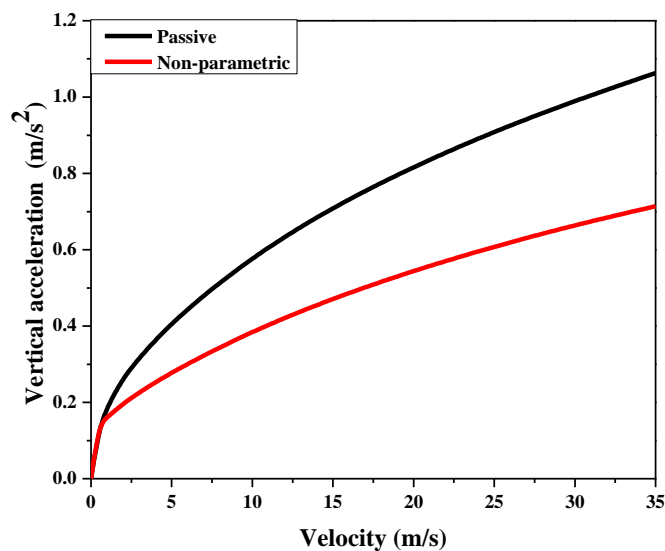


Figure 7.26 RMS acceleration of sprung mass v/s velocity

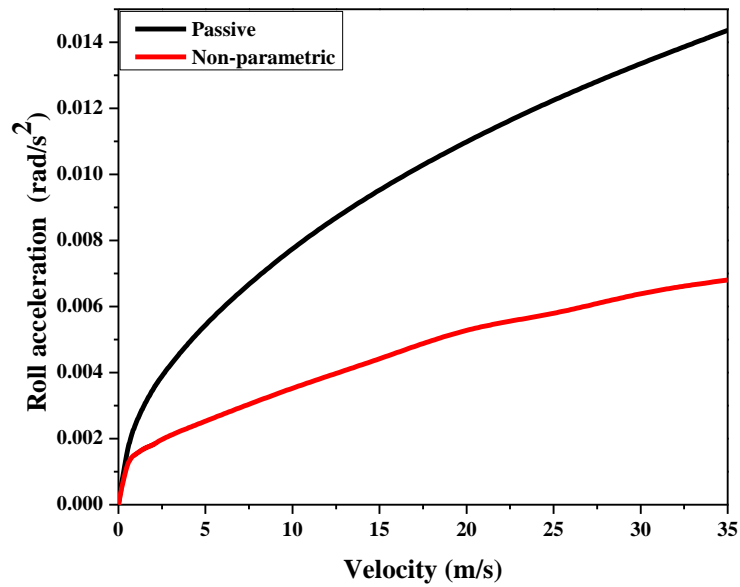


Figure 7.27 RMS acceleration of roll rate v/s velocity

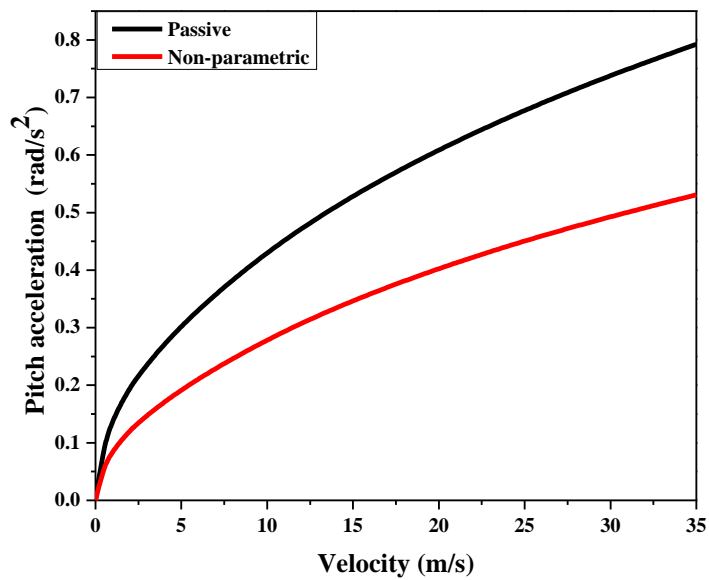


Figure 7.28 RMS acceleration of pitch rate v/s velocity

The road holding responses of four wheel such as front left and right side, rear right and left side of vehicle are given in Figures 7.29 to 7.32. In this case also, the semi-active suspension system shows considerable improvement in road holding than passive suspension system.

In comparison with passive suspension system, MR damper suspension system shows 32 % reduction vertical acceleration, 52 % reduction in roll motion, 33 % reduction in pitch motion of sprung mass and average 10% improvement in road holding attained.

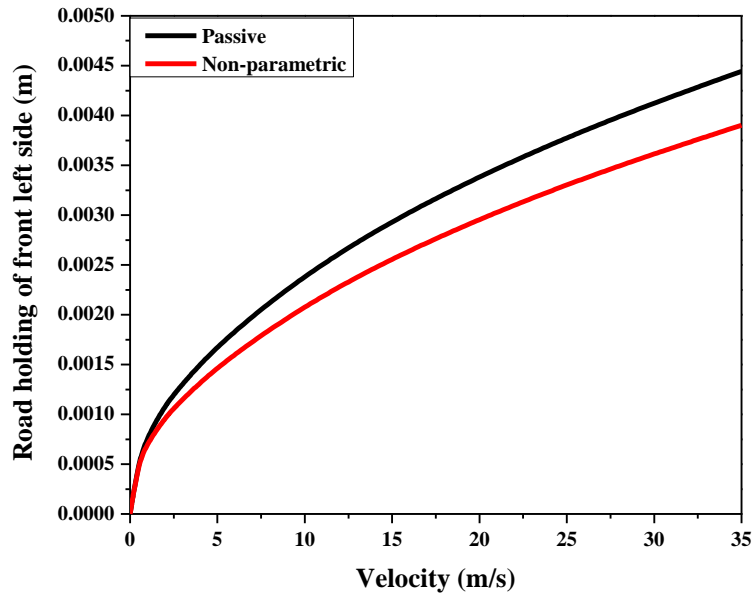


Figure 7.29 Road holding of front left wheel

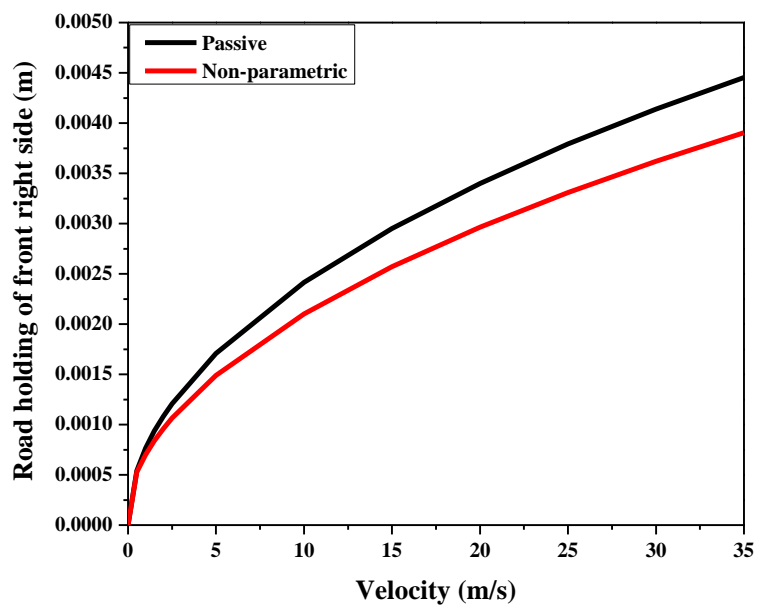


Figure 7.30 Road holding of front right wheel

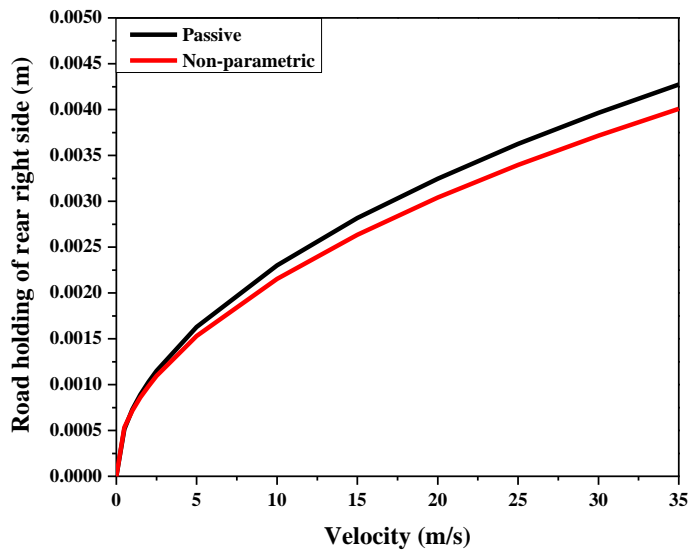


Figure 7.31 Road holding of rear right wheel

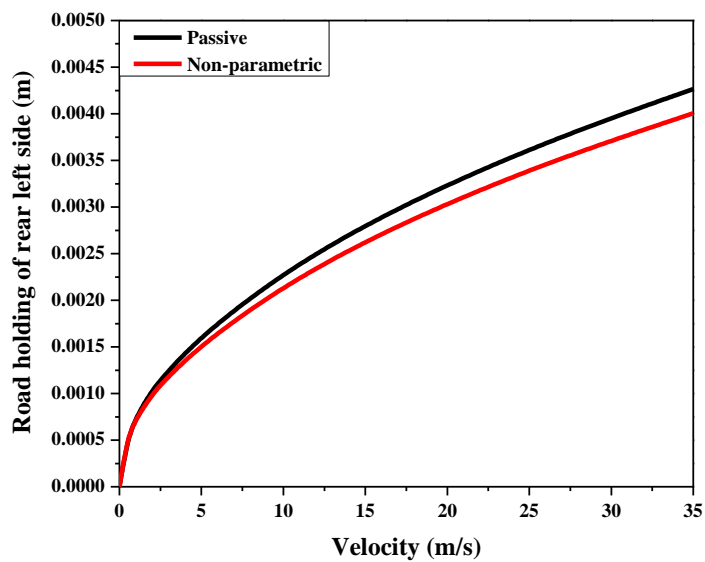


Figure 7.32 Road holding of rear left wheel

7.3.4.2. Dynamic response analysis of full car model subjected to road bump

Dynamic response of the full car vehicle model subjected to road bump profile and its acceleration response of vehicle body is depicted in Figure 7.33. It is demonstrated that, MR damper based suspension system shows 13% reduction in peak amplitude and 80% faster settling than passive suspension system.

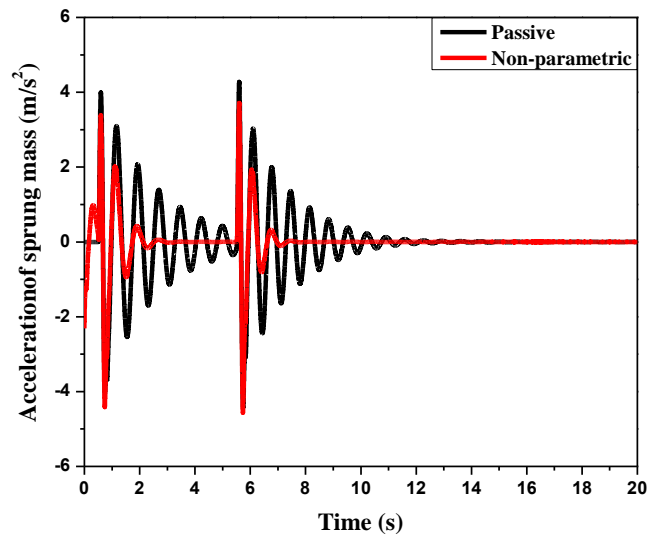


Figure 7.33 Acceleration of vehicle body under road bump

Figure 7.34 illustrates roll angle response of the vehicle body. Observation shows that the full car vehicle model with nonparametric MR based suspension system provides 58% peak amplitude reduction and 77% faster settling than passive suspension system.

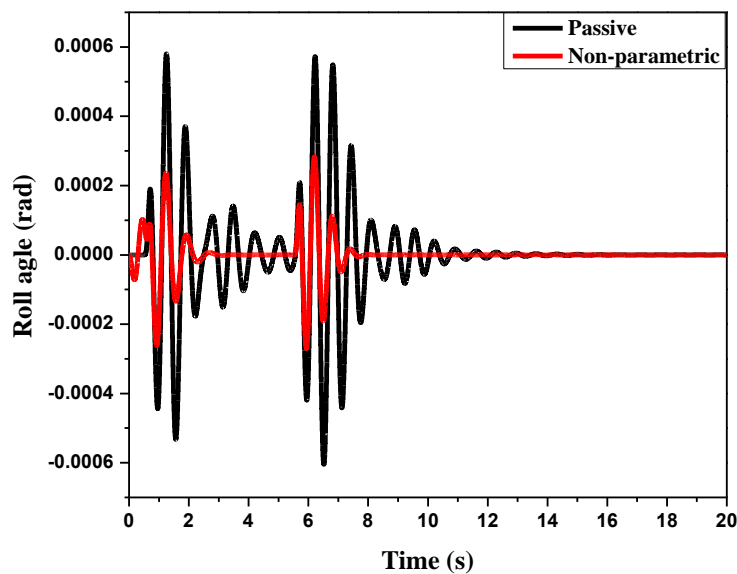


Figure 7.34 Roll angle of vehicle body under road bump

7.4. SUMMARY

The dynamic response analysis of vehicle with passive and semi-active suspension system is studied by using quarter car, half car and full car mathematical models subjected to random road and road bump as inputs. The comparative study between different control strategies such as sky-hook, fuzzy logic and PID controllers are carried out using quarter car model with developed non-parametric based MR suspension system. The result demonstrated that quarter car model with fuzzy logic control strategy provides better control performance for a vehicle than other control strategies. Also, quarter car model with Bouc-Wen MR model based suspension system is analyzed to benchmark the developed non parametric model and the responses of non-parametric model shows good agreement with Bouc-Wen model. Hence, the non-parametric MR model and fuzzy logic control strategy has been adopted in half car model and also in full car vehicle to study dynamic behaviour. The results of vehicle with nonparametric MR based suspension system are compared with passive suspension system. It shows that the vehicle with non-parametric based MR suspension system provides good vibration isolation for passenger vehicle than passive suspension system.

CHAPTER-8

CONCLUSIONS

8.1. SUMMARY

This research work started with design and optimization of MR damper to study the variation of magnetic flux density induced in the fluid flow gap with electromagnetic circuit parameters such as number of turns, current magnitude, fluid flow gap, core length and flange length by using FEA. The optimum fluid flow gap obtained from optimization study for maximizing the damper performance is used to fabricate the prototype MR damper. Along with geometrical parameters, other parameters such as proportion of MR fluid, operating frequencies and applied current also have influence on the damper performance. Based on the experimental result (damper force), the optimum level of these parameters are also evaluated by using Taguchi design of experimental technique. After evaluating the optimum parameters, dynamic behavior of MR damper with optimum parameters have been studied by using custom built dynamic testing machine.

In the present study, attempt has been made to develop nonparametric MR damper model by using magnetic flux density induced in fluid flow gap from “magneto-static analysis” results. By using statistical data categorizing technique, entire magnetic flux density developed in the fluid flow gap is divided into five categories based on the maximum and minimum total magnetic flux density for corresponding current value. The average total magnetic flux density from the statistical data categorizing technique has been used to determine the damper force. The polynomial model is used to describe force as a function of the current (I) applied to the MR damper. The hysteresis loop of MR damper is fitted by polynomial with sinusoidal displacement function ($x=a \sin (2\Pi ft)$). The Bouc-Wen MR model is considered to benchmark the developed nonparametric model. The parameters of the

Bouc-Wen models are evaluated by using NSGA-II optimization technique. The proposed novel nonparametric MR damper model is validated with experimental investigations and Bouc-Wen model result.

Performance of developed MR damper is analyzed by incorporating it into the vehicle model as suspension element. Dynamic response analysis of vehicle is studied by using mathematical models such as quarter car model, half car model and full car vehicle model subjected to the random road irregularities and road bump inputs. The comparative studies are conducted between passive and MR based suspension system.

8.2. CONTRIBUTIONS

- Found the optimal level of parameters on the performance of MR damper by using Taguchi design of experiments.
- Developed novel nonparametric MR damper model by using magnetic flux density induced in the fluid flow gap from “magneto-static analysis” results with help of statistical data categorizing technique.
- Developed mathematical model of quarter car, half car and full car vehicle model with passive and semi-active suspension system. The developed novel non-parametric model is used as MR damper in semi-active suspension system and studied performance of the vehicle in terms of ride comfort and road holding of vehicle under average road condition.

8.3. CONCLUSIONS

- The optimization of electromagnetic circuit of an MR damper is performed based on magnetostatic analysis to maximize magnetic flux density in the fluid flow gap considering different design parameters using DOE. Significant increase in magnetic flux density in the fluid flow gap is observed with increase of applied current, number of turns in a coil, coil core length while it decreases with increase of fluid flow gap and flange length. It was also found that the fluid flow gap size of less than 1.12 mm causes significant increase of magnetic flux density.
- Evaluation of optimal parameters such as proportion of MR fluid and operating frequencies on performance of the damper was carried out using

Taguchi design of experiments. The results show that, 30 % carbonyl iron powder and 70 % silicone oil proportion is optimal for better damper performance and 2 Hz frequency provides better damper performance than 1.5 Hz frequency.

- With reference to the characteristic curve (force v/s displacement) obtained experimentally, the Slope and area enclosed represent stiffness and energy dissipation of MR damper respectively. It can be concluded that slope and area enclosed increase with increase in applied current. Hence, maximum stiffness and energy dissipation was observed at higher currents. Observation shows that energy dissipated from MR damper at 0.4 A is three time greater than at 0.1 A.
- The results of the non-parametric MR damper model developed in the research work and standard parametric (Bouc-Wen) model are compared with experimental investigations and both the models have shown good agreement with experimental results.
- Dynamic response of quarter car vehicle model with semi-active suspension system has been evaluated with different control strategies such as sky-hook, fuzzy logic and PID controller in order to choose the efficient control strategy. Results of simulation show that fuzzy logic controller provides better vibration isolation of a passenger vehicle compared to other control strategies.
- Dynamic response analysis of quarter car, half car and full car vehicle models with nonparametric model of MR damper subjected to stationary random road input was conducted and the results were compared with passive suspension system. The quarter car model with non-parametric model of MR damper shows about 44% reduction in amplitude at resonance frequency. In case of road bump, it provides 65% faster settling time than passive suspension system.
- Dynamic response analysis of half car vehicle model with non-parametric model of MR damper performed better than passive suspension system with bounce acceleration reducing by 21%, 40% reduction in pitch motion and 16% improvement in road holding under stationary random road condition. In case

of road bump, it provides 13% reduction in peak amplitude and 63% faster settling than passive suspension system.

- Responses of full car vehicle model based on non-parametric model of MR damper has better performance compared to passive suspension system under random road excitation. In comparison with passive suspension system, MR damper suspension system shows 32 % reduction vertical acceleration, 52 % reduction in roll motion, 33 % reduction in pitch motion of sprung mass and 10% improvement in road holding attained. While in case of road bump excitation, it has provided 13 % reduction in peak amplitude and 80% faster settling than passive suspension system.

8.4. SCOPE OF FUTURE WORK

- Present study was focused on dynamic analysis of vehicle with MR damper using mathematical modelling. Further work in this direction could study the performance of a vehicle equipped with MR damper experimentally.
- Current investigations were limited to vertical dynamic analysis of a vehicle with MR damper. Further, lot of scope exists on lateral dynamic studies of a vehicle with MR damper giving special emphasis on handling and stability capabilities.
- Current research work was based on dynamic response studies of a vehicle subjected to stationary random road excitation. Further investigations can be carried out with non-stationary random road excitation.
- Dynamic response studies of a vehicle with twin tube MR damper are presented in this thesis. Future work can be in the direction of conducting dynamic analysis of a vehicle with monotube MR damper.
- Investigations can be carried out in preparing MR fluid with an arrangement to prevent settling of particles.
- Present work was based on development of non-parametric modelling of MR damper using magneto-static analysis. Coupled computational fluid dynamics (CFD) and discrete element model (DEM) of MR damper can be explored to enhance accuracy level.

REFERENCES

Agharkakli, A., Sabet, G.S. and Barouz, A. (2012). "Simulation and analysis of passive and active suspension system using quarter car model for different road profile." *International Journal of Engineering Trends and Technology*, 3(5), 636-644.

Aguirre, N., Ikhouane, F., Rodellar, J., Wagg, D. and Neild, S. (2010). "Modeling and identification of a small scale magnetorheological damper." *In Proceedings of the IFAC, International Workshop on adaptation and learning in control and signal processing*.

Ahmadian, M. and Pare, C.A. (2000). "A quarter-car experimental analysis of alternative semiactive control methods." *Journal of Intelligent Material Systems and Structures*, 11(8), 604-612.

Ahmadian, M. and Norris, J.A. (2008). "Experimental analysis of magnetorheological dampers when subjected to impact and shock loading." *Communications in Nonlinear Science and Numerical Simulation*, 13(9), 1978-1985.

Ali, S.F. and Ramaswamy, A. (2009). "Hybrid structural control using magnetorheological dampers for base isolated structures." *Smart Materials and Structures*, 18(5), 055011.

Alexandru, C. and Alexandru, P. (2011). "A comparative analysis between the vehicles passive and active suspensions." *International Journal of Mechanics*, 4(5), 371-378.

Alleyne, A., Neuhaus, P.D. and Hedrick, J.K. (1993). "Application of nonlinear control theory to electronically controlled suspensions." *Vehicle System Dynamics*, 22(5-6), 309-320.

Amato, F.J. and Viassolo, D.E. (2000). "Fuzzy control for active suspensions." *Mechatronics*, 10(8), 897-920.

Anakwa, W.K., Thomas, D.R., Jones, S.C., Bush, J., Green, D., Anglin, G.W., Rio, R., Sheng, J., Garrett, S. and Chen, L. (2002). "Development and control of a prototype pneumatic active suspension system." *IEEE Transactions on Education*, 45(1), 43-49.

Ashfak, A., Saheed, A., Rasheed, K.A. and Jaleel, J.A. (2011). "Design, fabrication and evaluation of MR damper." *International Journal of Aerospace and Mechanical Engineering*, 1, 27-33.

Atray, V.S. and Roschke, P.N. (2003). "Design, fabrication, testing, and fuzzy modeling of a large magnetorheological damper for vibration control in a railcar." *In IEEE/ASME 2003 Joint Rail Conference, American Society of Mechanical Engineers*, 223-229.

Avinash, B., Sundar, S.S. and Gangadharan, K.V. (2014). "Experimental study of damping characteristics of air, silicon oil, magneto rheological fluid on twin tube damper." *Procedia Materials Science*, 5, 2258-2262.

Bakshi, U.A. and Bakshi, A.V. (2009). *Electromagnetic field theory*. Technical Publications, India.

Balamurugan, L., Jancirani, J. and Eltantawie, M.A. (2014). "Generalized magnetorheological (MR) damper model and its application in semi-active control of vehicle suspension system." *International Journal of Automotive Technology*, 15(3), 419-427.

Barbosa, R. S. (2011). "Vehicle dynamic response due to pavement roughness." *Journal of the Brazilian Society of Mechanical Sciences and Engineering*, 33(3), 302-307.

Bajkowski, J. and Skalski, P. (2012). "Analysis of viscoplastic properties of a magnetorheological fluid in a damper." *acta mechanica et automatica*, 6, 5-10.

Berasategui, J., Elejabarrieta, M.J. and Bou-Ali, M.M. (2014). "Characterization analysis of a MR damper." *Smart Materials and Structures*, 23(4), 045025.

Boada, M.J.L., Calvo, J.A., Boada, B.L. and Diaz, V. (2011). "Modeling of a magnetorheological damper by recursive lazy learning." *International Journal of Non-Linear Mechanics*, 46(3), 479-485.

Bodgen, S. and Filus, J. (2003). "Analysis of parametric models of MR linear damper." *Journal of Theoretical and Applied Mechanics*, 41(2), 215-240.

Bossis, G., Lacin, S., Meunier, A. and Volkova, O. (2002). "Magnetorheological fluids." *Journal of magnetism and magnetic materials*, 252, 224-228.

Bose, H., Gerlach, T. and Ehrlich, J. (2013). "Magnetorheological torque transmission devices with permanent magnets." *In Journal of Physics: Conference Series*, 412(1), 012050.

Buciskas, V., Klevinskis, A., Sesok, N., Iljin, I. and Warsza, Z.L. (2016). "Evaluation of damping characteristics of a damper with magneto-rheological fluid." *In Advanced Mechatronics Solutions*, 411-420.

Butz, T. and Von Stryk, O. (2002). "Modelling and simulation of electro-and magnetorheological fluid dampers." *ZAMM*, 82(1), 3.

Campos, J., Davis, L., Lewis, F. L., Ikenaga, S., Scully, S. and Evans, M. (1999). "Active suspension control of ground vehicle heave and pitch motions." *In Proceedings of the 7th IEEE Mediterranean Control Conference on Control and Automation, Haifa, Israel*.

Çeşmeci, S. and Engin, T. (2010). "Modeling and testing of a field-controllable magnetorheological fluid damper." *International Journal of Mechanical Sciences*, 52(8), 1036-1046.

Changizi, N. and Rouhani, M. (2011). "Comparing PID and fuzzy logic control a quarter car suspension system." *The journal of mathematics and computer science*, 2(3), 559-564.

Chaudhuri, A., Wereley, N.M., Radhakrishnan, R. and Choi, S.B. (2006). "Rheological parameter estimation for a ferrous nanoparticle-based

magnetorheological fluid using genetic algorithms.” *Journal of intelligent material systems and structures*, 17(3), 261-269.

Chen, Y. (2009). “Skyhook surface sliding mode control on semi-active vehicle suspension system for ride comfort enhancement.” *Engineering*, 1(01), 23.

Chooi, W.W. and Oyadiji, S.O. (2008). “Design, modelling and testing of magnetorheological (MR) dampers using analytical flow solutions.” *Computers and structures*, 86(3), 473-482.

Choi, S.B., Jeon, J. and Ha, S.H. (2012). *Vibration Control of Flexible Structures Using Semi-Active Mount: Experimental Investigation*, INTECH

Choi, S.B., Lee, S.K. and Park, Y.P. (2001). “A hysteresis model for the field-dependent damping force of a magnetorheological damper.” *Journal of sound and vibration*, 245(2), 375-383.

Choi, J.S., Park, B.J., Cho, M.S. and Choi, H.J. (2006). “Preparation and magnetorheological characteristics of polymer coated carbonyl iron suspensions.” *Journal of Magnetism and Magnetic Materials*, 304(1), e374-e376.

Costa, E. and Branco, P.C. (2009). “Continuum electromechanics of a magnetorheological damper including the friction force effects between the MR fluid and device walls: analytical modelling and experimental validation.” *Sensors and Actuators-A*, 155(1), 82-88.

Cronje, J.M., Heyns, P.S., Theron, N.J. and Loveday, P.W. (2005). “Development of a variable stiffness and damping tunable vibration isolator.” *Journal of Vibration and Control*, 11(3), 381-396.

Deb, K. (2001). *Multi-objective optimization using evolutionary algorithms*, John Wiley and Sons.

Deb, K., Agrawal, S., Pratap, A. and Meyarivan, T. (2000). “A fast elitist non-dominated sorting genetic algorithm for multi-objective optimization: NSGA-II.” *In Parallel problem solving from nature PPSN VI*, 849-858.

Dong, X. M., Yu, M., Liao, C. R. and Chen, W. M. (2010). "Comparative research on semi-active control strategies for magneto-rheological suspension." *Nonlinear Dynamics*, 59(3), 433-453.

Du, H., Sze, K. Y. and Lam, J. (2005). "Semi-active H_{∞} control of vehicle suspension with magneto-rheological dampers." *Journal of Sound and Vibration*, 283(3), 981-996.

Dutta, S. and Chakraborty, G. (2014). "Performance analysis of nonlinear vibration isolator with magneto-rheological damper." *Journal of Sound and Vibration*, 333(20), 5097-5114.

Dutta, S., Narahari, S. and Chakraborty, G. (2013). "Semi-active vibration isolation of a quarter car model under random road excitations using magnetorheological damper." *In 1st International and 16th National Conference on Machines and Mechanisms*, 999-1005.

Ekkachai, K. and Nilkhamhang, I. (2012). "MR damper identification using EHM-based feed forward neural network." *In SICE Annual Conference IEEE*, 1138-1143.

Eltantawie, M.A. (2012). "Decentralized neuro-fuzzy control for half car with semi-active suspension system." *International Journal of Automotive Technology*, 13(3), 423-431.

Ehrgott, R.C. and Masri, S.F. (1992). "Modeling the oscillatory dynamic behaviour of electrorheological materials in shear." *Smart Materials and Structures*, 1(4), 275.

Enriquez-Zarate, J., Silva-Navarro, G. and Cabrera-Amado, A. (2015). "Semiactive Vibration Control in a Three-Story Building-Like Structure Using a Magnetorheological Damper." *Dynamics of Civil Structures*, 2, 475-483.

Ercan, Y. (2009). "Theoretical analysis and evaluation of an optimally controlled full-car vehicle model with a variable-damping semi-active vehicle suspension forced by measured road inputs." *In Journal of Physics: Conference Series*, 149(1), 012046.

- Eslaminasab, N., Biglarbegan, M., Melek, W.W. and Golnaraghi, M.F. (2007). "A neural network based fuzzy control approach to improve ride comfort and road handling of heavy vehicles using semi-active dampers." *International journal of heavy vehicle systems*, 14(2), 135-157.
- Esteki, K., Bagchi, A. and Sedaghati, R. (2014). "Dynamic analysis of electro-and magneto-rheological fluid dampers using duct flow models." *Smart Materials and Structures*, 23(3), 035016.
- Eski, I. and Yildirim, Ş. (2009). "Vibration control of vehicle active suspension system using a new robust neural network control system." *Simulation Modelling Practice and Theory*, 17(5), 778-793.
- Fateh, M.M. and Alavi, S.S. (2009). "Impedance control of an active suspension system." *Mechatronics*, 19(1), 134-140.
- Ferdous, M.M., Rashid, M.M., Hasan, M.H. and Rahman, M.A. (2014). "Optimal design of Magneto-Rheological damper comparing different configurations by finite element analysis." *Journal of mechanical science and technology*, 28(9), 3667-3677.
- Fengchen, T., Yang, Q., He, C. and Wang, L. (2012). "Experimental study and design on automobile suspension made of magneto-rheological damper." *Energy Procedia*, 16, 417-425.
- Fang, Z., Shu, W., Du, D., Xiang, B., He, Q. and He, K. (2011). "Semi-active suspension of a full-vehicle model based on double-loop control." *Procedia Engineering*, 16, 428-437.
- Gangrou, Peng. (2011). "Development of MR damper for motorcycle steering." ME thesis, University of Wollongong.
- Gavin, H., Hoagg, J. and Dobossy, M. (2001). "Optimal design of MR dampers." *In Proceedings of the US-Japan Workshop on Smart Structures for Improved Seismic Performance in Urban Regions*, 14, 225-236.

Gavin, H.P., Hanson, R.D. and Filisko, F.E. (1996). "Electrorheological dampers, part II: testing and modeling." *Journal of Applied Mechanics*, 63(3), 676-682.

Gaur, S. (2013). "Vibration Control of Bus Suspension System using PI and PID Controller." *International Journal of Advances in Engineering Sciences*, 3(3), 94-99.

Georgiou, G., Verros, G. and Natsiavas, S. (2007). "Multi-objective optimization of quarter-car models with a passive or semi-active suspension system." *Vehicle System Dynamics*, 45(1), 77-92.

Goldasz, J. and Sapiński, B. (2011). "Modeling of magnetorheological mounts in various operation modes." *acta mechanica et automatica*, 5, 29-40.

Gamota, D.R. and Filisko, F.E. (1991). "Dynamic mechanical studies of electrorheological materials: moderate frequencies." *Journal of Rheology*, 35(3), 399-425.

Gong, X.L., Zhang, X.Z. and Zhang, P.Q. (2005). "Fabrication and characterization of isotropic magnetorheological elastomers." *Polymer testing*, 24(5), 669-676.

Gravatt, J.W. (2003). "Magneto-rheological dampers for super-sport motorcycle applications." M.S. Thesis, Virginia Polytechnic and State University.

Grunwald, A. and Olabi, A. G. (2008). "Design of magneto-rheological (MR) valve." *Sensors and Actuators A*, 148(1), 211-223.

Gudmundsson, K.H., Jonsdottir, F. and Thorsteinsson, F. (2010). "A geometrical optimization of a magneto-rheological rotary brake in a prosthetic knee." *Smart Materials and Structures*, 19(3), 035023.

Guclu, R. (2005). "Fuzzy logic control of seat vibrations of a non-linear full vehicle model." *Nonlinear Dynamics*, 40(1), 21-34.

Guan, X., Guo, P. and Ou, J. (2009). "Multi-objective optimization of magnetorheological fluid dampers." *Engineering Mechanics*, 26, 30-35.

Harris, C.M. (1988). Shock and vibration handbook, McGraw-Hill, New York.

He, L., Qin, G., Zhang, Y. and Chen, L. (2008). "Non-stationary random vibration analysis of vehicle with fractional damping." *In International Conference on Intelligent Computation Technology and Automation (ICICTA)*, 2, 150-157.

Hasçalık, A. and Çaydaş, U. (2008). "Optimization of turning parameters for surface roughness and tool life based on the Taguchi method." *The International Journal of Advanced Manufacturing Technology*, 38(9-10), 896-903.

Hato, M.J., Choi, H.J., Sim, H.H., Park, B.O. and Ray, S.S. (2011). "Magnetic carbonyl iron suspension with organoclay additive and its magnetorheological properties." *Colloids and Surfaces A: Physicochemical and Engineering Aspects*, 377(1), 103-109.

Havelka, F. and Musil, M. (2012). "Optimal semi-active preview control of a quarter car model with magnetorheological damper with respect to tire lift off." *Engineering Mechanics*, 355-365.

Hong, M.K., Park, B.J. and Choi, H.J. (2009). "Preparation and characterization of MR fluid consisting of magnetite particle coated with PMMA." *In Journal of Physics: Conference Series*, 149 (1), 012055.

Holdmann, P. and Holle, M. (1999). "Possibilities to improve the ride and handling performance of delivery trucks by modern mechatronic systems." *JSAE review*, 20(4), 505-510.

Hrovat D. (1993). "Applications of optimal control to advanced automotive suspension design." *Journal of Dynamic Systems, Measurement, and Control*, 115(2B), 328-342.

Huang, S.J. and Lin, W.C. (2003). "A self-organizing fuzzy controller for an active suspension system." *Journal of Vibration and Control*, 9(9), 1023-1040.

Hu, G., Xie, Z. and Li, W. (2015). "Optimal design of a double coil magnetorheological fluid damper with various piston profiles." *World Congress on Structural and Multidisciplinary Optimization*, 1–6.

Hu, G., Zhou, W. and Li, W. (2015). "A new magnetorheological damper with improved displacement differential self-induced ability." *Smart Materials and Structures*, 24(8), 087001.

Hu, W. and Wereley, N.M. (2008). "Hybrid magnetorheological fluid–elastomeric lag dampers for helicopter stability augmentation." *Smart Materials and Structures*, 17(4), 045021.

Ikhoulane, F. and Dyke, S.J. (2007). "Modeling and identification of a shear mode magnetorheological damper." *Smart Materials and Structures*, 16(3), 605.

Imaduddin, F., Mazlan, S. A. and Zamzuri, H. (2013). "A design and modelling review of rotary magnetorheological damper." *Materials and Design*, 51, 575-591.

Jolly, M.R., Bender, J.W. and Carlson, J.D. (1998). "Properties and applications of commercial magnetorheological fluids." *In 5th annual international symposium on smart structures and materials*, 262-275.

Javarehshkian, M.H. and Esmaeli, A. (2015). "Optimal Design of Magnetorheological Fluid Damper Based on Response Surface Method." *International Journal of Engineering*, 28.

Jahromi, A.F. and Zabihollah, A. (2010). "Linear quadratic regulator and fuzzy controller application in full-car model of suspension system with magnetorheological shock absorber." *In International Conference on Mechatronics and Embedded Systems and Applications*, 522-528.

Jeon, D., Park, C. and Park, K. (1999). "Vibration suppression by controlling an MR damper." *International Journal of Modern Physics B*, 13(14n16), 2221-2228.

Jonasson, M. and Roos, F. (2008). "Design and evaluation of an active electromechanical wheel suspension system." *Mechatronics*, 18(4), 218-230.

Jun, J.B., Uhm, S.Y., Ryu, J.H. and Suh, K.D. (2005). "Synthesis and characterization of monodisperse magnetic composite particles for magnetorheological fluid materials." *Colloids and Surfaces A: Physicochemical and Engineering Aspects*, 260(1), 157-164.

Jha, S. and Jain, V.K. (2009). "Rheological characterization of magnetorheological polishing fluid for MRAFF." *The International Journal of Advanced Manufacturing Technology*, 42(7-8), 656-668.

Kamalakkannan, K., Elayaperumal, A. and Managlaramam, S. (2013). "Input advanced control of semi active half car heave model." *Journal of Mechanical Science and Technology*, 27(5), 1225-1231.

Karkoub, M.A. and Zribi, M. (2006). "Active/semi-active suspension control using magnetorheological actuators." *International journal of systems science*. 37(1), 35-44.

Kargulewicz, M., Iordanoff, I., Marrero, V. and Tichy, J. (2012). "Modeling of Magnetorheological Fluids by the Discrete Element Method." *Journal of Tribology*, 134(3), 031706.

Kasprzyk, J. and Krauze, P. (2014). "Vibration control for a half-car model with adaptation of the magnetorheological damper model." *In Proceedings of the 6th International Conference on Modelling, Identification and Control (ICMIC)*, 243-248.

Khiavi, A. M., Mirzaei, M. and Hajimohammadi, S. (2013). "A new optimal control law for semi-active suspension system considering nonlinear magneto-rheological damper model." *Journal of Vibration and Control*, 1077546313478292.

Klingenberg, D. J. (2001). "Magnetorheology: applications and challenges." *AICHE Journal*, 47(2), 246-249.

Kim, J. and Park, K.M. (2005). "Material characterization of MR fluid at high frequencies." *Journal of sound and vibration*, 283(1), 121-133.

Kim, Y., Choi, S., Lee, J., Yoo, W. and Sohn, J. (2011). "Damper modeling for dynamic simulation of a large bus with MR damper." *International Journal of Automotive Technology*, 12(4), 521-527.

Kolekar, S., Kurahatti, R.V., Prashanth, P.K., Kamble, V. and Reddy, N. (2014). "Preparation of a silicon oil based magneto rheological fluid and an experimental study of its rheological properties using a plate and cone type Rheometer." *Journal of Institute of smart structures and system*, 3, 23-26.

Kordonski, W. and Golini, D. (1999). "Progress update in magnetorheological finishing." *International Journal of Modern Physics B*, 13(14n16), 2205-2212.

Kumbhar, B. K., Patil, S. R. and Sawant, S. M. (2015). "Synthesis and characterization of magneto-rheological (MR) fluids for MR brake application." *Engineering Science and Technology, an International Journal*, 18(3), 432-438.

Kuzhir, P., Bossis, G., Bashtovoi, V. and Volkova, O. (2003). "Flow of magnetorheological fluid through porous media." *European Journal of Mechanics-B/Fluids*, 22(4), 331-343.

Kciuk, M., and Turczyn, R. (2006). "Properties and application of magnetorheological fluids." *Journal of Achievements in Materials and Manufacturing Engineering*, 18(1-2), 127-130.

Kciuk, M., Kciuk, S. and Turczyn, R. (2009). "Magnetorheological characterisation of carbonyl iron based suspension." *Journal of Achievements in Materials and Manufacturing Engineering*, 33(2), 135-141.

Kciuk, S., Turczyn, R. and Kciuk, M. (2010). "Experimental and numerical studies of MR damper with prototype magnetorheological fluid." *Journal of Achievements in Materials and Manufacturing Engineering*, 39(1), 52-59.

Kulkarni, P., Ciocanel, C., Vieira, S. L., and Naganathan, N. (2003). "Study of the behavior of MR fluids in squeeze, torsional and valve modes." *Journal of intelligent material systems and structures*, 14(2), 99-104.

- Kumbhar, B. K. and Patil, S. R. (2014). "A Study on Properties and Selection Criteria for Magneto-Rheological (MR) Fluid Components." *International Journal of ChemTech Research*, 16 (6), 3303-3306.
- Kurczyk, S. and Pawelczyk, M. (2013). "Fuzzy control for semi-active vehicle suspension." *Journal of Low Frequency Noise, Vibration and Active Control*, 32(3), 217-225.
- Kwok, N. M., Ha, Q. P., Nguyen, M. T., Li, J. and Samali, B. (2007). "Bouc–Wen model parameter identification for a MR fluid damper using computationally efficient GA." *ISA transactions*, 46(2), 167-179.
- Lam, H.F., Lai, C.Y. and Liao, W.H. (2002). "Automobile Suspension Systems with MR Fluid Dampers." Technical Report, Department of Mechanical and Automation Engineering, The Chinese University of Hong Kong.
- Lee, D.Y., Choi, Y.T. and Wereley, N.M. (2002). "Performance analysis of ER/MR impact damper systems using Herschel-Bulkley model." *Journal of Intelligent Material Systems and Structures*, 13(7-8), 525-531.
- Liao, W.H. and Lai, C.Y. (2002). "Harmonic analysis of a magnetorheological damper for vibration control." *Smart Materials and Structures*, 11(2), 288.
- Lin, T.R. (2002). "Optimisation technique for face milling stainless steel with multiple performance characteristics." *The International Journal of Advanced Manufacturing Technology*, 19(5), 330-335.
- Lin, J., Lian, R.J., Huang, C.N. and Sie, W.T. (2009). "Enhanced fuzzy sliding mode controller for active suspension systems." *Mechatronics*, 19(7), 1178-1190.
- Lindler, J. and Wereley, N.M. (2003). "Quasi-steady Bingham plastic analysis of an electrorheological flow mode bypass damper with piston bleed." *Smart materials and structures*, 12(3), 305.

Liu, Y., Waters, T.P. and Brennan, M.J. (2005). "A comparison of semi-active damping control strategies for vibration isolation of harmonic disturbances." *Journal of Sound and Vibration*, 280(1), 21-39.

Li, W.H., Yao, G.Z., Chen, G., Yeo, S.H. and Yap, F.F. (2000). "Testing and steady state modeling of a linear MR damper under sinusoidal loading." *Smart Materials and Structures*, 9(1), 95-102.

Li, W.H., Guo, N.Q. and Du, H. (2003). "Finite element analysis and simulation evaluation of a magnetorheological valve." *The international journal of advanced manufacturing technology*, 21(6), 438-445.

Li, W.H., Wang, X.Y., Zhang, X.Z. and Zhou, Y. (2009). "Development and analysis of a variable stiffness damper using an MR bladder." *Smart Materials and Structures*, 18(7), 074007.

Li, W.H., Du, H., Chen, G. and Guo, N.Q. (2003). "Experimental and modeling approaches of MR behaviors under large step strains." *Materials Science and Engineering: A*, 340(1), 251-257.

Liu, Y., Matsuhisa, H., Utsuno, H. and Park, J.G. (2006). "Variable damping and stiffness vibration control with magnetorheological fluid dampers for two degree-of-freedom system." *JSME International Journal Series C Mechanical Systems, Machine Elements and Manufacturing*, 49(1), 156-162.

Mangal, S.K. and Kumar, A. (2015). "Geometric parameter optimization of magnetorheological damper using design of experiment technique." *International Journal of Mechanical and Materials Engineering*, 10(1), 1-9.

McLaughlin, G., Hu, W. and Wereley, N.M. (2014). "Advanced magnetorheological damper with a spiral channel bypass valve." *Journal of Applied Physics*, 115(17), 17B532.

- Metered, H., Bonello, P. and Oyadiji, S.O. (2010). "The experimental identification of magnetorheological dampers and evaluation of their controllers." *Mechanical Systems and Signal Processing*, 24(4), 976-994.
- Milecki, A. (2001). "Investigation and control of magneto-rheological fluid dampers." *International journal of machine tools and manufacture*, 41(3), 379-391.
- Muhammad, A., Yao, X.L. and Deng, Z.C. (2006). "Review of magnetorheological (MR) fluids and its applications in vibration control." *Journal of Marine Science and Application*, 5(3), 17-29.
- Naik, R.D. and Singru, P.M. (2009). "Establishing the limiting conditions of operation of magneto-rheological fluid dampers in vehicle suspension systems." *Mechanics Research Communications*, 36(8), 957-962.
- Nakai, H., Oosaku, S. and Motozono, Y. (2000). "Application of practical observer to semi-active suspensions." *Journal of dynamic systems, measurement, and control*, 122(2), 284-289.
- Nalbant, M., Gökkaya, H. and Sur, G. (2007). "Application of Taguchi method in the optimization of cutting parameters for surface roughness in turning." *Materials and design*, 28(4), 1379-1385.
- Narayanan, S. and Raju, G.V. (1990). "Stochastic optimal control of non-stationary response of a single-degree-of-freedom vehicle model." *Journal of Sound and Vibration*, 141(3), 449-463.
- Nguyen, Q.H., Han, Y.M., Choi, S.B. and Wereley, N.M. (2007). "Geometry optimization of MR valves constrained in a specific volume using the finite element method." *Smart Materials and Structures*, 16(6), 2242.
- Nguyen, Q.H. and Choi, S.B. (2009). "Optimal design of MR shock absorber and application to vehicle suspension." *Smart materials and Structures*, 18(3), 035012.

Nguyen, Q.H., Choi, S.B., Lee, Y.S. and Han, M.S. (2009). "An analytical method for optimal design of MR valve structures." *Smart Materials and Structures*, 18(9), 095032.

Nguyen, Q.H., Choi, S.B., and Woo, J.K. (2014). "Optimal design of magnetorheological fluid-based dampers for front-loaded washing machines." *Proceedings of the Institution of Mechanical Engineers, Part C: Journal of Mechanical Engineering Science*, 228(2), 294-306.

Nguyen, S.D., Nguyen, Q.H. and Choi, S.B. (2015). "A hybrid clustering based fuzzy structure for vibration control - Part 2: An application to semi-active vehicle seat-suspension system." *Mechanical Systems and Signal Processing*, 56, 288-301.

Nugroho, P.W., Du, H., Li, W. and Alici, G. (2013). "Implementation of Adaptive Neuro Fuzzy Inference System controller on magneto rheological damper suspension." *In International Conference on Advanced Intelligent Mechatronics (AIM)*, 1399-1403.

Nitin, H., Ambhore, pangavhane, D.R. and Shyamsundar, D., Hivarale. (2013). "A study of some nonparametric model of magnetorheological fluid damper for vibration control." *International journal of current Engineering and Technology*, 3(2), 388-392.

Olabi, A.G. and Grunwald, A. (2007). "Design and application of magneto-rheological fluid." *Materials and design*, 28(10), 2658-2664.

Paksoy, M., Guclu, R. and Cetin, S. (2014). "Semiactive self-tuning fuzzy logic control of full vehicle model with MR damper." *Advances in Mechanical Engineering*, 6, 816813.

Park, E. J., da Luz, L. F. and Suleman, A. (2008). "Multidisciplinary design optimization of an automotive magnetorheological brake design." *Computers and structures*, 86(3), 207-216.

- Parlak, Z., Engin, T., Ari, V., Sahin, I. and Calli, I. (2010). "Geometrical optimisation of vehicle shock dampers with magnetorheological fluid." *International journal of vehicle design*, 54(4), 371-392.
- Parlak, Z. and Engin, T. (2012). "Time-dependent CFD and quasi-static analysis of magnetorheological fluid dampers with experimental validation." *International Journal of Mechanical Sciences*, 64(1), 22-31.
- Parlak, Z., Engin, T. and Çallı, İ. (2012). "Optimal design of MR damper via finite element analyses of fluid dynamic and magnetic field." *Mechatronics*, 22(6), 890-903.
- Parlak, Z., Engin, T. and Şahin, İ. (2013). "Optimal magnetorheological damper configuration using the Taguchi experimental design method." *Journal of Mechanical Design*, 135(8), 081008.
- Parthasarathy, M. and Klingenberg, D.J. (1996). "Electrorheology: mechanisms and models." *Materials Science and Engineering: R: Reports*, 17(2), 57-103.
- Premalatha, S.E., Chokkalingam, R. and Mahendran, M. (2012). "Magneto mechanical properties of iron based MR fluids." *American Journal of Polymer Science*, 2(4), 50-55.
- Paul, M.D., Moinuddin, M.A. and Islam, M.M.N. (2014). "Finite Element Analysis and Simulation of A Magneto-Rheological Damper." *International Journal for Innovative Research in Science and Technology*, 1(5), 12-19.
- Paul, P.S., Iasanth, J.A., Vasanth, X.A. and Varadarajan, A.S. (2015). "Effect of nanoparticles on the performance of magnetorheological fluid damper during hard turning process." *Friction*, 3(4), 333-343.
- Potter, J.N., Neild, S.A. and Wagg, D.J. (2011). "Quasi-active suspension design using magnetorheological dampers." *Journal of Sound and Vibration*, 330(10), 2201-2219.

Prabakar, R.S., Sujatha, C. and Narayanan, S. (2013). "Response of a quarter car model with optimal magnetorheological damper parameters." *Journal of Sound and Vibration*, 332(9), 2191-2206.

Prabakar, R.S., Sujatha, C. and Narayanan, S. (2009). "Optimal semi-active preview control response of a half car vehicle model with magnetorheological damper." *Journal of sound and vibration*, 326(3), 400-420.

Priyandoko, G., Mailah, M. and Jamaluddin, H. (2009). "Vehicle active suspension system using skyhook adaptive neuro active force control." *Mechanical Systems and Signal Processing*, 23(3), 855-868.

Rajamani, R. (2012). Design and Analysis of Passive Automotive Suspensions. *Vehicle Dynamics and Control*, 267-300.

Rao, T., Mohan, R., Rao, G.V., Rao, K.S. and Purushottam, A. (2010). "Analysis of passive and semi active controlled suspension systems for ride comfort in an omnibus passing over a speed bump." *International Journal of Research and Reviews in Applied Sciences*, 5(1), 7-17.

Rao, L. G. and Narayanan, S. (2009). "Sky-hook control of nonlinear quarter car model traversing rough road matching performance of LQR control." *Journal of Sound and Vibration*, 323(3), 515-529.

Rao, M.V.C. and Prahlad, V. (1997). "A tunable fuzzy logic controller for vehicle-active suspension systems." *Fuzzy sets and systems*, 85(1), 11-21.

Rosenfeld, N. C. and Wereley, N. M. (2004). "Volume-constrained optimization of magnetorheological and electrorheological valves and dampers." *Smart Materials and Structures*, 13(6), 1303.

Rossi, C., and Lucente, G. (2004). " H_{∞} control of automotive semi-active suspensions." *In Proceedings of the 1st IFAC Symposium on Advances in Automotive Control (AAC)*. Salerno, Italy.

- Sapinski, B. and Filus, J. (2003). "Analysis of parametric models of MR linear damper." *Journal of Theoretical and Applied Mechanics*, 41(2), 215-240.
- Sarkar, C. and Hirani, H. (2013). "Synthesis and characterization of antifriction magnetorheological fluids for brake." *Defence Science Journal*, 63(4), 408-412.
- Savaresi, S.M., Bittanti, S. and Montiglio, M. (2005). "Identification of semi-physical and black-box non-linear models: the case of MR-dampers for vehicles control." *Automatica*, 41(1), 113-127.
- Salloom, M.Y. and Samad, Z. (2011). "Finite element modeling and simulation of proposed design magneto-rheological valve." *The International Journal of Advanced Manufacturing Technology*, 54(5-8), 421-429.
- Sahasrabudhe, S.S. and Nagarajaiah, S. (2005). "Semi-active control of sliding isolated bridges using MR dampers: an experimental and numerical study." *Earthquake engineering and structural dynamics*, 34(8), 965-983.
- Schurter, K.C. and Roschke, P.N. (2000). "Fuzzy modeling of a magnetorheological damper using ANFIS." *In the Ninth IEEE International Conference on Fuzzy Systems*, 1, 122-127.
- Seong, M.S., Sung, K.G. and Choi, S.B. (2011). Control Strategies for Vehicle Suspension System Featuring Magnetorheological (MR) Damper, INTECH.
- Shaji, S. and Radhakrishnan, V. (2003). "Analysis of process parameters in surface grinding with graphite as lubricant based on the Taguchi method." *Journal of Materials Processing Technology*, 141(1), 51-59.
- Sharkawy, A.B. (2005). "Fuzzy and adaptive fuzzy control for the automobiles active suspension system." *Vehicle system dynamics*, 43(11), 795-806.
- Shivaram, A.C. and Gangadharan, K.V. (2007). "Statistical modeling of a magneto-rheological fluid damper using the design of experiments approach." *Smart materials and structures*, 16(4), 1310.

Shibayama, A., Miyazaki, T., Otomo, T., Fujita, T. and Shimada, K. (2002). "Relationship between chain structures and viscosity in the magneto-rheological suspensions stable dispersing different concentration of iron particles with smectite." *International Journal of Modern Physics B*, 16(17n18), 2364-2370.

Simon, T.M., Reitich, F., Jolly, M.R., Ito, K. and Banks, H.T. (2001). "The effective magnetic properties of magnetorheological fluids." *Mathematical and Computer Modelling*, 33(1), 273-284.

Sims, N.D. and Stanway, R. (2007). "Modelling of force-velocity hysteresis in smart fluid dampers." *Journal of sound and vibration*, 300(1), 429-431.

Sireteanu, T. and Stoia, N. (2003). "Damping optimization of passive and semi-active vehicle suspension by numerical simulation." *Proceedings of the Romanian Academy*, 4(2), 121-127.

Slaski, G. and Maciejewski, M. (2011). "Skyhook and fuzzy logic controller of a semi active vehicle suspension." *Prace Naukowe Politechniki Warszawskiej, Transport*, 97-111.

Song, X., Ahmadian, M. and Southward, S.C. (2005). "Modeling magnetorheological dampers with application of nonparametric approach." *Journal of Intelligent Material Systems and Structures*, 16(5), 421-432.

Spencer, B.F., Dyke, S.J., Sain, M.K. and Carlson, J. (1997). "Phenomenological model for magnetorheological dampers." *Journal of engineering mechanics*, 123(3), 230-238.

Spelta, C., Previdi, F., Savaresi, S.M., Fraternali, G. and Gaudiano, N. (2009). "Control of magnetorheological dampers for vibration reduction in a washing machine." *Mechatronics*, 19(3), 410-421.

Sapinski, B. and Filus, J. (2003). "Analysis of parametric models of MR linear damper." *Journal of Theoretical and Applied Mechanics*, 41(2), 215-240.

Sternberg, A., Zemp, R. and de la Llera, J.C. (2014). "Multiphysics behavior of a magneto-rheological damper and experimental validation." *Engineering Structures*, 69, 194-205.

Stanway, R.S.J.L., Sproston, J.L. and Stevens, N.G. (1987). "Non-linear modelling of an electro-rheological vibration damper." *Journal of Electrostatics*, 20(2), 167-184.

Stribrsky, A., Hyniová, K., Honců, J. and Kruczek, A. (2003). "Using fuzzy logic to control active suspension system of one-half-car model." *Acta Montanistica Slovaca, Ročník*, 8.

Talib, A., Hussin, M., Darns, M. and Zaurah, I. (2013, April). "Self-tuning PID controller for active suspension system with hydraulic actuator." *In IEEE Symposium on Computers and Informatics (ISCI)*, 86-91.

Thakkar, R.M., Shah and Mohammed, Y.M. (2013). "Modeling and simulation of magnetorheological fluid damper for predicting the saturation limit to applied field current". *Global research analysis*, 2(3).

Ting, C.S., Li, T.H.S. and Kung, F.C. (1995). "Design of fuzzy controller for active suspension system." *Mechatronics*, 5(4), 365-383.

Tosun, N., Cogun, C. and Tosun, G. (2004). "A study on kerf and material removal rate in wire electrical discharge machining based on Taguchi method." *Journal of Materials Processing Technology*, 152(3), 316-322.

Truong, D.Q. and Ahn, K.K. (2012). MR fluid damper and its application to force sensorless damping control system, INTECH.

Tu, F., Yang, Q., He, C. and Wang, L. (2012). "Experimental study and design on automobile suspension made of magneto-rheological damper." *Energy Procedia*, 16, 417-425.

Turnip, A., Park, S. and Hong, K.S. (2010). "Sensitivity control of a MR-damper semi-active suspension." *International Journal of Precision Engineering and Manufacturing*, 11(2), 209-218.

Tyan, F., Hong, Y.F., Tu, S.H. and Jeng, W.S. (2009). "Generation of random road profiles." *Journal of Advanced Engineering*, 4(2), 1373-1378.

Wang, D.H. and Liao, W.H. (2004). "Modeling and control of magnetorheological fluid dampers using neural networks." *Smart Materials and Structures*, 14(1), 111-126.

Wang, J. and Meng, G. (2001). "Magnetorheological fluid devices: principles, characteristics and applications in mechanical engineering." Proceedings of the Institution of Mechanical Engineers, Part L: *Journal of Materials Design and Applications*, 215(3), 165-174.

Wen, Y.K. (1976). "Method for random vibration of hysteretic systems." *Journal of the engineering mechanics division*, 102(2), 249-263.

Wereley, N.M., Pang, L. and Kamath, G.M. (1998). "Idealized hysteresis modeling of electrorheological and magnetorheological dampers." *Journal of Intelligent Material Systems and Structures*, 9(8), 642-649.

Wereley, N.M., and Pang, L. (1998). "Nondimensional analysis of semi-active electrorheological and magnetorheological dampers using approximate parallel plate models." *Smart Materials and Structures*, 7(5), 732.

Wong, P.L., Bullough, W.A., Feng, C. and Lingard, S. (2001). "Tribological performance of a magneto-rheological suspension." *Wear*, 247(1), 33-40.

Yang, G., Spencer, B.F., Carlson, J.D. and Sain, M.K. (2002). "Large-scale MR fluid dampers: modeling and dynamic performance considerations." *Engineering structures*, 24(3), 309-323.

Yang, W.P. and Tarng, Y.S. (1998). "Design optimization of cutting parameters for turning operations based on the Taguchi method." *Journal of materials processing technology*, 84(1), 122-129.

- Yeh, E.C. and Tsao, Y.J. (1994). "A fuzzy preview control scheme of active suspension for rough road." *International Journal of Vehicle Design*, 15(1-2), 166-180.
- Yazid, I.I.M., Mazlan, S.A., Kikuchi, T., Zamzuri, H. and Imaduddin, F. (2014). "Design of magnetorheological damper with a combination of shear and squeeze modes." *Materials and Design*, 54, 87-95.
- Yue, C., Butsuen, T., and Hedrick, J.K. (1989). "Alternative control laws for automotive active suspensions." *Journal of Dynamic Systems, Measurement, and Control*, 111, 286–291
- Yao, G.Z., Yap, F.F., Chen, G., Li, W. and Yeo, S.H. (2002). "MR damper and its application for semi-active control of vehicle suspension system." *Mechatronics*, 12(7), 963-973.
- Yoshimura, T., Kume, A., Kurimoto, M. and Hino, J. (2001). "Construction of an active suspension system of a quarter car model using the concept of sliding mode control." *Journal of Sound and Vibration*, 239(2), 187-199.
- Yu, G.J., Du, C.B. and Li, Z.Q. (2012). "Optimum Design of a Magnetic Circuit in a Magneto-Rheological Damper." *In Applied Mechanics and Materials*, 130, 1400-1403.
- Zhang, L.J., Lee, C.M. and Wang, Y.S. (2002). "A study on nonstationary random vibration of a vehicle in time and frequency domains." *International Journal of Automotive Technology*, 3(3), 101-109.
- Zhang, J., Zhang, J.Q. and Jia, J.F. (2008). "Characteristic analysis of magnetorheological fluid based on different carriers." *Journal of Central South University of Technology*, 15, 252-255.
- Zhang, H., Wang, E., Min, F., Subash, R. and Su, C. (2013). "Skyhook-based semi-active control of full-vehicle suspension with magneto-rheological dampers." *Chinese Journal of Mechanical Engineering*., 26(3), 498-505.

Zheng, L., Li, Y.N., Shao, J. and Sun, X.S. (2007). "The design of a fuzzy-sliding mode controller of semi-active suspension systems with MR dampers." *Fourth International Conference on Fuzzy Systems and Knowledge Discovery IEEE*, 4, 514-518.

Zhu, C. (2005). "A disk-type magneto-rheological fluid damper for rotor system vibration control." *Journal of sound and vibration*, 283(3), 1051-1069.

Zhou, Y. and Zhang, Y.L. (2013). "Optimal design of a shear magnetorheological damper for turning vibration suppression." *Smart Materials and Structures*, 22(9), 095012.

Zhou, Y., Wang, X., Zhang, X. and Li, W. (2009). "Variable stiffness and damping magnetorheological isolator." *Frontiers of Mechanical Engineering in China*, 4(3), 310-315.

Zhao, H., Liu, Z. and Liu, Y. (2000). "Mechanical properties of a new electrorheological fluid." *Solid state communications*, 116(6), 321-325.

APPENDIX-I

OPTIMIZATION OF THE BOUC-WEN PARAMETERS USING GENETIC ALGORITHM (GA)

A genetic algorithm (GA) is an intelligent probabilistic search algorithm which can be applied to a variety of optimization problems. The idea of GAs is based on the evolutionary process of biological organisms in nature. During the course of the evolution, natural populations evolve according to the principles of natural selection and "survival of the fittest". Individuals which are more successful in adapting to their environment will have a better chance of surviving and reproducing, while individuals which are less fit will be eliminated. In optimization terms, each individual in the population is encoded into a string or chromosome which represents a possible solution to a given problem (Deb, 2001).

GA process starts with the initialization of the population with the calculation of the fitness function. The fitness of an individual is evaluated with respect to a given objective. The best individual is selected and the mating is prioritized based on the fittest individual. An individual's characteristics or features are stored in their genes that make up chromosomes. When a species breeds, these traits are exchanged and altered by genetic processes called crossover and mutation. Crossover is the exchange of a random portion of chromosomes, while mutation is the random alteration of a gene, changing its feature of function.

Steps Involved in GA process

Genetic Algorithm operates on a population of designs. Major components of Genetic Algorithm including encoding scheme, fitness evaluation, parent selection, crossover operators and mutation operators are explained in the following sections.

Encoding: - Encoding is the first and important part of GAs process, because problem related to information is encoded in a structure called chromosome or string. Chromosome is generally a sequence of the variables of problems in an organized manner. Every variable sequenced to construct the chromosome called gene.

Fitness evaluation: - GAs mimic the “survival of the fittest” principle of nature to make a search process. Therefore, GAs are naturally suitable to solve maximization problems. Minimization problems are usually transformed to maximization problems by some suitable transformation. In general, a fitness function $F(x)$ is first derived from the objective function $f(x)$ and used in successive genetic operations. For maximization problems, the fitness function can be considered the same as the objective function ($F(x) = f(x)$). The minimization problem is an equivalent maximization problem such that the optimum point remains unchanged. A number of such transformations are possible. Generally the fitness function used in such cases is

$$F(x) = \frac{1}{1 + f(x)}$$

Genetic operators: - The operations of GAs begin with a population of random strings representing design variables and each string is evaluated to find the fitness value. The population is then operated by three main operators such as reproduction, crossover and mutation to create a new population of points.

Reproduction: - Reproduction is the first operator applied on a population. Reproduction selects good strings in a population and form mating pool. There exist a number of selection operators in GA, but the essential idea is that above-average design strings are picked from the current population and duplicates of them are inserted in the mating pool in prescribed manner. The commonly used reproduction operator is the proportionate reproduction where a string in the current population is selected with a probability proportional to its fitness. Thus, good strings in a population are probabilistically assigned a large number of copies and a mating pool is formed.

Crossover: - Crossover is the exchange information between the individuals among randomly selected pairs from the parent pool and produces new chromosomes from two parents. Crossover is performed after selection of a subpopulation of individuals according to their fitness values and gathering of the selected individuals into a gene

pool. Generally crossover is achieved by three stages. The first stage is matching and it is the selection of two individuals in the gene pool randomly. In the second stage, a crossover point is determined in each of the individuals. In final stage, two part of the individuals are replaced each other.

Mutation: - Mutation is the operation that defines the variation of chromosome. This variation may be local or global. Mutation process is very important to improving the population. Since the initial population is a subset of possible solutions and an important bit of all chromosomes may be 0 while it must be 1 to be optimal.

Non-Dominated Sort: - The population is initialized based on the problem range and constraints. Once the population is initialized the population is sorted based on non-domination into each front. The first front being completely with non-dominant set in the current population, and the second front being dominated by the individuals in the first front only. The fast sort algorithm (Deb et al. 2000) is described below

- For each individual p in the main population P
 - Initialize $S_p = \theta$. This set would contain all the individuals that are being dominated by p .
 - Initialize $n_p = 0$. This would be the number of individuals that dominate p .
 - For each individual q in P
 - if p dominated q then add q to the set S_p i.e. $S_p = S_p \cup \{q\}$
 - if q dominates p then increment the domination counter for p i.e. $n_p = n_p + 1$
 - If $n_p = 0$, i.e., no individuals dominate p , then p belongs in the first front, update the rank of p to one and add p to front one, i.e., $F_1 = F_1 \cup \{p\}$.
- This is carried out for all the individuals in the main population P .
- Initialize the front counter to one, $i=1$
- Following is carried out while the i th front is nonempty i.e. F_i is not empty.

1. $Q = \theta$, the set for sorting the individuals for the $(i+1)^{\text{th}}$ front.
2. For each individual p in front F_i
 - For each individual q in S_p
 - $n_q = n_q - 1$, decrement the domination count for individual q .
 - if $n_q = 0$ then none of the individuals in the subsequent fronts would dominate q , hence set $q_{\text{rank}} = i+1$
 - Increment the front counter by one
 - Now the set q is the next front and hence $F_i = Q$.

This algorithm is better than the original NSGA since it utilizes the information about the set that an individual dominates and number of individuals that dominate the individual.

Crowding Distance: - Once the non-dominated sort is completed the crowding distance is assigned. Since the individuals are selected based on rank and crowding distance all individuals in the population are assigned a crowding distance value. Crowding distance is assigned front wise and comparing crowding distance between two individuals in different fronts is unnecessary.

1. Initially all the crowding distance values are assigned zero for all individuals.
2. The individuals are then sorted based on objective
3. The boundary values for each individual is assigned infinity
4. The remaining individuals are given crowding distance depending on the objective functions

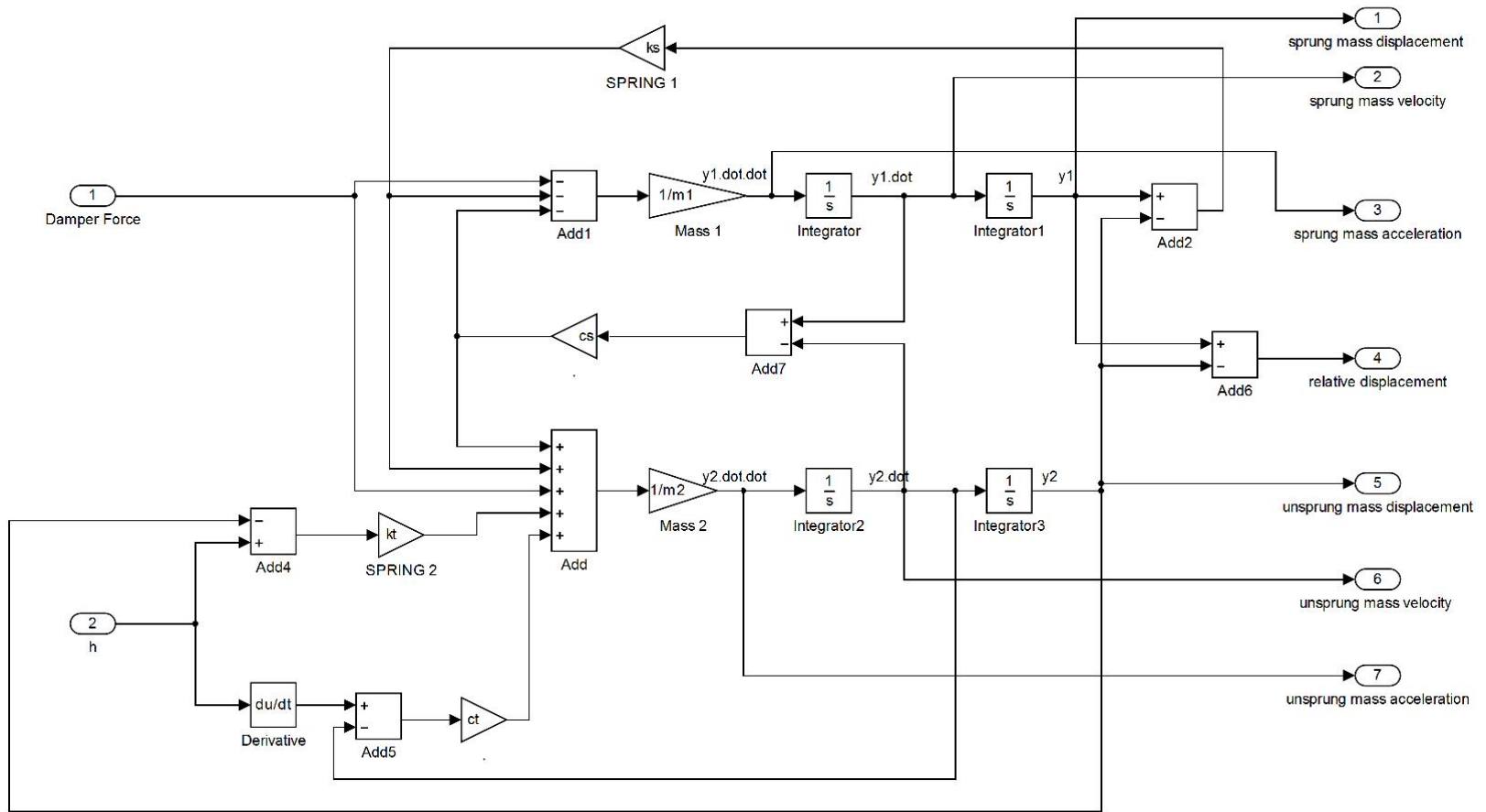
The basic idea behind crowding distance is finding the Euclidian distance between each individual in a front based on their objectives. The individuals in the boundary are always selected since they have infinite distance.

APPENDIX-II

DESCRIPTION OF SOFTWARE MODULE USED

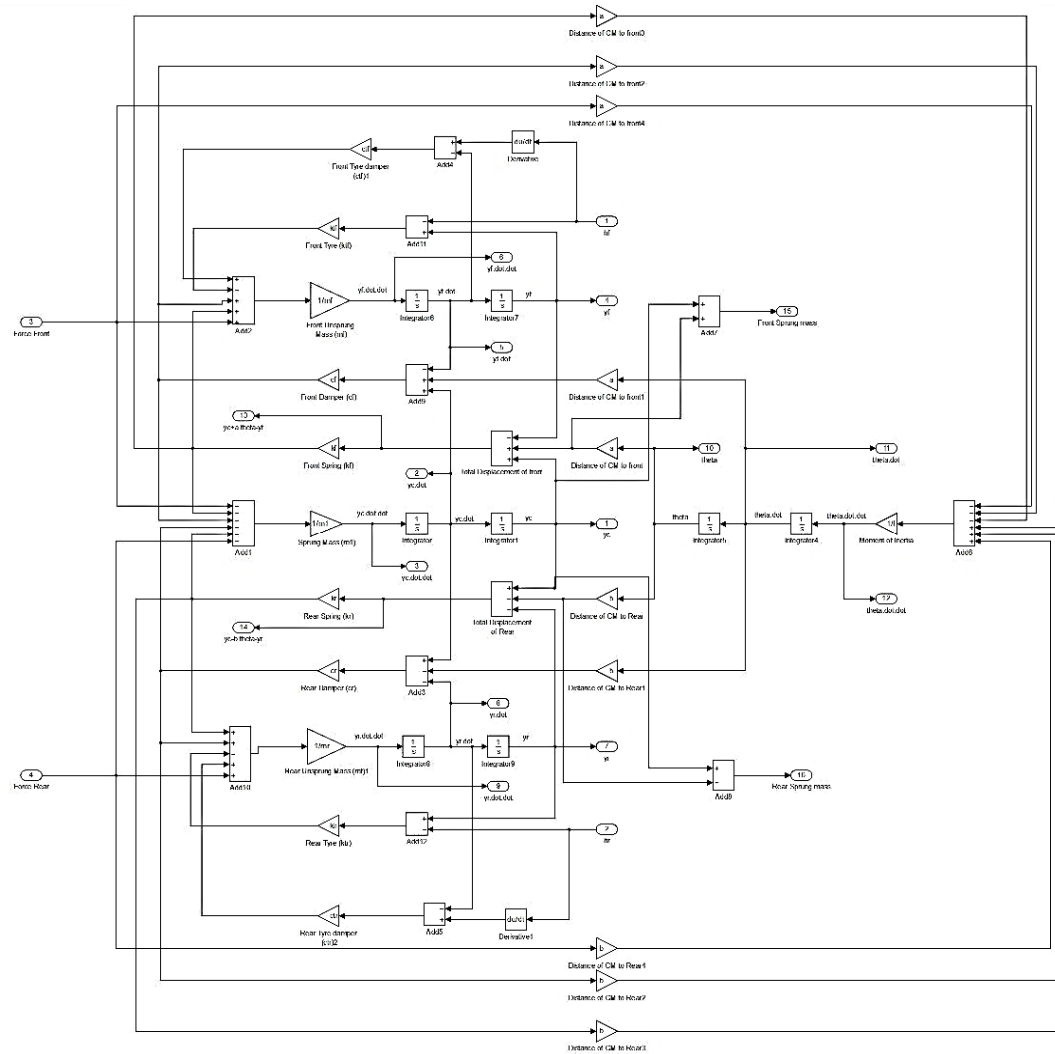
Software	Module	Descriptions
Ansys workbench	Magnetostatic	Magnetostatic analysis is used to find the magnetic field and its related quantities such as magnetic flux density, field intensity, inductance and flux linkage due to application of electric current. It is also used to verify the risks of magnetic saturation in the devices, which could limit the performance of the devices.
Minitab	Design of experiments	DOE (design of experiments) helps you investigate the effects of input variables (factors) on an output variable (response) at the same time. These experiments consist of a series of runs, or tests, in which purposeful changes are made to the input variables. Data are collected at each run. By using DOE the process conditions and product components that affect quality to be identify, and then determine the factor settings that optimize results.
MATLAB	Simulink	Simulink provides a graphical editor, customizable block libraries, and solvers for modeling and simulating dynamic systems. It is integrated with MATLAB, enabling you to incorporate MATLAB algorithms into models and export simulation results to MATLAB for further analysis.

APPENDIX-II (a)
QUARTER CAR MODEL

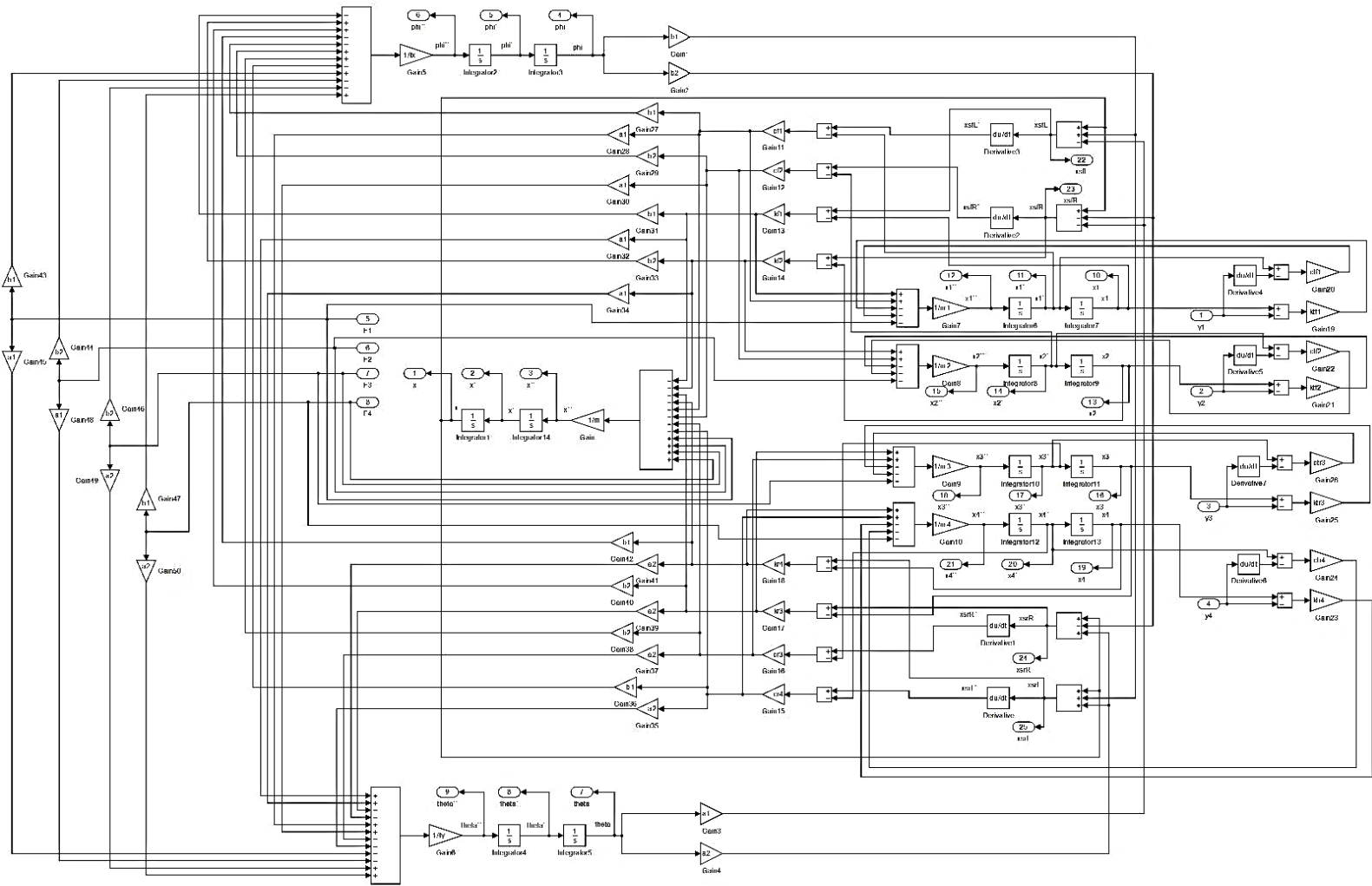


APPENDIX-II (b)

HALF CAR MODEL



APPENDIX-II (c)
FULL CAR MODEL



LIST OF PUBLICATIONS

1. **Hemanth K.**, Hemantha Kumar and Gangadharan K. V. (2016). Vertical dynamic analysis of a quarter car suspension system with MR damper. *Journal of the Brazilian Society of Mechanical Sciences and Engineering*, 1-11. (Springer Publications, Impact factor- 0.963, SCI Indexed)
2. **Hemanth K.**, Hemantha Kumar and Gangadharan K. V. (2016). Optimization of Magneto-Rheological Damper for Maximizing Magnetic Flux Density in the Fluid Flow Gap Through FEA and GA Approaches. *Journal of The Institution of Engineers (India): Series C*, 1-7. (Springer Publications)
3. **Hemanth K.**, Ganesha A., Hemantha Kumar and Gangadharan K. V. (2014). Analysis of MR damper based on finite element approach. In *Applied Mechanics and Materials*, 592, 2006-2010. (Trans Tech Publications, Impact factor- 0.15, SCI Indexed)
4. **Hemanth K.**, Hemantha Kumar and Gangadharan K. V. “Comparative study between non-parametric magneto-rheological (MR) damper model with parametric Bouc-Wen magneto-rheological model” *ICCMS-2016, IIT-B, 27th June - 1st July 2016*.
5. **Hemanth K.**, Lohit S K, Hemantha Kumar and Gangadharan K. V. “Evaluate the performance of quarter car suspension system with nonlinear hysteresis Magnetorheological damper” *ICCMS-2016, IIT-B, 27th June - 1st July 2016*.
6. Lohit S.K., **Hemanth K.**, Hemantha Kumar and Gangadharan K. V. “Experimental and Analytical Studies on Magnetorheological Damper” *ICFIMEMM, March -2016*.
7. **Hemanth K.**, Hemantha Kumar and K.V.Gangadharan “Dynamic analysis of half car model with MR damper.” *International Journal of Acoustics and Vibration* (Revised and sent). Impact factor-0.47, SCI indexed
8. **Hemanth K.**, Lohit S.K., Hemantha Kumar and K.V.Gangadharan “Ride comfort analysis of a vehicle with semi-active suspension system with fuzzy logic control strategy subjected to random road irregularities.” *Journal of Vibration Engineering and Technologies* (under review). Impact factor-0.2, SCI indexed
9. **Hemanth K.**, Hemantha Kumar and K.V.Gangadharan “Evaluate the optimal level of parameters on the performance of MR damper by using Taguchi design of experiments.” *Indian Journal of Engineering and Materials Sciences* (under review). Impact factor-0.56, SCI indexed.

BIO-DATA

1. **Name** : Hemanth K.
2. **Father's Name** : Krishna
3. **Date of Birth** : 14/07/1988
4. **Nationality** : Indian
5. **Marital Status** : Single
6. **Address** :

Permanent Address

S/o. C. N. Krishna
Shivanilaya, Kote
Marigudistreet, Channarayapatna-573116
Hassan

Present Address

Department of Mechanical Engineering
National Institute of Technology Karnataka
Surathkal-575025, Srinivasanagar P.O.
Dhakshina Kannada (Dist), Karnataka, India

7. **Mobile Number** : +91-996498185
8. **E-mail id.** : ckh454@gmail.com
9. **Educational Qualification** :

Qualification	College/school	University/Board	Year of Passing	Performance
Ph.D. in Mechanical Engineering	National Institute of Technology Karnataka	National Institute of Technology Karnataka	2016	8.32 (CGPA)
M.Tech in Machine design	NCET, Bangalore	Visvesvaraya Technological University	2012	75.25%
B.E in Mechanical Engineering	MCE, Hassan	Visvesvaraya Technological University	2010	68.32%

10. **Work Experience** :

Name of the Organization	Duration	Position
St. Joseph College of Engineering and Technology	Aug 2012 to July 2013	Assistant Professor

I declare that above information is true and correct to best of my knowledge and belief.

(Hemanth K.)